

# Journal of Engineering and Technology for Industrial Applications



**ISSN 2447-0228**

**April 2023**

**Volume 09 / No 40**

**Editor-in-Chief: J. C. Leite**

**[www.itegam-jetia.org](http://www.itegam-jetia.org)**



O **ITEGAM-JETIA: Journal of Engineering and Technology for Industrial Applications** is a publication of the Galileo Institute of Technology and Education of the Amazon (ITEGAM), located in the city of Manaus since 2008. JETIA publishes original scientific articles covering all aspects of engineering. Our goal is the dissemination of research original, useful and relevant presenting new knowledge on theoretical or practical aspects of methodologies and methods used in engineering or leading to improvements in professional practice. All the conclusions presented in the articles It should be state-of-the-art and supported by current rigorous analysis and balanced assessment. Public magazine scientific and technological research articles, review articles and case studies.

**JETIA** will address topics from the following areas of knowledge: Mechanical Engineering, Civil Engineering, Materials and Mineralogy, Geosciences, Environment, Information and Decision Systems, Processes and Energy, Electrical and Automation, Mechatronics, Biotechnology and other Engineering related areas.

**Publication Information:**

**ITEGAM-JETIA** (ISSN 2447-0228), (online) is published by Galileo Institute of Technology and Education of the Amazon on a every two months (February, April, June, August, October and December).

**Contact information:**

Web page: [www.itegam-jetia.org](http://www.itegam-jetia.org)

Email: [editor@itegam-jetia.org](mailto:editor@itegam-jetia.org)

Galileo Institute of Technology and Education of the Amazon (ITEGAM).

Joaquim Nabuco Avenue, No. 1950. Center. Manaus, Amazonas. Brazil.

Zip Code: 69020-031. Phone: (92) 3584-6145.

**Copyright 2014. Galileo Institute of Technology and Education of the Amazon (ITEGAM)**

The total or partial reproduction of texts related to articles is allowed, only if the source is properly cited. The concepts and opinions expressed in the articles are the sole responsibility of the authors.

**Previous Notice**

All statements, methods, instructions and ideas are the sole responsibility of the authors and do not necessarily represent the view of ITEGAM -JETIA. The publisher is not responsible for any damage and / or damage to the use of the contents of this journal. The concepts and opinions expressed in the articles are the sole responsibility of the authors.

**Directory**

Members of the ITEGAM Editorial Center - Journal of Engineering and Technology for Industrial Applications (ITEGAM-JETIA) of the Galileo Institute of Technology and Education of the Amazon (ITEGAM). Manaus-Amazonas, Brazil.

**Jandecy Cabral Leite**, CEO and Editorial Editor-in-Chief

**Ivan Leandro Rodriguez Rico**, Editorial Assistant

**Ricardo Silva Parente**, Information Technology Assistant

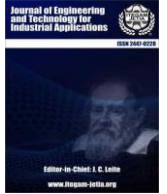


ITEGAM-JETIA. v.9, n.40. April of 2023. Manaus - Amazonas, Brazil. ISSN 2447-0228 (ONLINE)

<https://www.itegam-jetia.org>

## SUMMARY

- EXPLANATION OF AN INNOVATIVE PROGRAMMING APPROACH TO CREATE A PROGRESSIVE TWO-DIMENSIONAL DATA FILE OF THREE INTER-DEPENDANT VARIABLES IN A FULLY AUTOMATED DATA ACQUISITION SYSTEM** 4  
*Avijit Das*
- INVESTIGATIVE ANALYSIS OF SELECTED FSO MODELS WITH VARYING WAVELENGTHS FOR TROPICAL WEATHER** 10  
*Ibukunoluwa A. Olajide, Samson A. Oyetunji, Yekeen O. Olasoji, Wasiu O. Popoola and Muhammad Ijaz*
- FACTORS AFFECTING TECHNICAL EFFICIENCY SCORES ESTIMATED FOR THE COTTON SECTOR OF THE HARRAN PLAIN IN TURKIYE: A STOCHASTIC FRONTIER ANALYSIS** 18  
*Tamer İşgün, Remziye Özel, Abdalbaki Bilgiç and Mehmet Reşit Sevinç*
- NEPHROPROTECTIVE EFFECTS OF ELEUTHERINE AMERICANA MERR AGAINST LEAD ACETATE-INDUCED CYTOTOXICITY IN MICE BALB/C** 27  
*Neti Eka Jayanti, Rozzana Mohd Said, Choo Chee Yan, Suhaidah Mohd Jofrry and Sa'adah Siregar*
- INFLUENCE OF GRADATION ON THE PERFORMANCE OF ASPHALTIC MIXES** 33  
*Akintunde Akinola Oyedele*
- DESIGN AND CONSTRUCTION OF A FUZZY LOGIC SOLAR TRACKER PROTOTYPE FOR THE OPTIMIZATION OF A PHOTOVOLTAIC SYSTEM** 39  
*Omar Beltrán González, Jesús Hernández Aguilar, Francisco Eneldo López Monteagudo, Rafael Villela Varela, Aurelio Beltrán Telles and Claudia Reyes Rivas*



## EXPLANATION OF AN INNOVATIVE PROGRAMMING APPROACH TO CREATE A PROGRESSIVE TWO-DIMENSIONAL DATA FILE OF THREE INTER-DEPENDANT VARIABLES IN A FULLY AUTOMATED DATA ACQUISITION SYSTEM

Avijit Das\*<sup>1</sup>

<sup>1</sup> Saha Institute of Nuclear Physics, 1/AF, Bidhan Nagar, Kolkata - 700064, West Bengal, India.

<sup>1</sup> <http://orcid.org/0000-0001-5754-5245> 

Email \* [avijit.das@saha.ac.in](mailto:avijit.das@saha.ac.in)

### ARTICLE INFO

#### Article History

Received: March 23<sup>th</sup>, 2023

Accepted: April 26<sup>th</sup>, 2023

Published: April 29<sup>th</sup>, 2023

#### Keywords:

LabVIEW,  
2D array,  
Data acquisition,  
Automation,  
CSV file.

### ABSTRACT

This technical document explains a programming model for recording data of a special case in a comma-separated (.csv) file. Generally, in any data acquisition system storing of data increments in one direction; that is in rows. In this article a different programming concept has been illustrated for an automated application to store data in two dimensions; that not only expands in rows but also in columns during the progress of next all successive data acquisition loops for the same set of parameters with a new updated value of the third variable. The effectiveness of the program me has been verified based on a practical proto type test made by monitoring and recording several sets of resultant values of DC current at different values of applied DC voltage and had performed these tests consecutively at different values of temperature. All these acquired data sets were saved in a single comma separated (.csv) data file. The full process can be completed in a single test run and most importantly, without any intervention from a human being. By following the logic and method demonstrated, a similar application could be developed also by other text-based programming languages like Java or Python.



Copyright ©2023 by authors and Galileo Institute of Technology and Education of the Amazon (ITEGAM). This work is licensed under the Creative Commons Attribution International License (CC BY 4.0).

### I. INTRODUCTION

This article describes a fully automated data acquisition programming process in LabVIEW to implement a non-conventional idea of creating a comma-separated data file. Here an uncommon programming method demonstrates how several sequential measurement cycles of a set of variables against variation of a third variable can be saved in a data file without any human intervention. In general, in the case of any data acquisition system in a scientific or engineering laboratory, we normally measure and collect data from one or more variables, that vary against another common and periodically changing variables, like time, voltage or current, temperature etc. Such data collection cycles continue to add on rows of data one after another, which may be of two or more columns depending on the number of parameters under assessment. But sometimes a specific situation demands creating and saving sets of data by monitoring of the

first variable against periodic variation of the second variable at different values of a third variable. One such a very common example is the output characteristic of an NPN transistor at common-emitter configuration, where individual sets of data are collected by monitoring of collector current (IC) against linear variation of collector-emitter voltage (VCE) at different values of base current (IB).

Conventionally, this can easily be done by performing several tests runs at different values of the third variable (like, IB) and manually combining all the results in an excel sheet. But in a completely automated data acquisition process suggested in this article without any attention from a human being, the automatic creation of a new column on the right side of the latest one is done. This process requires an additional programming trick, and that is the goal of writing this article. A sample example has been shown in Table 1 to illustrate my programming idea in an

apprehensible way. Where the initial set of measurements of current (first variable) in a load with linear variation of voltage (second variable) records at some temperature T1. The same acquisition cycles repeat with different values of temperature, such as T2, T3, T4, etc and all the sets of data is being saved in a

single .csv file. In this document, LabVIEW graphical programming language (version 8.0 on Windows XP OS) has been used to explain the procedure [1]. But the same methodology can be followed for other popular high-level programming languages like C++, Java or Python.

Table 1: an example to show how a .csv data file creates different sets of data of variable-2 (I) against variable-1 (V) at different values of the third variable (T).

		Loops of several cycles						
		Loop 1	Loop 2	Loop 3	Loop 4	Loops 5 to 8	Loop 9	Loop 10
		T <sub>1</sub>	T <sub>2</sub>	T <sub>3</sub>	T <sub>4</sub>	T <sub>5</sub> to T <sub>8</sub>	T <sub>9</sub>	T <sub>10</sub>
Acquisition Cycles	V <sub>1</sub>	I <sub>1</sub>	I <sub>11</sub>	I <sub>21</sub>	I <sub>31</sub>	.....	I <sub>81</sub>	I <sub>91</sub>
	V <sub>2</sub>	I <sub>2</sub>	I <sub>12</sub>	I <sub>22</sub>	I <sub>32</sub>	.....	I <sub>82</sub>	I <sub>92</sub>
	V <sub>3</sub>	I <sub>3</sub>	I <sub>13</sub>	I <sub>23</sub>	I <sub>33</sub>	.....	I <sub>83</sub>	I <sub>93</sub>
	V <sub>4</sub> to V <sub>9</sub>	.....	.....	.....	.....	.....	.....	.....
	V <sub>10</sub>	I <sub>10</sub>	I <sub>20</sub>	I <sub>30</sub>	I <sub>40</sub>	.....	I <sub>90</sub>	I <sub>100</sub>
Handles by Sub_Prog_1.vi		Handles by Sub_Prog_2.vi						

Source: Author, (2023).

## II. PROGRAMME DESIGN METHOD

The programming model has been designed to handle three variables that are interlinked with each other. A single data acquisition cycle consists of monitoring the values of variable-2 (Current, abbreviated as I) against stepwise increment of variable-1 (Voltage, abbreviated as V). Several such sets of acquisition cycles had been performed at different values of the third variable (Temperature, abbreviated as T) and designated as acquisition loops.

Several graphical programme files had been developed (listed in Table-2) to demonstrate the process. Among these, the main file is Main\_Prog\_GUI.vi which acts as the user interface where data file name and other parameters can be entered in designated text boxes as well as acquired data is being displayed (Figure 1). Graphical interface for Sub\_Prog\_1.vi and Sub\_Prog\_2.vi was not compulsory to build, but I had made it to check the variables visually to understand the progress. An in-built 'File Dialog' VI (virtual instrument used in LabVIEW

programming) that displays a dialog box, where the user can specify a file name with a directory to save the data file with an *Open/Create/Replace File* option. The total programme architecture has been shown graphically in Figure 2. Different parts of the main or parent programme file have been marked with distinguished part numbers to help the readers to identify the segment of the programme under discussion.

In this programme, a 'Flat Sequence Structure' (marked as FSS-1 in Figure 2) executes statements sequentially (P2, P3, and P4) one after another within a main programme 'While Loop'. In the first sub-diagram or frame (P2) of this FSS-1, another internal 'Flat Sequence Structure' (FSS-2) executes eleven times within a 'For Loop' (For Loop 1) and creates eleven numbers of rows in the first data file. In its first frame (P2.1A), voltage increases to its next value and calls Sub\_Prog\_3.vi. Sub\_Prog\_3 sends a set of SCPI commands to the Keithley meter via GPIB interface method to source this voltage and measure the corresponding current.

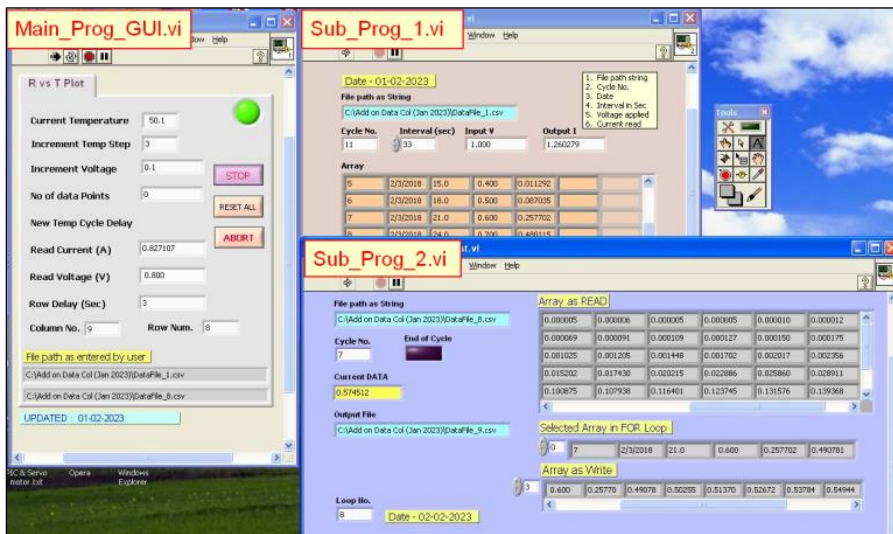


Figure 1: Screenshot of three graphical interface files among them, Main\_Prog\_GUI.vi control the parameters, and the other two display the data while acquisition is in progress.

Source: Author, (2023).

These parameters are then sent to Sub\_Prog\_1 to store eleven rows of data with five columns. It saves the first spreadsheet data file (DataFile\_1.csv) using an in-built VI file called 'Write To Spreadsheet File.vi' with serial numbers, date, elapsed time in second, the voltage applied (second variable) and noted current (first variable) - all are separated by comma (Figure 3). All these parameters were in string format and created rows of

data with 'Build Array' in-built function [2]. Every sequential call of this VI file (Sub\_Prog\_1.vi) from the programme-part P2.1A during each cycle within the For Loop-1 adds new rows of data with five columns. A cycle delay was added in frame-2 (P2.1B) of FSS-2 as desired by the user. Once the first round of data collection is made at an initial value of the third variable, this VI file (Sub\_Prog\_1.vi) is never invoked any further.

Table 2: List of project files and the functions performed by them.

Project file names mentioned in this article	Function / Purpose of the programme code
Main_Prog_GUI.vi	* Creates the main graphical user interface (GUI). It is likely to be modified according to the need. * It shows all necessary parameters in text boxes and clickable buttons.
Sub_Prog_1.vi	* Creates first spreadsheet file named as DataFile_1.csv
Sub_Prog_2.vi	* Creates a new data file and manipulates the old file name to generate a new data file name. * Reads latest spreadsheet file row by row and adds new data at the end of each row with a comma added afterward, * And saves all data sets in the newly created spreadsheet file.
Sub_Prog_3.vi	* Communicates with Keithley 2450 via GPIB Port. * Sources some voltage and reads output current from the DUT.
Sub_Prog_4.vi	* Read the current temperature from the Autonics PID controller
Sub_Prog_5.vi	* Send new Set Point (SP) to the Autonics PID controller.
Sub_Prog_6.vi	* Set Auto-Tune On or Off for the Autonics PID controller.9

Source: Author, (2023).

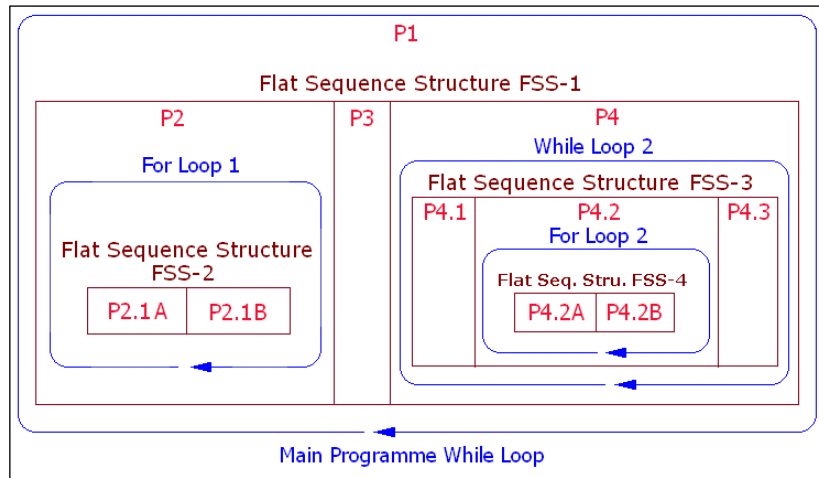


Figure 2: Block diagram of the programme Main\_Prog\_GUI.vi that revokes other two sub-programme files from 'For Loop 1' and 'For Loop 2'.

Source: Author, (2023).

	A	B	C	D	E	F	G	H	I	J	K	L	M	N
1	1	02-03-2023	3	0	0									
2	2	02-03-2023	6	0.1	0.000004									
3	3	02-03-2023	9	0.2	0.000056									
4	4	02-03-2023	12	0.3	0.000733									
5	5	02-03-2023	15	0.4	0.011292									
6	6	02-03-2023	18	0.5	0.087035									
7	7	02-03-2023	21	0.6	0.257702									
8	8	02-03-2023	24	0.7	0.480115									
9	9	02-03-2023	27	0.8	0.727761									
10	10	02-03-2023	30	0.9	0.989532									
11	11	02-03-2023	33	1	1.260279									
12														
13														

Figure 3: Screenshot of the data file (DataFile\_1.csv) displayed within the Excel sheet after completing the first round of data acquisition in Loop-1 by the programme Sub\_Prog\_1.vi.

Source: Author, (2023).

Time is incremented at every 3 seconds and voltage is incremented by 0.1v at each step starting from zero to one volt. Column E is showing the resultant current.

In the next frame P3, the main programme calls another two sub-programmes Sub\_Prog\_4.vi and Sub\_Prog\_5.vi which communicate with the PID temperature controller from a USB port using the RS-485 method. A USB-to-RS485 converter was used for this purpose. Sub\_Prog\_4.vi reads the current temperature (PV) and Sub\_Prog\_5.vi writes a new set point (SP) of temperature to the controller. Instruction codes within these two sequences part P2 and P3 is executed only once and never called any further till the end of the programme.

In the third frame (P4) of FSS-1, programme performs the most important and little complex processes. In this part of the programme P4, another 'Flat Sequence Structure' (FSS-3 in Figure 2) executes nine times within a conditional 'While Loop' (While Loop 2). This number is restricted exclusively for my programme only and has been discussed later. All programme sequences inside this recursive 'While Loop' repeats depending upon the number of data acquisition loops wanted by the programmer. Each such acquisition loop creates a new data file with an added data column.

Within the first frame (P4.1) of the Flat Sequence Structure (FSS-3) Sub\_Prog\_3.vi is called to reset the source meter voltage to zero and prepare it to start a new measurement cycle from the initial stage. Sub\_Prog\_4.vi is also called from this part to read the current process temperature.

In the second part (P4.2) of FSS-3 programme reads the first data file name and manipulates it to generate a new file name depending upon the serial number of the data column it is going to create. It reads the initial data file name string (i.e. DataFile\_1.csv) and to determine a new file name, it subtracts the

last five characters from the file name string using 'String Subset' function.

With this character subtraction, the file name string becomes, "DataFile\_"

It takes the current column number and adds the remaining string with this column number and .csv extension ("N.csv", where N is the current column or plot number).

While recording data in the second column, the file name becomes, "DataFile\_" + "2.csv" = "DataFile\_2.csv".

A 'For Loop' (named as For Loop 2 in Figure 2) executes eleven times. Inside this For Loop, another set of programme instructions executes sequentially inside FSS-4. Inside the first frame (P4.2A) of FSS-4, Sub\_Prog\_3.vi is called to send commands to the Keithley sourcemeter to measure the load current against the application of some amount of source voltage incremented from its previous value. In the next frame, (P4.2B) Sub\_prog\_2.vi is called, which performs the addition of recent data (that is load current in our case) to a new and fresh data column on the right side of the previous column. Figure 4 can explain the process clearly. The programme reads each row as a 1D Array from the previous and latest spreadsheet file and adds the recent value of variable-1 (i.e. Current,  $I_{31}$ ) as an array element using the in-built function 'Insert into Array'. The sub-programme file 'Sub\_Prog\_2.vi' is called eleven times from the 'For Loop-2' to read all the rows sequentially as a 1-D array and add the newly acquired data at its end as a new array element. Within part P4 the 'While Loop-2' iterates maximum of nine times to create total ten ( $1+9 = 10$ ) data collection loops. The reason for this number restriction has been discussed in the section 'Conclusion'. The output 1D array from the 'Insert into Array' function writes into the new spreadsheet file that has been generated with a new file name (i.e. DataFile\_4.csv in Figure 4) using the in-built VI file 'Write To Spreadsheet File.vi'.

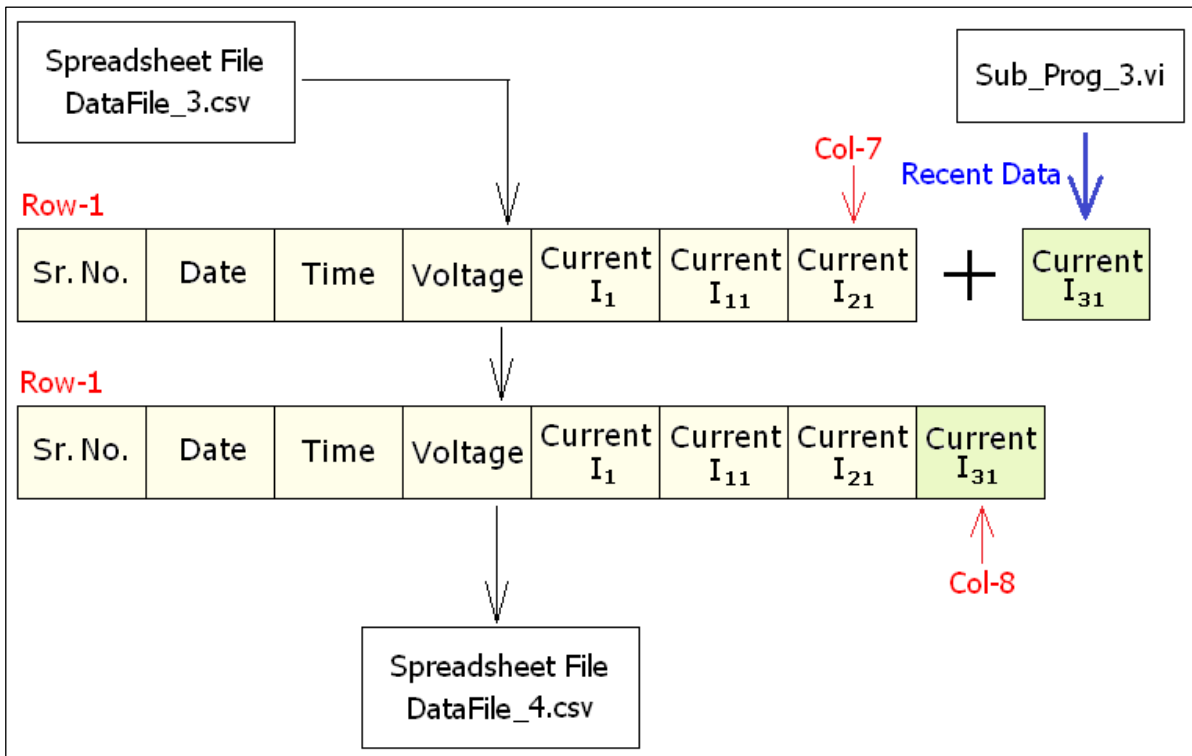


Figure 4: Reading of 1D array from a single row of the previous data file (DataFile\_3.csv) and appending of recently collected latest data to it that saves in a newly created file DataFile\_4.csv.

Source: Author, (2023).

As a next step of the 'Sequential Structure' within the 'While Loop', in part P4.3 code instructs the PID controller to change the third variable. Thus it increments the temperature from  $T_2$  to  $T_3$ , waits for 2 min. to allow the temperature to be stable at its new value, resets the voltage to zero ( $V_1$ ) again to initiate a new data collection cycle in the next loop, and repeats the same

process already defined. One such complete programme loop creates and saves another data files on the hard drive. The number of columns of variable-2 is created in a data file depending upon the number of programme loops iterates. Figure 5 shows the excel sheet of DataFile\_10.csv after ten iteration loops.

	A	B	C	D	E	F	G	H	I	J	K	L	M	N
1	1	02-03-2023	3	0	0	0.000004	0.000005	0.000006	0.000005	0.000005	0.00001	0.000012	0.000014	0.000017
2	2	02-03-2023	6	0.1	0.000004	0.000062	0.000069	0.000091	0.000109	0.000127	0.00015	0.000175	0.000214	0.00025
3	3	02-03-2023	9	0.2	0.000056	0.000858	0.001025	0.001205	0.001448	0.001702	0.002017	0.002356	0.002901	0.003405
4	4	02-03-2023	12	0.3	0.000733	0.013042	0.015202	0.01743	0.020215	0.022886	0.02586	0.028911	0.033252	0.036898
5	5	02-03-2023	15	0.4	0.011292	0.093493	0.100875	0.107938	0.116401	0.123745	0.131576	0.139368	0.149271	0.157594
6	6	02-03-2023	18	0.5	0.087035	0.26715	0.277639	0.287516	0.299174	0.309114	0.319617	0.329949	0.342414	0.353084
7	7	02-03-2023	21	0.6	0.257702	0.490781	0.502559	0.513709	0.526726	0.537844	0.549442	0.56128	0.574512	0.586357
8	8	02-03-2023	24	0.7	0.480115	0.739005	0.751341	0.763475	0.776839	0.788593	0.800904	0.813699	0.827107	0.839336
9	9	02-03-2023	27	0.8	0.727761	1.001112	1.013743	1.026497	1.040051	1.052179	1.064806	1.07805	1.091961	1.104061
10	10	02-03-2023	30	0.9	0.989532	1.271964	1.284771	1.297856	1.311613	1.323818	1.33695	1.350212	1.364786	1.376675
11	11	02-03-2023	33	1	1.260279	1.548791	1.561664	1.574889	1.588887	1.601122	1.614645	1.628063	1.642713	1.654591
12														
13														

Figure 5: Screenshot of the data file (DataFile\_10.csv) displayed within Excel sheet after completing tenth round of data acquisition in Loop-10 by the programme Sub\_Prog\_2.vi.  
Source: Author, (2023).

#### IV. VERIFICATION OF THE CODE WITH A COUPLE OF PRACTICAL DATA ACQUISITION PROCESSES

The effectiveness of the programming process has been verified by two prototype data acquisition projects those are very common in a scientific or engineering laboratory. The first one was Current versus Voltage (I-V) characteristic of a Silicon diode (1N4007) against variation of temperature and in second case, the device under test (DUT) was a 470 ohm quarter watt resistance.

A Keithley Source meter (Model 2450) was used to generate voltage ranges from zero to 1v DC in the case of the diode and zero to 10v DC while the DUT was the resistance [3,4]. The source meter was interfaced with the desktop PC via GPIB interface. A PCI GPIB card (Make: National Instruments, USA)

was used for this purpose. The front-panel connections are safety banana-type jacks.

To heat the copper sample holder, two 40 watt, and 12v cartridge heaters were used with a small size 3x2 mm<sup>2</sup> PT-100 RTD Sensor (Make: Hayashi Denko, Japan, Model: CRZ-2005-100-A-1) to sense the temperature of the copper block (Figure 6). A PID temperature controller (Make: Autonics, Model: TK4S-T4CR) with RS-485 interface facility was used to read, display and control the temperature with the help of an external relay [5,6]. A USB-to-RS485 converter (Model: SCM-US481) allows the device to interface with the PC through one of its USB port and it behaves just like a COM Port (Figure 7) [7].



Figure 6: (a) Keithley Model-2450 Source Meter and heater power supply integrated with an Autonics TK series temperature controller connected via a USB-to-RS-485 converter. (b) View of the copper-made heating plate mounted with two cartridge heaters, one PT-100 sensor, and a common silicon diode IN-4007 as the device under test (DUT).

Source: Author, (2023).



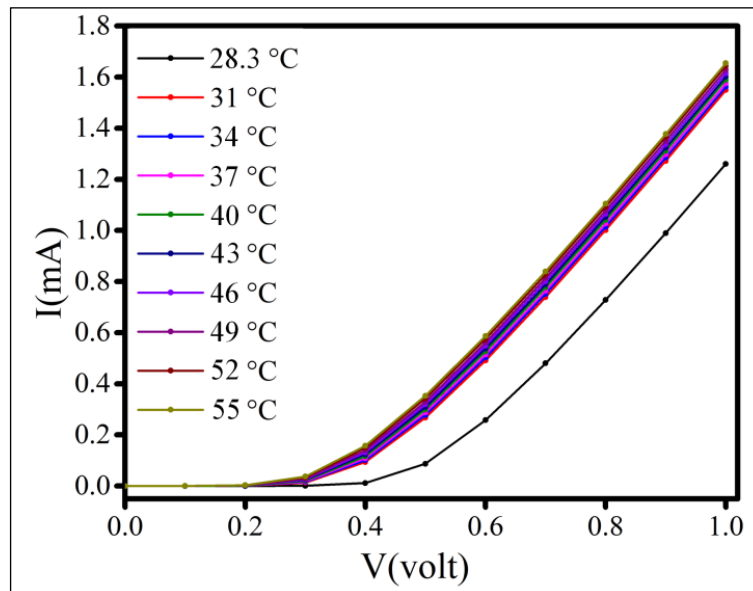


Figure 7. V-I curve of the Si diode plotted from DataFile\_10.csv at different plate temperatures.  
Source: Author, (2023).

A main graphical user interface file (Main\_Prog\_GUI.vi) was created to select the data file name and folder, range and increment value of applied DC voltage, display of monitored current, increment value of temperature at every cycle, etc. Several other LabVIEW vi files were prepared those were called from the main graphical user interface (GUI) file, and performed like subprograms of C++ or Java. One such VI file (Sub\_Prog\_3.vi) was used to source voltage and measure current by the Keithley source meter. Other VI files perform several other tasks like sending temperature set point to the Autonics controller, reading current process value (PV), setting the auto-tune facility on or off, etc.

## V. DISCUSSION - RELEVANCE AND IMPORTANCE

A prototype test was performed to monitor the temperature dependency of a Silicon diode PN junction. The purpose of this sample study was to construct and develop an effective, efficient, and fully automated data acquisition system several independent measurement cycles can be performed automatically in a single test run without any human intervention.

## VI. CONCLUSIONS

This software model has a few limitations that can be attended in the future for further improvement. I have kept the total number of acquisition loops within ten to avoid a problem during assigning new data file names when the number exceeds nine. If the file number becomes two digits i.e. more than nine then while manipulating the new file name by subtracting the last five characters (N.csv) from the end, it generates an erroneous file name. Interested programmers may focus on this point to avoid this limitation with improved logic.

The values of the third parameter (i.e. Temperature in my program me) are never recorded in the data file. It may be recorded at the end of the last row or prior to the first row to avoid ambiguity. Column titles are also not printed on the topmost row to identify the type of data for each column. That results in a kind of incompleteness in the data file. Both these drawbacks can be addressed in a future version either in LabVIEW or other programming languages.

## VII. AUTHOR'S CONTRIBUTION

**Conceptualization:** Avijit Das.

**Methodology:** Avijit Das.

**Investigation:** Avijit Das.

**Discussion of results:** Avijit Das.

**Writing – Original Draft:** Avijit Das.

**Writing – Review and Editing:** Avijit Das.

**Resources:** Avijit Das.

**Supervision:** Avijit Das.

**Approval of the final text:** Avijit Das.

## VII. ACKNOWLEDGMENTS

I am grateful to Mr. Subhadip Chowdhury, Senior Research Fellow of our institute, who generated the graphs from my data files and helped me to present it in my manuscript.

## VIII. REFERENCES

- [1] LabVIEW User Manual, National Instruments Corp.
- [2] LabVIEW Arrays and Clusters Explained. Available in: <https://www.ni.com/en-in/support/documentation/supplemental/08/labview-arrays-and-clusters-explained.html>
- [3] Keithley Model 2450 User Manual, Tektronix Inc. Available in: [https://download.tek.com/manual/2450-900-01E\\_Aug\\_2019\\_User.pdf](https://download.tek.com/manual/2450-900-01E_Aug_2019_User.pdf)
- [4] Keithley Model 2450 Reference Manual, Tektronix Inc. Available in: <https://www.tek.com/en/keithley-source-measure-units/keithley-smu-2400-series-sourcemeter-manual/model-2450-interactive-sou>
- [5] Autonics TK series PID Controller communication. Manual, Available in: <https://www.autonics.com/>
- [6] Autonics TK series PID Controller user manual. Available in: [https://autonics.se/wp-content/uploads/2018/03/tk\\_en\\_manual\\_170829\\_hw.pdf](https://autonics.se/wp-content/uploads/2018/03/tk_en_manual_170829_hw.pdf)
- [7] Wikipedia – Modbus. Available in: <https://en.wikipedia.org/wiki/Modbus>
- [8] What is the Modbus Protocol & How Does It Work?, National Instruments Corp. Available in: <https://www.ni.com/en-in/innovations/white-papers/14/the-modbus-protocol-in-depth.html>



ISSN ONLINE: 2447-0228








## INVESTIGATIVE ANALYSIS OF SELECTED FSO MODELS WITH VARYING WAVELENGTHS FOR TROPICAL WEATHER

Ibukunoluwa A. Olajide\*<sup>1</sup>, Samson A. Oyetunji<sup>2</sup>, Yekeen O. Olasoji<sup>3</sup>, Wasiu O. Popoola<sup>4</sup> and Muhammad Ijaz<sup>5</sup>

<sup>1,2,3</sup> Department of Electrical and Electronics Engineering, The Federal University of Technology, Akure, Nigeria.

<sup>4</sup> Institute for Digital communication, University of Edinburgh, United Kingdom.

<sup>5</sup> Department of Electrical and Electronics Engineering, Manchester Metropolitan University, United Kingdom.

<sup>1</sup> <http://orcid.org/0000-0001-9647-876X> , <sup>2</sup> <http://orcid.org/0000-0001-8171-0327> , <sup>3</sup> <http://orcid.org/0000-0002-1978-1930> ,  
<sup>4</sup> <http://orcid.org/0000-0002-2954-7902> , <sup>5</sup> <http://orcid.org/0000-0002-0050-9435> 

Email: \*[iaadebanjo@futa.edu.ng](mailto:iaadebanjo@futa.edu.ng), [saoyetunji@futa.edu.ng](mailto:saoyetunji@futa.edu.ng), [yoolasoji@futa.edu.ng](mailto:yoolasoji@futa.edu.ng), [w.popoola@ed.ac.uk](mailto:w.popoola@ed.ac.uk), [m.ijaz@mmu.ac.uk](mailto:m.ijaz@mmu.ac.uk)

### ARTICLE INFO

#### Article History

Received: March 14<sup>th</sup>, 2023

Accepted: April 26<sup>th</sup>, 2023

Published: April 29<sup>th</sup>, 2023

#### Keywords:

Scattering,  
Visibility,  
Attenuation,  
Rain Intensity.

### ABSTRACT

In this paper, an investigation of some selected Mie and geometric Scattering models for free space optical (FSO) communication was done on available atmospheric data in Nigeria. The Kim and Kruse models have been established for the temperate region. In this work, the models were examined using the visibility data from the year 2008 to 2019. The models were examined under the 2% and 5% transmission threshold and under the wavelengths 780nm, 850nm, 1100nm, and 1550nm. The results indicates a higher attenuation at 780nm, supporting what is available in literature. The Suriza et al, ITU-R(Carbonneau) and Gailani et al models were investigated using the rain intensity data. The Suriza et al model indicates a reduced attenuation compared to the other two models.



Copyright ©2023 by authors and Galileo Institute of Technology and Education of the Amazon (ITEGAM). This work is licensed under the Creative Commons Attribution International License (CC BY 4.0).

### I. INTRODUCTION

Free space optical (FSO) communication is a recent technology in wireless communication that is gradually becoming explorable and deplorable. Emergence of Internet of Things (IoT) and increased demand for internet penetration has resulted in unending congestion of the Radio Frequency (RF) spectrum. The effect on licensed band is high cost of data transfer. This is compounded by the cost of infrastructural deployment of optical fiber cables. In handling this bottleneck, an alternative technological approach is to be considered to ease off the strain on RF infrastructure. The need to develop a viable alternative becomes inevitable if the desire to increase penetration and teledensity which are the fulcrum of digital economy is to be realized even with population growth. Free space optical communication (FSO) was developed in response to the increase in demand for high speed and tap- proof communication system [1]. It is a promising communication technique that has great advantage in handling losses, security issues, central connectivity, spectrum, and bandwidth management. Radio frequency (RF) and Millimeter

wave technologies offer data rates from tens mbps to several Hundreds mbps, but spectrum congestion, license issues and unwanted interference from other bands are their known limitations, though emerging license-free bands of RF technology stand promising, yet bandwidth limitation places FSO ahead as a substitute to address the last and first mile problem in wireless communication [2]. Despite the huge advantages of FSO, it has its peculiar disadvantages. Due to the narrowness of its beams, stiff alignment and pointing is required to prevent beam dispersion [4][5]. Another principal factor of limitation is the effect of the propagating medium- the atmosphere. FSO suffers easily from absorption, rain, fog, and snow -general atmospheric condition and turbulence. Nigeria as a tropical country has its inherent climatic conditions that is needed to be studied in order to implement the free space optical communication technology. In this paper, a fundamental and investigative study of established Mie and Geometric scattering models in FSO were used on sets of atmospheric data obtained for Akure, Nigeria. Kim and Kruse models were examined under the 2% and 5% transmission

threshold for the wavelengths 780nm, 850nm, 1100nm, and 1550nm. The results indicates a higher attenuation at 780nm. The Suriza et al, ITU-R (Carbonneau) and Gailani et al models were investigated using the rain intensity data. The Suriza et al model gave a reduced attenuation compared to the other two models. It provides a preliminary analysis of simulated results of what to expect when a thorough experimental analysis is carried out within the southern region of Nigeria. The paper is organized as follows: literature review is presented in Section II, the methodological approach is provided in Section III, while the graphical analysis and discussion is given in Section IV. The conclusion is drawn in Section V.

## II. THEORETICAL REFERENCE

### II.1 FSO LOSSES

Propagated power from an FSO transmitter to the receiver is affected by various factors. They are system loss, Geometric and misalignment losses, atmospheric losses, atmosphere turbulence induced fading, and ambient noise [5]. All these losses do have relative to high effects on FSO propagation, but the scope of this study is atmospheric losses.

#### II.1.1 Atmospheric Losses

The Earth's surface layers are broadly classed into two spheres: Homosphere and the Heterosphere. The Homosphere ranges from 0-9 km while the Heterosphere is above 90 km [4]. The Homosphere is where free space optical communication takes place. Furthermore, the Homosphere can be classed / divided into (i) Troposphere (0-20 km), (ii) Stratosphere (20-50 km) and Mesosphere (50-90 km). The Homosphere is resident to many gases, water vapours, pollutants and chemicals. These tenants of the Homosphere induce atmosphere effects on the propagated signals, whether RF or IR signals. These interaction causes absorption and scattering of the signals leading to signal attenuation. Beers Law expresses the attenuation of travelling light through the atmosphere under the influence of absorption and scattering [6][3]. According to Beers Law, the transmission,  $\tau$  of radiation in the atmosphere as a function of distance,  $d$  is given as [6],

$$\tau = \exp(-\gamma d) \tag{1}$$

where  $\tau = \frac{I_R}{I_0}$ , which could be called atmospheric attenuation,  $\gamma$  is the attenuation/extinction coefficient.  $\gamma$  is the sum of the absorption and the scattering coefficients from aerosols and molecular constituents, given as [2].

$$\gamma = \alpha_m + \alpha_a + \beta_m + \beta_a \tag{2}$$

The first two terms represents the molecular and aerosol absorption while the last two, the molecular and aerosol scattering.

#### II.1.2 Absorption

Absorption is caused by the collision of photons with various dispersed liquid and solid particles in the atmosphere [3]. Some of these photons are extinguished, and energy is absorbed [7]. Atmospheric absorption is a wavelength-dependent phenomenon, therefore, it is selective. These absorbing particles are divided into Molecule and Aerosol absorbers [4]. Molecule absorbers are Nitrogen, Hydrogen, Ozone, Oxygen, Carbon dioxide etc.; they are gases present in the atmosphere. Aerosols are suspended particles in the medium [7]. The suspended particles could be liquid or solid particles. Liquid particles are mist and water vapour, while solid particles are dust, smoke, volcanic particles, maritime droplets. These particles create reducing effects on optical link margin, and link availability.

Absorption causes the atmosphere to have transparent zones, called atmospheric transmission windows [2][3]. This transmission window allows specific frequencies of light to pass through it. However, the wavelength of transmission is usually chosen to match the atmospheric transmission window, thereby resulting in the attenuation / extinction coefficient being a scattering parameter alone. Therefore, Equation (2) becomes.

$$\gamma = \beta_a \tag{3}$$

#### II.1.3 Scattering

Scattering occurs when the optical beam collides with a scatterer. This leads to a redistribution of light or deflection in angle of beam arrival [7]. As light is redistributed, optical energy is redistributed with and without wavelength change [4]. The redistribution leads to reduction in the intensity of beam for longer distance [8]. The scattering effect depends on the radius,  $r$  of the particles (fog, aerosol) experienced during propagation [2]. There are three main types of scattering: Rayleigh, Mie, and Non-Selective scattering.

In Rayleigh scattering, the size of the colliding particle is less than the wavelength of the beam. For Rayleigh,  $x_0 \ll 1$ ; therefore, it is known as Molecule scattering [8].

In Mie scattering, the size of the colliding particle is comparable to the wavelength of the beam,  $x_0 \approx 1$ . In the Non-selective scattering also known as geometric scattering, the colliding particles size is larger than the wavelength of the beam,  $x_0 \gg 1$  [9]. A summary of typical atmospheric scattering particles is presented in Table 1.

Table 1: Atmospheric Scattering Particles.

Type	Radius( $\mu$ m)	Size Parameter, $x_0$	Scattering Process
Air Molecules	0.0001	0.00074	Rayleigh
Haze particle	0.01-1	0.074-7.4	Rayleigh – Mie
Fog droplets	1-20	7.40-147.8	Mie– Geometric
Rain	100-10000	740-74000	Geometric/ Non-Selective
Snow	1000-5000	7400-37000	Geometric/Non-Selective
Hail	5000-50000	37000-50000	Geometric/Non-Selective

Source: Ghassemlooy and Popoola, (2010), Kim et al (2001).

### II.1.4 Atmosphere Turbulence

The variation in the temperature, wind, and pressure of air sets a random phenomenon, which is spatial and temporal fluctuations of refractive index [7]. This turbulence results in eddies, cells or air particles having varying sizes from 0.1 m to 10 m. These eddies deflect optical transmission path. Atmospheric turbulence depends on (i) atmospheric pressure/ altitude (ii) wind speed, and (iii) variation of index of refraction [2]. When a plane wave passes through these eddies, part of the wave are reflected causing a distorted wave with varied intensity, and a warping of the isophase surface [3]. This is shown from the relationship between temperature, pressure and refractive index:

$$n \approx 79 \times \frac{P}{T} \quad (4)$$

where P is the atmosphere pressure is [mbar], T is the temperature in kelvin [K].

Atmosphere turbulence is measured in terms of refractive index structure coefficient,  $C_n^2$  [7]. It is the most important parameter for the checking turbulence strength.  $C_n^2$  depends on geographical location, altitude and time of the day. The value of  $C_n^2$  for weak turbulence at ground level could be little as  $10^{-17} \text{m}^{-2/3}$ , and for a strong turbulence, it can be up to  $10^{-13} \text{m}^{-2/3}$  [7]. Some of the commonly used models are presented in [11].

## III. MATERIALS AND METHODS

### III.1 MIE SCATTERING

Characterisation of atmospheric Mie scattering was carried out using MATLAB. Two established models will be investigated to check the suitability to the atmospheric structure of the selected region

#### III.1.1 Kim and Kruse Model

The prediction of fog attenuation based on visibility was employed for this work. The Koschmieder law expresses the visibility by the extinction coefficient at 550 nm. At 550 nm, visibility is given as [12]:

$$V = \frac{\ln\left[\frac{1}{\tau_{th}}\right]}{\gamma(\lambda_0)} \quad (5)$$

where  $\tau_{th}$  is transmission threshold over the atmospheric path,  $\gamma$  is the extinction coefficients ( $\text{km}^{-1}$ ), and  $\lambda_0$  equals 550 nm. The specific attenuation  $\alpha$  can be expressed in terms of the visibility range, thereby as

$$\alpha = \frac{\log[1/\tau_{th}]}{V} \quad (6)$$

For the prediction of the fog attenuation, the following equation was considered:

$$\beta_a(\lambda) \approx y(\lambda) = \frac{\ln\left[\frac{1}{\tau_{th}}\right]}{V} \left[\frac{\lambda}{\lambda_0}\right]^{-q} \quad (7)$$

where  $\tau_{th}$  is the transmission threshold and it was taken as 2% and 5% of the transmitted power for this study,  $\lambda_0$  is the maximum spectrum at 550 nm, V is the visibility, and q is the coefficient of particle size distribution. The values of q will be taken as noted by Kim and Kruse to be [13].

$$q = \begin{cases} 1.6 & \text{for } V > 50 \text{ km} \\ 1.3 & \text{for } 6 < V < 50 \text{ km} \\ 0.16V + 0.34 & \text{for } 1 < V < 6 \text{ km} \\ V - 0.5 & \text{for } 0.5 < V < 1 \text{ km} \\ 0 & \text{for } V < 0.5 \text{ km} \end{cases} \quad (8)$$

## III.2 NON-SELECTIVE SCATTERING

Raindrops do have transient effects on optical signals. In the tropics, heavy rain is the major cause of attenuation of an FSO link [14]. Usually, the rain intensity data is often used to determine the specific rain attenuation in FSO. The international Telecommunication union sector (ITU-R- Carbonneau), Suriza et al, and Gailani et al model [14] was examined in this research. These models are based on rain rate distribution, but other prediction models exist which are based on rain-drop size distribution, which may not appropriately apply to the tropical region [13]. Rain specific attenuation is represented by the Power Law [16]:

$$A = kR^\alpha \quad (9)$$

where R is the rain rate in millimeter per hour, k and  $\alpha$  are power law parameters.

Power law parameters are frequency, rain drop size and rain temperature dependent, therefore it will be assumed that rain drop size is oblong. Table II gives the parameters of the adopted models.

Table 2: Selected Rain Models.

Rain Model	k	$\alpha$	Region
Carbonneau	1.076	0.67	Temperate
Gailini et al	2.03	0.70	Tropics
Suriza et al	0.3988	0.7601	Tropics

Source: Authors, (2023).

## IV. RESULTS AND DISCUSSIONS

### IV.1 MIE SCATTERING

Visibility data was obtained from The World Weather Online in Hong Kong for Akure, from July 2008 to October 2022. The historical data runs for 12 years. Definite analysis of the data was done using two known models in Mie scattering- KIM and Kruse models. Analytical examination of data sets was done on yearly basis under varying parameters.

Yearly Analysis with varying wavelengths was carried out and is observed in figure 1 to Figure 17.

The transmission threshold  $\tau_{th}$  at 2 % is presented and a comparison is made with a transmission threshold at 5 % Four (4) operating transmission windows, namely 780nm, 850nm, 1100nm and 1550nm were used for comparison. Figure 1 gives the result for varying transmission window when  $\tau_{th}$  at 2% for the year 2011. The result shows a general trend in the relationship between attenuation (dB/km) and visibility (km). Selected plots are presented in this paper. The transmission window of 1550nm performs best for both models giving a reduced equivalent attenuation. This result agrees with theoretical postulations.

The graph obtained for the year 2014 given in Figure 3, shows an even distribution with a similar resemblance to what was obtained in the year 2011. Figure 4 gives the graphical analysis of the years 2016. It is also observed that the curve appears closer in the year 2012 (Figure 2) and 2016 due to the closeness of the visibility data obtained for those years. At transmission window of 780 nm, the highest attenuation in dB/km is observed for all results

presented. A combined graph of  $\tau_{th}$  at 2% and 5% is presented in Figure 5. The plots obtained for the years have a close segmentation observed. It is observed that the attenuation obtained at transmission window of 1550 nm when  $\tau_{th}$  is at 5% lies closely in attenuation value obtained at transmission window of 1100 nm when  $\tau_{th}$  is at 2%. Further observed, is the closeness in attenuation values of the models at varied value of  $\tau_{th}$ . It is noted from the results obtained that from visibility of 6 km upwards, the attenuation in dB/km for both models at either 2% or 5% of  $\tau_{th}$  are the same. This is in accordance with the rules guiding the usage of the models. At this level, the only point of argument for any reasonable deployment of FSO is the choice value of  $\tau_{th}$ .

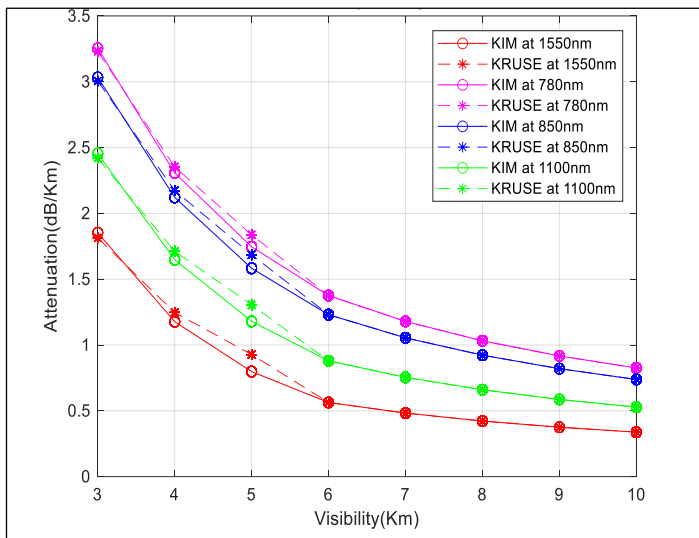


Figure 1: Varied transmission window for attenuation/visibility performance for the year 2011 @  $\tau_{th} = 2\%$ . Source: Authors, (2023).

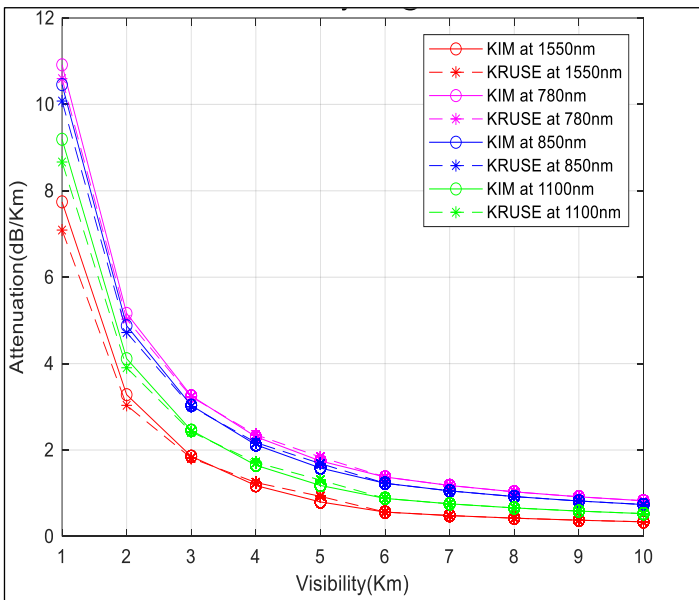


Figure 2: Varied transmission window for attenuation/visibility performance for the year 2012 @  $\tau_{th} = 2\%$ . Source: Authors, (2023).

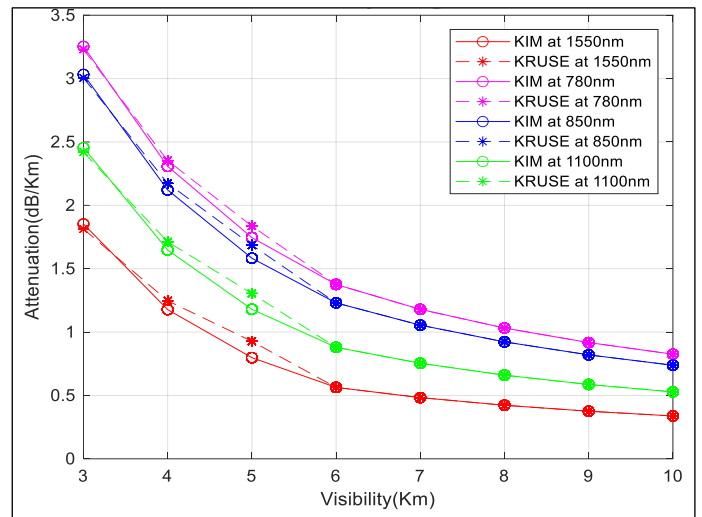


Figure 3: Varied transmission window for attenuation/visibility performance for the year 2014 @  $\tau_{th} = 2\%$ . Source: Authors, (2023).

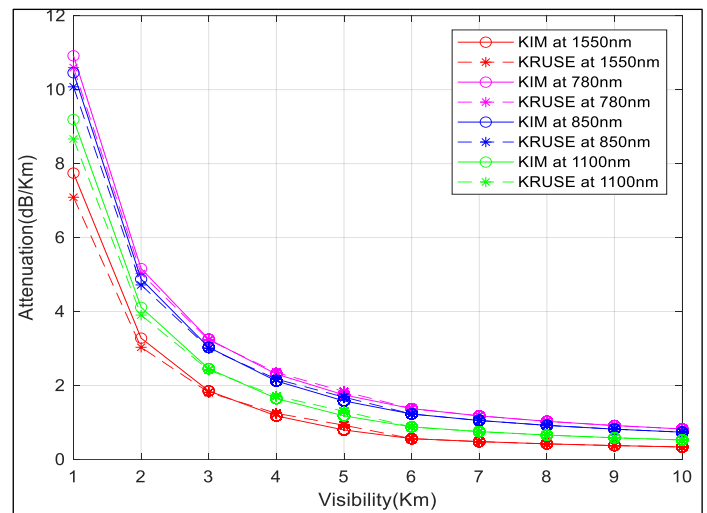


Figure 4: Varied transmission window for attenuation/visibility performance for the year 2016 @  $\tau_{th} = 2\%$ . Source: Authors, (2023).

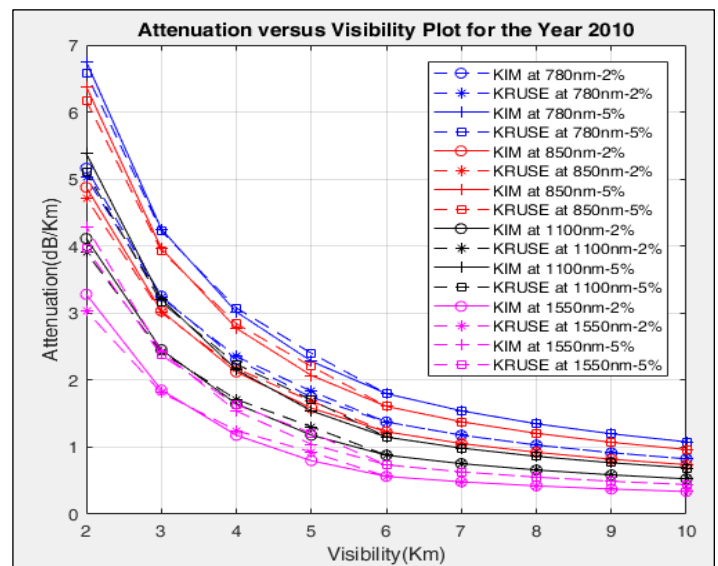


Figure 5: Combined attenuation plot when  $\tau_{th}$  is at 2% and 5% for the year 2019. Source: Authors, (2023)

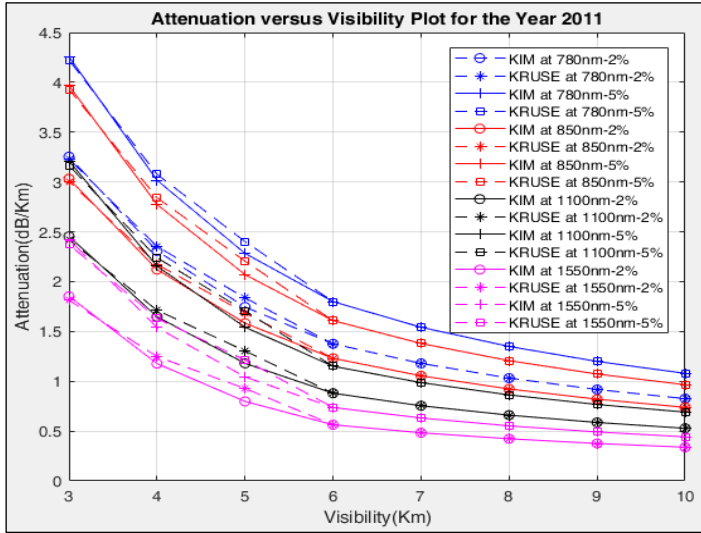


Figure 6: Combined attenuation plot when  $\tau_{th}$  is at 2% and 5% for the year 2019. Source: Authors, (2023).

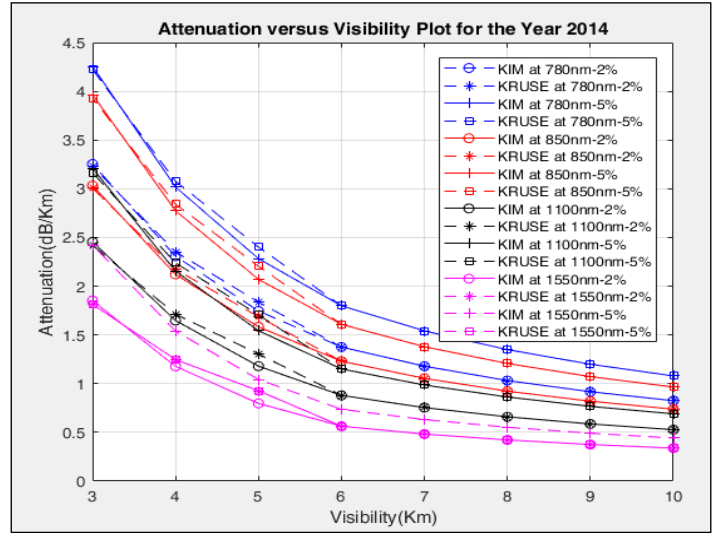


Figure 9: Combined attenuation plot when  $\tau_{th}$  is at 2% and 5% for the year 2019. Source: Authors, (2023).

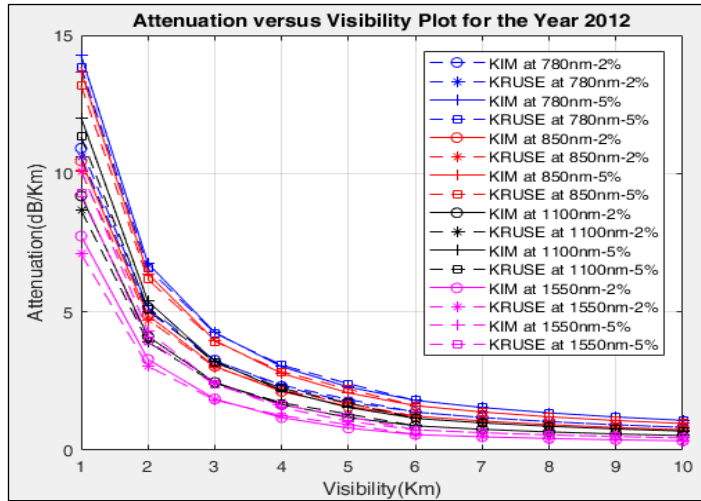


Figure 7: Combined attenuation plot when  $\tau_{th}$  is at 2% and 5% for the year 2019. Source: Authors, (2023).

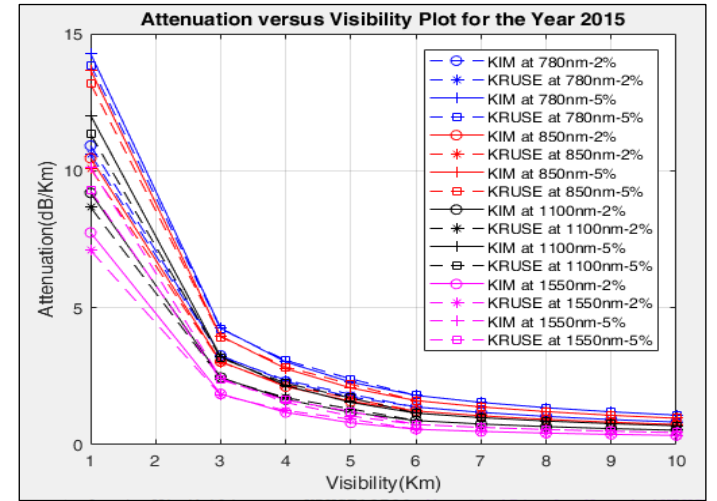


Figure 10: Combined attenuation plot when  $\tau_{th}$  is at 2% and 5% for the year 2019. Source: Authors, (2023).

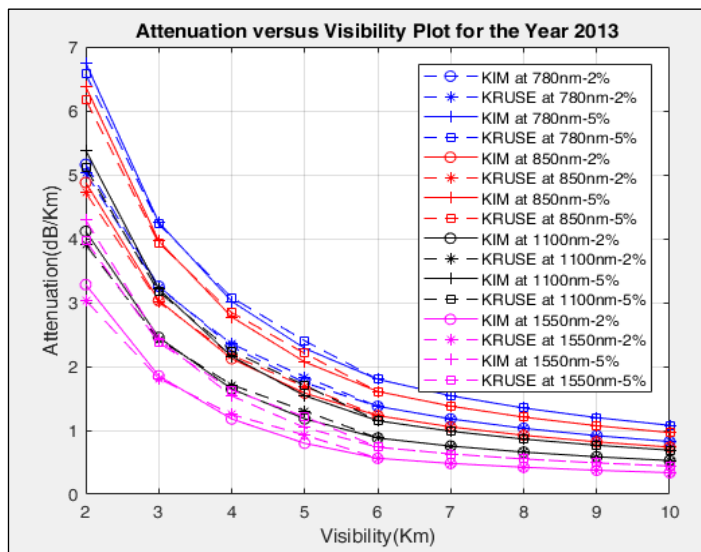


Figure 8: Combined attenuation plot when  $\tau_{th}$  is at 2% and 5% for the year 2019. Source: Authors, (2023).

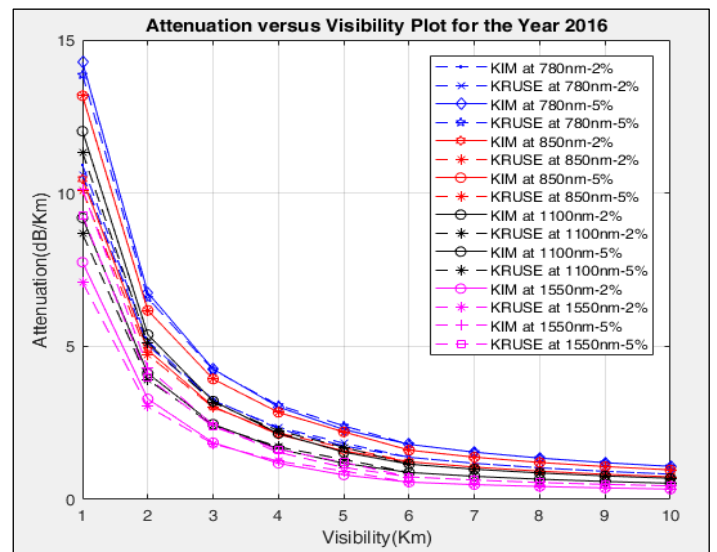


Figure 11: Combined attenuation plot when  $\tau_{th}$  is at 2% and 5% for the year 2019. Source: Authors, (2023).

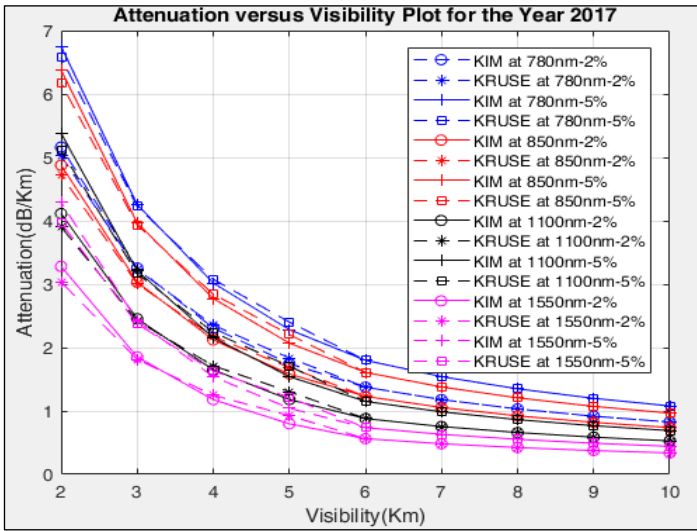


Figure 12: Combined attenuation plot when  $\tau_{th}$  is at 2% and 5% for the year 2019. Source: Authors, (2023).

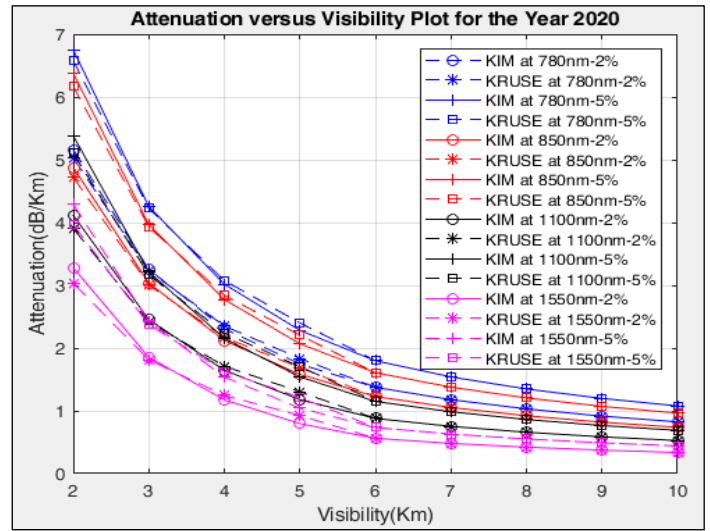


Figure 15: Combined attenuation plot when  $\tau_{th}$  is at 2% and 5% for the year 2019. Source: Authors, (2023).

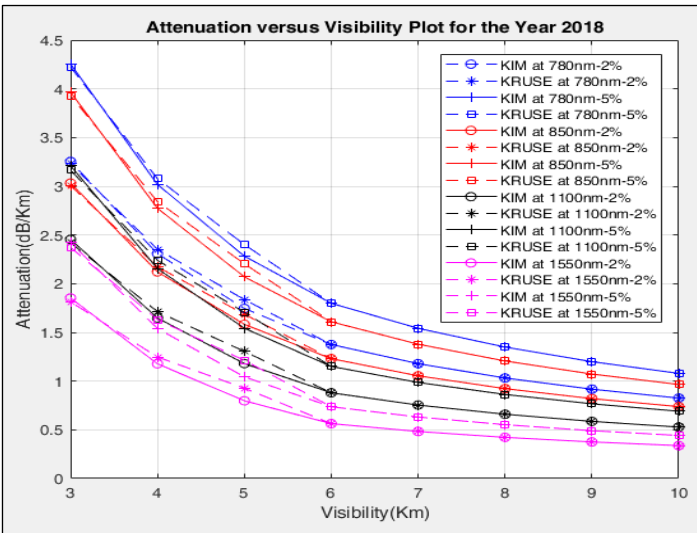


Figure 13: Combined attenuation plot when  $\tau_{th}$  is at 2% and 5% for the year 2019. Source: Authors, (2023).

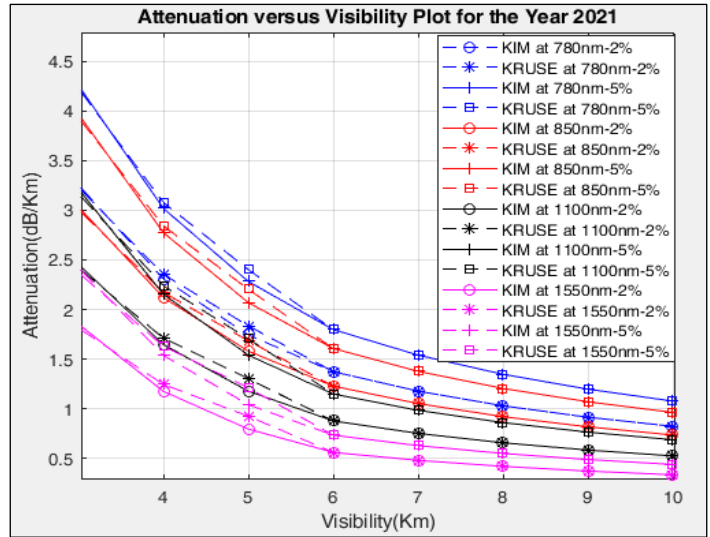


Figure 16: Combined attenuation plot when  $\tau_{th}$  is at 2% and 5% for the year 2019. Source: Authors, (2023).

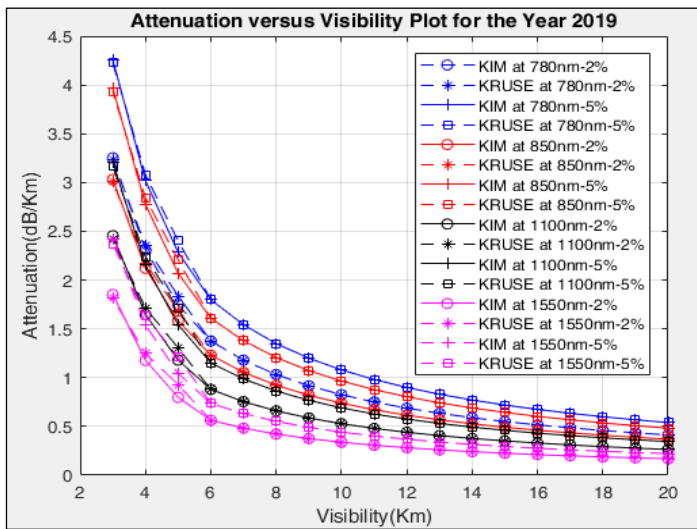


Figure 14: Combined attenuation plot when  $\tau_{th}$  is at 2% and 5% for the year 2019. Source: Authors, (2023).

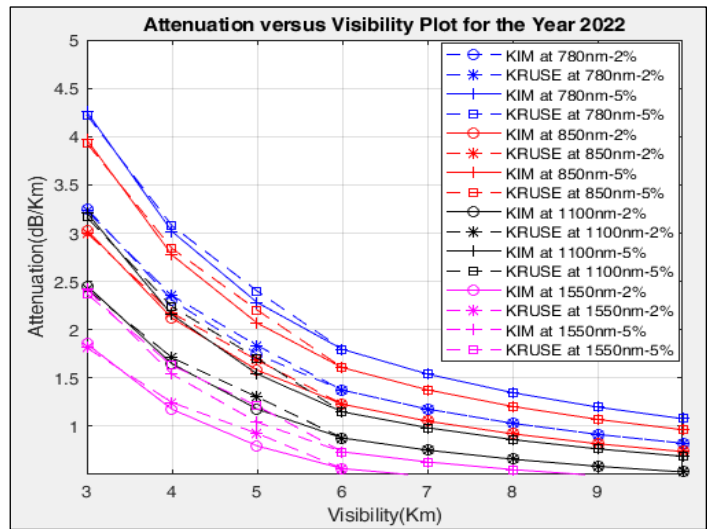


Figure 17: Combined attenuation plot when  $\tau_{th}$  is at 2% and 5% for the year 2019. Source: Authors, (2023).

## IV.2 NON-SELECTIVE SCATTERING

### IV.2.1 Conversion Factor

The Rain data obtained has a precipitation interval of 1 hour. This scale does not adequately provide a proper window for investigation. In order to verify the authenticity of the data and form an adaptive time-series data, a conversion factor was developed. Terrestrial data taken on site at the Department of Physics, The Federal University of Technology, Akure was plotted against the available data. This is necessary because conversion factor is dependent on the location. Fig.5 shows the regression plot of conversion. To check for congruence in the data, the Root Mean Square (RMSE) value was calculated to be 0.022123154 and the chi-square value was obtained as 1.

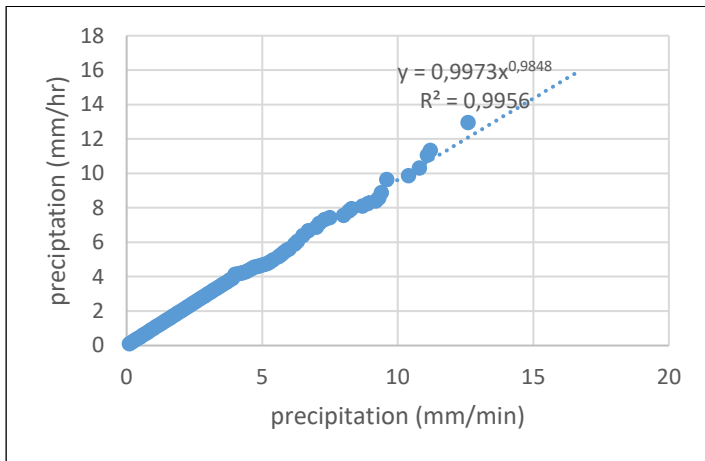


Figure 18: The regression plot of Rain Conversion.  
Source: Authors, (2023).

### IV.2.2 Examination of the Selected Rain Models

The rain intensity values were examined using the selected rain models. Fig. 6 provides the Rain attenuation (dB/km) against Rain intensity (mm/min) plot of the three models. It is clearly observed that the Suriza et al model shows close results to that of ITU-R model.

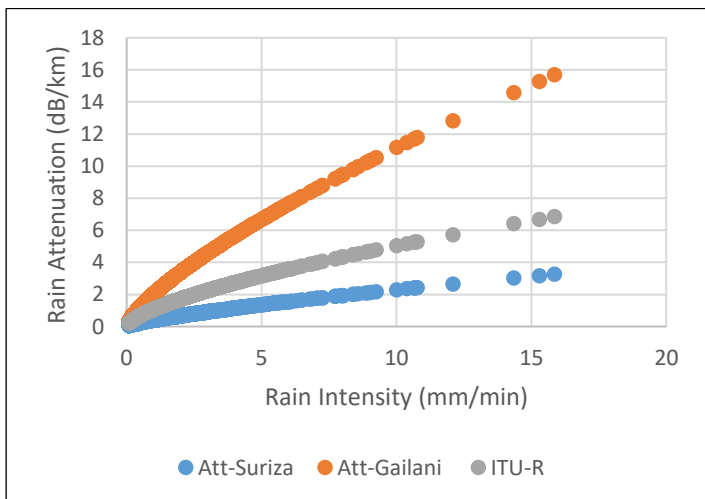


Figure 19: Rain Attenuation plots.  
Source: Authors, (2023).

## V. CONCLUSIONS

In this paper, we were able to analyse selected FSO model for Mie scattering and Geometric scattering on obtained

atmospheric data of Akure, in the southern region of Nigeria. An examination of the Kim and Kruse model was carried out on the data at 2% transmission threshold with a comparison at 5% transmission threshold for 780nm, 850nm, 1100nm and 1550nm transmission windows. It was observed that in all the years the highest attenuation occurred at 780nm transmission window. For the Geometric scattering, the Suriza et al, Gailani et al and ITU-R (Carbonneau) Models were examined with Rain intensity data. The Suriza et al model gave the lowest attenuation result. Since this work is limited to certain models, and in order to further study the effects of the atmosphere on FSO communication in the southern region of Nigeria, an empirical study is recommended.

## VI. AUTHOR'S CONTRIBUTION

**Conceptualization:** Samson A. Oyetunji, Ibukunoluwa A. Olajide and Wasii O. Popoola.

**Methodology:** Samson A. Oyetunji and Ibukunoluwa A. Olajide.

**Investigation:** Ibukunoluwa A. Olajide.

**Discussion of results:** Samson A. Oyetunji and Ibukunoluwa A. Olajide, Yekeen O. Olasoji, and Muhammad Ijaz.

**Writing – Original Draft:** Ibukunoluwa A. Olajide.

**Writing – Review and Editing:** Ibukunoluwa A. Olajide, and Muhammad Ijaz.

**Resources:** Ibukunoluwa A. Olajide.

**Supervision:** Samson A. Oyetunji, Yekeen O. Olasoji, and Wasii O. Popoola.

**Approval of the final text:** Ibukunoluwa A. Olajide, Samson A. Oyetunji, Yekeen O. Olasoji, Wasii O. Popoola and Muhammad Ijaz.

## VII. ACKNOWLEDGMENTS

The authors would like to acknowledge the input received from Prof. J. S. Ojo of the Department of Physics, The Federal University of Technology, Akure, Nigeria.

## VIII. REFERENCES

- [1] H. Henniger, and O. Wilfert, "An Introduction to Free-space Optical Communications," *RadioEngineering*, vol.19 no 2, 2010.
- [2] Z. Ghassemlooy, and W. O. Popoola, "Terrestrial free-space optical communications," *InTech*, pp. 355-392, 2010
- [3] A.G. Alkholidi, and K. S. Altowij, "Free space optical communications—Theory and practices" In *Contemporary Issues in Wireless Communications*. InTech., 2014
- [4] H. Kaushal, V.K. Jain, and S. Kar, "Free space optical communication," Springer India, 2017.
- [5] M.A. Khalighi, and M. Uysal, "Survey on free space optical communication: A communication theory perspective," *IEEE Communications Surveys & Tutorials*, vol. 16 no 4, pp. 2231-2258, 2014.
- [6] H. Willebrand, and B.S. Ghuman" *Free space optics: enabling optical connectivity in today's networks*". SAMS publishing, Indiana, 2002.
- [7] K. Anbarasi, C. Hemanth, and R.G. Sangeetha, "A review on channel models in free space optical communication systems," *Optics and Laser Technology*, vol. 97, pp.161-171, 2017.
- [8] A. Malik, and P. Singh, "Free space optics: current applications and future challenges," *International Journal of Optics*, Hindawi Publishing Corporation, 2015.
- [9] E. J. McCartney, "Optics of the atmosphere: scattering by molecules and particles," John Wiley and Sons, Inc., New York, 1976.



- [10] I. I. Kim, B. McArthur, and E. J. Korevaar, "Comparison of laser beam propagation at 785 nm and 1550 nm in fog and haze for optical wireless communications," In *Optical Wireless Communications III International Society for Optics and Photonics*, vol. 4214, pp. 26-38, 2001.
- [11] H. Kaushal, and G. Kaddoum, "Optical communication in space: Challenges and mitigation techniques," *IEEE communications surveys & tutorials*, vol.19 no.1, pp. 57-96, 2017.
- [12] S. S. Muhammad, B. Flecker, E. Leitgeb, and M. Gebhart. "Characterization of fog attenuation in terrestrial free space optical links," *Optical engineering*, vol. 46 no. 6, 2007.
- [13] M. Ijaz, Z. Ghassemlooy, H. Le-minh, S. Zvanovec, J. Perez, J. Pesek, and O. Fiser, "Experimental validation of fog models for FSO under laboratory controlled conditions". *IEEE Personal Indoor and Mobile Radio Communication*, pp. 19-23, 2013.
- [14] A. Z. Suriza, I. M. Rafiqul, A. K. Wajdi, and A. W. Naji, "Proposed parameters of specific rain attenuation prediction for free space optics link operating in tropical region". *Journal of Atmospheric and Solar-Terrestrial Physics*, vol 94, pp.93-99, 2013.
- [15] S. A. Al-Gailani, A.B. Mohammad, U.U. Sheikh, and R. Q. Shaddad, "Determination of rain attenuation parameters for free space optical link in tropical rain". *Optik*, 125(4), pp.1575-1578, 2014.
- [16] S. A, Zabidi, M. R., Islam, W, Al-Khateeb, and A. W. Naji. "Analysis of rain effects on terrestrial free space optics based on data measured in tropical climate". *IIUM Engineering Journal*, vol.12 no. 5, 2012.







## FACTORS AFFECTING TECHNICAL EFFICIENCY SCORES ESTIMATED FOR THE COTTON SECTOR OF THE HARRAN PLAIN IN TURKIYE: A STOCHASTIC FRONTIER ANALYSIS

Tamer Işgın<sup>1</sup>, Remziye Özel<sup>2</sup>, Abdulbaki Bilgiç<sup>3</sup> and Mehmet Reşit Sevinç\*<sup>4</sup>

<sup>1,2,4</sup> Department of Agricultural Economics, Faculty of Agriculture, Harran University, Sanlıurfa 63050, Turkiye.

<sup>3</sup> Department of Management Information Systems, Faculty of Economics and Administrative Sciences, Bilecik Şeyh Edebali University, Bilecik 11320, Turkiye.

<sup>1</sup> <http://orcid.org/0000-0001-8583-6525> , <sup>2</sup> <http://orcid.org/0000-0001-9240-3453> , <sup>3</sup> <http://orcid.org/0000-0001-5946-0915> , <sup>4</sup> <http://orcid.org/0000-0002-0617-7822> 

Email: [tisgin@harran.edu.tr](mailto:tisgin@harran.edu.tr), [rozal@harran.edu.tr](mailto:rozal@harran.edu.tr), [abdulbaki.bilgic@bilecik.edu.tr](mailto:abdulbaki.bilgic@bilecik.edu.tr), \*[rsevinc@harran.edu.tr](mailto:rsevinc@harran.edu.tr)

### ARTICLE INFO

#### Article History

Received: March 15<sup>th</sup>, 2023

Accepted: April 26<sup>th</sup>, 2023

Published: April 29<sup>th</sup>, 2023

#### Keywords:

Cotton,  
Frontier,  
Function,  
Stochastic,  
Harran Plain-Turkiye.

### ABSTRACT

The current study deals with the technical efficiency of cotton farmers operating on the Harran Plain of Turkiye with an application to the two well-known stochastic approaches, i.e., the Cobb-Douglas and the translog stochastic frontier production functions. Using farm-level cross-sectional data, a specialized maximum likelihood technique incorporates both stochastic frontiers and inefficiency effects models into a single equation model to estimate these efficiency scores along with their determinants simultaneously. Calculations indicate that technical inefficiency effects were present in these models. The data used in this research proved to be the best fit for the translog production function in comparison to the specification of the corresponding Cobb-Douglas frontier model. Although partial influences of some of the variables included in the inefficiency effects model were found to be insignificant, all these variables jointly had significant impacts in shaping the inefficiency of the sampled farmers. Results show that factors such as farm experience, education, land fragmentation, off-farm job availability, irrigation frequency, and farm location influence the technical inefficiency effects.



Copyright ©2023 by authors and Galileo Institute of Technology and Education of the Amazon (ITEGAM). This work is licensed under the Creative Commons Attribution International License (CC BY 4.0).

### I. INTRODUCTION

There are interesting concerns both in terms of poverty reduction and national economic aspects arising from the role of cotton production in national development in Turkiye. Cotton farming has traditionally been considered the main livelihood of the farm households operating in the major plains of Turkiye. The cotton sector on the Harran Plain, one of the largest plains of the Southeastern Anatolia region in Turkiye, is almost entirely characterized by middle-income cotton producers who were responsible for about 21 percent of the national cotton production. With cotton the most-planted field crop on the Harran Plain, it is commonly accepted among local farmers that cotton is the most profitable agricultural commodity. Between 1995 and 2019, the area under cotton cultivation in Turkiye increased more than twenty times and reached 477,868 hectares with a production amount reaching 2.2 million metric tons [1].

The cotton sector, loaded with a lot of roles in farmers' livelihoods as such, has been disrupted by several problems. First of all, inefficient production techniques lead to low levels of yield and quality factors. Based on a dataset compiled using information gathered from a sample of cotton farmers operating in the Harran Plain, Binici et al. (2006a) reported that most cotton farmers in the region are inefficient input users. In addition, excessive irrigation practices, which are widely applied in the Harran Plain, are the main drivers of increased soil salinity. This problem is due to the shallow groundwater table and can seriously disrupt cotton production [2]–[4].

In addition, the prevailing marketing system in the area is not sufficient to provide local cotton farmers with the possibility of supplying their products at reasonable prices. Factors like these have reducing effects on farmer incomes. As a result, poverty will continue to be a trap for most households. Therefore, improving production performance while ensuring sustainable use of

resources is the main challenge for the growth of middle-income cotton farmers. However, the opportunity to improve farm production based on the expansion of cultivated land is limited to meeting the growing demand for cotton required for Türkiye's ever-increasing population. Therefore, advances in technology and productivity/efficiency are the only hope of production increase to meet the increasing demand for cotton.

While production functions of farmers operating at full efficiency level were assumed to be known, it was necessary to estimate these functions based on data using either parametric or non-parametric (also known as Stochastic Frontier Analysis and Data Envelopment Analysis, respectively) techniques as the parameters of such functions always remained unknown in practice. Starting from this point, literature on efficiency has evolved in two directions of which is to use parametric techniques [5]–[17] and the other one is to use non-parametric techniques [18], [19].

The bulk of the literature focusing on parametric techniques has developed in the area where technical efficiency and inefficiency factors are incorporated simultaneously within a stochastic model [7], [9], [15]–[17], [20]–[26]. However, in some empirical papers by opponents of the above method, a two-step procedure was adopted, i.e. stochastic frontier production function parameters were estimated first, and then the estimated technical inefficiency effects were retracted on the various farmer-specific variables that are expected to be important in explaining the level of technical incompetence of the farmers sampled. This two-step approach contradicts standard assumptions that inefficiency effects are independently and identically distributed to estimate unknown values. However, using predicted technical inefficiency effects in a regression model that includes other explanatory variables is not consistent with the assumption of uniformly distributed technical inefficiency effects in the stochastic model [27]. Despite this debate over whether or not either analysis of the impacts of farm-specific factors on productive efficiency should be handled within a simultaneous model, the two-step procedure is still quite popular in determining the linkage between productive efficiency and firm-specific factors.

In Turkish agriculture, it is important to measure efficiency and productivity for several reasons. Firstly, efficiency and productivity are the key indicators to evaluate farm households as they are the accepted performance measures and success parameters. Secondly, to hypothesize the determinants of inefficiency it is important to isolate the impacts of efficiency and productivity from the environmental impacts once they are estimated. Improving the performance of farm households is then closely related to policies that are formed by identifying sources of inefficiency.

## II. MATERIALS AND METHODS

### II.1 DATA COLLECTED AND THE MATERIAL USED

The research project was started by the University of Harran and funded by the Scientific and Technological Research Council of Türkiye (TUBITAK) with reference number 110K374. Individual units and a subset of survey data were used in this analysis.

The information acquired using a data collecting method also known as the farmer registration information and financial incentive systems, applied to a random sample of cotton farmers working on the Harran Plain, constitutes the majority of the core materials utilized in this article. This method addresses the problem of survey respondents having trouble recalling their responses to

questions about their agricultural practices. Farmers are frequently confronted with queries about their previous farming techniques. The study reported in this paper uses farmer diaries based on payments to motivate farmers to voluntarily participate in the survey and so limit the problems generated by the problem of misremembering the answers to comprehensive survey questions.

The implementation of a financial inducement system that allows for the financial and production record keeping with the least amount of information loss would ensure that participant farmers are provided an incentive to complete farmer diaries on a daily or at least weekly basis. As a result, a payment schedule was established, allowing our member farmers to get a one-time-only payment after finishing the diaries after the season.

We used a stratified random sample technique to choose several representative cotton farmers who would be given diaries to fill out beginning with the 2012 crop season. We then administered frequent visits (10 to 20 depending on the location) to these farmers throughout the season to control these diaries. Two steps were taken to carry out the sampling. First, we purposely identified 51 villages based on their representative properties. On the Harran Plain, 1,029 registered cotton farmers were actively farming the crop and these farmers are to be counted as the overall farmer population. In the second stage, a stratified random selection strategy with a 5% acceptable error margin was used to choose a total of 126 cotton farmers to furnish the farmer diaries. This procedure yields four size strata that represent the region's entire farmer population. There will be 49, 49, 21, and 7 cotton growers sampled in each of the four size strata, respectively.

### II.2 ANALYTICAL FRAMEWORK

To estimate frontier production functions for efficiency assessments, stochastic frontier analysis (SFA) has been utilized extensively in the literature. The stochastic frontier analysis pays particular attention to how the composite error term takes the form, differentiating between measurement errors and other sources of statistical noise. This is in contrast to Data Envelopment Analysis (DEA), which makes no assumptions about the distributional form for inefficiency terms or the functional forms of production functions. Contrary to what DEA claims, not all deviations from the maximum production are considered to be the result of technological inefficiency from the SFA perspective. With Farrell (1957) [28] reporting that production functions of firms must be estimated using data on individual levels and functional forms, stochastic frontiers have since been developed further capitalizing on this notion [29].

The two major representations of the stochastic frontiers are the Cobb-Douglas model and the Transcendental logarithmic (hereafter, translog) model [30], [31]. The Cobb-Douglas stochastic frontier model imposes several technological constraints, such as requiring constant elasticity of scale and unity elasticity of input substitution. However, the translog stochastic frontier model, which has a flexible functional form, does not impose any such limitations, and the range of the elasticity of substitution ranges from negative infinity to positive infinity. Hence the Cobb-Douglas model is nested in the Translog model.

We can specify these models as:

Cobb-Douglas:

$$\ln Y_i = \beta_0 + \sum_{i=1}^6 \beta_i \ln X_i + \varepsilon_i \quad (1)$$

Translog

$$\ln Y_i = \beta_0 + \sum_{j=1}^6 \beta_j \ln X_{ji} + \sum_{j=1}^6 \sum_{k=1}^6 \beta_{jk} \ln X_{ji} \ln X_{ki} + \varepsilon_i \quad (2)$$

where  $Y_i$  is the  $i$ -th firm's output,  $X_i$  is a  $K \times 1$  vector holding the input logarithms;  $\beta$  is a vector of unknown parameters; and  $\varepsilon_i$  is the composite error term, which is made up of two distinct error components from different sources, i.e.,  $\varepsilon_i = v_i - u_i$  where  $v_i$ s are the error component resulting from measurement errors and other factors beyond the farmer's control and are assumed to follow a normal distribution  $N(0, \sigma_v^2)$ . The  $u_i$ s, on the other hand, are non-negative random variables linked to technological inefficiency and are supposed to come from a normal distribution with mean  $\mu$  and variance  $\sigma_u^2$ , which is truncated at zero from below, where  $\mu$  is defined as

$$\begin{aligned} \mu_i = & \delta_0 + \delta_1 Z_{1i} + \delta_2 Z_{2i} + \delta_3 Z_{3i} + \delta_4 Z_{4i} + \delta_5 Z_{5i} \\ & + \delta_6 Z_{6i} + \delta_7 Z_{7i} + \delta_8 Z_{8i} + \delta_9 Z_{9i} + \delta_{10} Z_{10i} \end{aligned} \quad (3)$$

and where  $Z_{is}$  are farm and farmer-specific variables that are hypothesized to have an impact on technical inefficiency level.

Following the  $\gamma$  parameterization of Battese & Cora [6];

$$\gamma = \frac{\sigma_u^2}{\sigma_v^2 + \sigma_u^2} \quad (4)$$

The log-likelihood function for normal and truncated normal pairs may then be written as

$$\ln L = \sum_{i=1}^N \left\{ -0.5 \ln(2\pi) - \ln \sigma_s - \ln \Phi \left( \frac{\mu_i}{\sigma_s \sqrt{\gamma}} \right) + \ln \Phi \left[ \frac{(1-\gamma)\mu_i - \gamma\varepsilon_i}{\{\sigma_s^2 \gamma(1-\gamma)\}^{1/2}} \right] - 0.5 \left( \frac{\varepsilon_i + \mu_i}{\sigma_s} \right)^2 \right\} \quad (5)$$

Where  $\mu_i$  is specified as before,  $\sigma_s^2 = \sigma_v^2 + \sigma_u^2$ ,  $\Phi(\cdot)$  represents the cumulative distribution function of a standardized normal variable, and  $\varepsilon_i$  is the composite error term for each firm in

question. The parameters,  $\beta$ ,  $\sigma_s^2$ , and  $\gamma$  in the above likelihood function are the choice variables for which the values are to be estimated by maximizing the function using the FRONTIER 4.1 computer program developed by Coelli in 1996 [32]. The ratio of the observed output to matching stochastic frontier output is the technical efficiency term for a single data point in SFA:

$$TE_i = \frac{Y_i}{e^{X_i \beta}} = \frac{e^{X_i \beta - u_i}}{e^{X_i \beta}} = e^{-u_i} \quad (6)$$

However, the inefficiency term,  $u_i$  is not observed while the composite error term is. Thus estimating technical efficiency scores requires taking the expected value of  $u_i$  conditional on  $\varepsilon_i = v_i - u_i$  [13]:

$$\begin{aligned} TE_i = e^{-u_i} &= E[e^{-u_i} | \varepsilon_i = v_i - u_i] \\ &= \frac{1 - \Phi(\sigma_\Lambda + \gamma \varepsilon_i / \sigma_\Lambda)}{1 - \Phi(\gamma \varepsilon_i / \sigma_\Lambda)} e^{(\gamma \varepsilon_i + \sigma_\Lambda^2 / 2)} \end{aligned} \quad (7)$$

where  $\sigma_\Lambda = \sqrt{\gamma(1-\gamma)\sigma_s^2}$ ;  $\varepsilon_i = \ln(Y_i) - X_i \beta$ , and the cumulative distribution function of a standardized normal variable is again represented by  $\Phi(\cdot)$ .

### II.3 VARIABLES USED IN THE ANALYSIS

Participants in the survey were also interviewed to answer questions in two categories: (1) production characteristics, which included measures such as the size of operation, type of ownership, commodity yields, and land characteristics; and (2) farmer characteristics, which included gender, age, and education, among others. Table 1 describes the output and input variables that are used to estimate frontier production functions, while Table 2 summarizes the description of the dependent and explanatory (Z) variables that are used in our econometric analysis. These tables per se are self-explanatory and describe the variables used in the analyses quite comprehensively.

Table 1: Definition of the variables used to estimate frontier production functions.

Variables	Definition
<b>Output Variable</b>	
OUTPUT	Quantity of cotton produced in total (kilograms)
<b>Input Variables</b>	
SEED ( $X_1$ )	Quantity of seeds used in cotton production (kilograms)
FERTILIZER ( $X_2$ )	The variable denoted as FERTILIZER represents the net total amount of ammonium and phosphate contained in commercial brand fertilizers used in cotton production and is measured in kilograms.
LABOR ( $X_3$ )	Working hours depleted (family as well as hired labor).
PESTICIDE ( $X_4$ )	Value of herbicidal and insecticidal chemicals (TL <sup>1</sup> ).
CAPITAL ( $X_5$ )	Capital input includes the annualized flow of capital services required by cotton production and is measured in TL.
LAND ( $X_6$ )	Land area input is considered as the land area under cotton cultivation and measured in hectares.

<sup>1</sup> Abbreviated for Turkish Liras

Source: Authors, (2023).

Table 2: Z variables' definition for the stochastic frontier analysis (inefficiency determinants).

Variable	Definition
<b>Dependent Variable</b>	
TE <sub>VRS</sub>	Technical efficiency is calculated using the assumption of variable returns to scale, with a value ranging from 0 to 1.
<b>Explanatory Variables</b>	
EXPERIENCE (Z <sub>1</sub> )	Farmer experience (Years)
EDUCATION (Z <sub>2</sub> )	If the farmer attended high school or high school and college, the dummy variable will have a value of 1, otherwise, it will have a value of 0.
HSIZE (Z <sub>3</sub> )	Household size; the number of people living in the household.
OFF-FARM (Z <sub>4</sub> )	The value of the dummy variable is 1 if the farmer works outside the farm and 0 otherwise.
FMLYLBOR (Z <sub>5</sub> )	Share of the family labor force in total labor input (%)
LSEGMENT (Z <sub>6</sub> )	Parcel segmentation on land is the number of parcels under the farmer's ownership or tenancy.
LNDOWNR (Z <sub>7</sub> )	If the farmer owns the land he farms, the dummy variable will have a value of 1; otherwise, it will have a value of 0.
LOCNHRN (Z <sub>8</sub> )	Dummy variable that indicates the location of the agricultural activity has a value of 1 if it is situated in Sanliurfa's Harran district.
LOCNACKL (Z <sub>9</sub> )	Dummy variable that indicates the location of the agricultural activity and returns 1 if the land is in Sanliurfa's Akcakale district.
IRRGFREQ (Z <sub>10</sub> )	Frequency of irrigation applied to the land under cultivation.

Source: Authors, (2023).

Table 3 shows descriptive statistics for the input variables used to estimate production frontiers, whereas Table 4 shows descriptive statistics for farm and farmer characteristics (Z variables) utilized as explanatory factors for examining the drivers of technical efficiency scores.

The variable designated "OUTPUT" is the quantity of cotton produced in total kilograms. Six inputs capturing all the production factors that are used in cotton production (SEED, FERTILIZER, LABOR, PESTICIDE, CAPITAL, and LAND) are considered. Some of these input variables are measured in mass units (i.e., kilograms), while others are expressed in Turkish Liras (TL). The labor input (LABOR) is measured in working hours depleted by the farmer and considers paid and unpaid labor. The variable denoted as CAPITAL quantifies the annualized flow of capital services required by cotton production and is estimated by summing up all the expenses on fixed and variable inputs other than

seed, fertilizer, labor, and pesticides. These expenses typically include yearly depreciation, rental costs for the land and/or machinery used in production plus other expenses on fuels and repair and maintenance services for the farm machinery. The variable designated "FERTILIZER" is the net amount of nitrogen plus phosphorus contained in commercial fertilizers applied and measured in kilograms. The variable "SEED" represents the amount of cotton seeds used to sow the field and is measured in kilograms as well. The variable designated "PESTICIDE" consists of such variable expenditures including those for both herbicidal and insecticidal chemicals and is measured in TL.

Using Coelli's FRONTIER 4.1 software developed in 1996 and SFA methodologies separately applied to each frontier production function under the assumptions of variable returns to scale, technical efficiency ratings utilized as the dependent variable in our econometric studies are estimated [32].

Table 3: The input variables' descriptive statistics for estimating stochastic frontiers.

Variables	Mean	Std. Dev.	Minimum	Maximum
Y: Amount of cotton produced (kg)	47,642.619	45,253.108	3,209.000	290,000.000
X <sub>1</sub> : Seeds (kg)	306.024	489.567	10.000	4,500.000
X <sub>2</sub> : Fertilizer (ammonium+phosphate; kg)	2,925.405	3,081.784	2,200.000	16,740.000
X <sub>3</sub> : Labor (Family + hired; hours)	3,944.772	4,217.881	175.300	20,499.000
X <sub>4</sub> : Values of Pesticides used (TL)	2,881.470	3,905.217	50.000	31,320.000
X <sub>5</sub> : Fixed and variable capital (TL)	31,473.694	35,152.091	933.000	261,271.438
X <sub>6</sub> : Land area (ha)	10.790	11.140	0.650	80.000

Source: Authors, (2023).

Table 4: Explanatory variables' descriptive statistics used to assess the inefficiency effects model.

Explanatory Variables	Mean	Std. Dev.	Minimum	Maximum	Obs
EXPERIENCE (Z <sub>1</sub> )	17.3016	10.1155	2.0	45.0	126
EDUCATION (Z <sub>2</sub> )	0.3730	0.4855	0.0	1.0	126
HSIZE (Z <sub>3</sub> )	9.8968	7.4176	2.0	55.0	126
OFF-FARM (Z <sub>4</sub> )	0.3016	0.4608	0.0	1.0	126
FMLYLBOR (Z <sub>5</sub> )	0.3167	0.3135	0.0	1.0	126
LSEGMENT (Z <sub>6</sub> )	1.9762	1.3234	1.0	7.0	126
LNDOWNR (Z <sub>7</sub> )	0.8254	0.3811	0.0	1.0	126
LOCNHRN (Z <sub>8</sub> )	0.2698	0.4456	0.0	1.0	126
LOCNACKL (Z <sub>9</sub> )	0.2381	0.4276	0.0	1.0	126
<b>IRRGFREQ (Z<sub>10</sub>)</b>	<b>6.6746</b>	<b>1.5688</b>	<b>3.0</b>	<b>12.0</b>	<b>126</b>

Source: Authors, (2023).

Some of the farm and farmer characteristics anticipated to influence technical efficiency scores include single dummy

variables quantifying off-farm work status (OFF-FARM), land ownership status (LNDOWNR), and education level

(EDUCATION), as well as a mutually exclusive multiple dummy variable representing farm location (LOCNCNTR, LOCNHRRN, and LOCNACKL). Other determinants affecting farmer performances are farming experience in years (EXPERIENCE), household size (HSIZE), number of parcels under the farmer's ownership or tenancy (LSEGMENT), and number of irrigation applied (IRRGFREQ). To quantify the effects of the proportion of family labor input in the entire labor force (measured in continuous percentages), we lastly incorporate the variable FMLYLBOR. The location dummies are used to identify the impacts of farmer locality on their performance measures. Due to improved access to knowledge, it is speculated that farmers in the central area are technically more efficient than those working in the Harran and Akcakale districts. Dropping one of the dummy variables from the analysis and using it as a reference variable instead would help avoid dummy trap problems and thus we followed this rule for all the dummy variables in our econometric analysis to keep the consistency throughout. The variable designated LNDOWNR quantifies the effects of land ownership status and could have an ambiguous impact on efficiency. Efficiency might be enhanced by applying soil-improving techniques, an incentive created by land ownership status. However, the tenant farmer may be encouraged to use inputs more effectively by his or her status as a land renter.

A bigger percentage of hired labor may indicate a more specialized, and hence productive, labor input, but it may also be a source of moral hazard. The influence of the amount of family labor might go either way (positive or negative) [33]. Experienced farmers tend to operate more professionally; therefore, it would stand to reason that experience would increase efficiency. However, other writers explore reasons for the reverse connection [34], maybe because farming becomes more physically demanding as the farmer ages (e.g., age impairments-non linearity). Similarly, we hypothetically attach higher efficiency scores to those full-time experienced farmers who are more educated with smaller household sizes, operate on a smaller land tract divided by a smaller number of parcels, and finally irrigate the land more sensibly.

### III. RESULTS AND DISCUSSION

In Table 5, the maximum likelihood estimates of the coefficients for the translog stochastic frontier model and the Cobb-Douglas model are shown. All the  $\beta$  coefficients from the Cobb-Douglas frontier model have expected signs and three of these coefficients turn out to be considered significant demonstrating the robustness of the model. In the translog frontier model, nine out of the twenty-seven coefficients are significant at the %1 level, four are significant at the %5 levels, and just one is significant at the %10 levels. Thus the translog frontier model is robust as well.

We check to see if the technical efficiency estimates produced from the two models have different means and variances. Even though the generalized likelihood ratio (LR) test indicates that the translog stochastic frontier model is an appropriate representation, we additionally investigate the sensitivity of technical efficiency levels to the functional form choice. Table 6 shows the production elasticities of individual inputs along with scale parameters. Both models yield production elasticities with all their signs (positive) in the direction expected. The land has the highest production elasticity indicating that it is the most prevalent factor of production. This finding is consistent when we particularly consider how scarce the land is to the farm households

in Turkiye. This implies that farm households may be encouraged to continue cultivating their current land parcels.

The factors designated CAPITAL and PESTICIDE appear to be the second and third important factors of production, respectively, for the Cobb-Douglas frontier model while FERTILIZER and SEED inputs for the translog frontier model. These inputs (SEED, PESTICIDE, and FERTILIZER) are land-enforcing factors of production tending to increase the productivity of existing land tracts and thereby promoting yields per hectare. In Turkiye, land degradation brought by elevated soil salinity and wind erosion is the number one constraint on the production and it is possible to state that efficient utilization of fertilizer, seed, and pesticides as well as a suitable combination of the three can mitigate the effects of this constraint. The scale elasticities for the Cobb-Douglas and translog frontier models are 0.96639 and 0.95124, respectively, implying slightly diminishing returns to scale. This means that the farmers are not the best operators in terms of production size.

#### III.1 EFFECTS OF TECHNICAL INEFFICIENCY

The two key metrics used to assess the overall consequences of technical inefficiency are  $\sigma^2$  and  $\gamma$ . Both the Cobb-Douglas and the Translog frontier models' predicted values of  $\sigma^2$  and  $\gamma$  are statistically significant to differing degrees (5% in the Cobb-Douglas model and 1% in the Translog model). This result agrees with previous findings. The Cobb-Douglas and Translog frontier models' estimated values are very substantially different from zero, indicating that the random component of the inefficiency effects considerably affects the level and variability of production for these sampled farmers. This finding is consistent with those found by Wadud (2003) [30], Sharma et al. (1999) [24], and Coelli and Battese (1996) [35]. The Cobb-Douglas and Translog frontier models' respective generalized LR tests, designated as test number 1 in Table 7, lead us to strongly reject the null hypothesis that there is no technological inefficiency at the 5% level. This reveals the randomness of technical inefficiency effects in both models for the farm households operating on the Harran Plain of Turkiye. As a result, their standard response functions are insufficient representations of cotton output.

The generalized LR test presented in Table 7 further illustrates that the stochastic frontier model's explanatory factors, which are unique to the farm setting, have collectively influenced the level of technical inefficiency at the 5 percent level for both frontier models. Given that these factors are likely to have an impact on the productivity of local cotton farmers, it is crucial to look at the signs of the predicted coefficients for  $\delta_i$  parameters linked to the various explanatory variables in both stochastic frontier models.

In all models, the signs of the estimates for the coefficients of farming experience are positive, showing that experienced farmers are technically less efficient than rookie farmers. While this compares to previous results obtained by several researchers [9], [30], [36], it contradicts the finding obtained by Sesabo and Tol (2007) [25]. This could be attributable to easier credit availability for younger farmers. The coefficients of education in the two models as measured by a dummy variable (taking on values of 1 if the farmer has a high school or college degree) have positive signs indicating that higher education causes inefficiency which is not in the direction expected (significant at 10% and 5% significance levels, respectively). This conforms to the results found elsewhere [24], [35].

Table 5: Estimates of the stochastic frontier models using the maximum likelihood technique.

Variables	Parameters	Cobb-Douglas		Translog	
		Coefficient	t-ratio	Coefficient	t-ratio
Intercept	$\beta_0$	6.80800***	13.63900	1.22817	0.93423
Ln X <sub>1</sub>	$\beta_1$	0.00684	0.09622	4.78501***	4.26456
Ln X <sub>2</sub>	$\beta_2$	0.02476	1.04251	-2.36477***	-2.82885
Ln X <sub>3</sub>	$\beta_3$	0.00158	0.07597	-0.31636	-0.54166
Ln X <sub>4</sub>	$\beta_4$	0.09822***	3.21313	2.55431***	3.23434
Ln X <sub>5</sub>	$\beta_5$	0.14152**	2.18146	-0.20837	-0.24001
Ln X <sub>6</sub>	$\beta_6$	0.69347***	7.27066	-3.09795***	-3.18605
Ln X <sub>1</sub> x Ln X <sub>1</sub>	$\beta_7$	-	-	-0.21986	-1.57440
Ln X <sub>2</sub> x Ln X <sub>2</sub>	$\beta_8$	-	-	0.00384	0.25583
Ln X <sub>3</sub> x Ln X <sub>3</sub>	$\beta_9$	-	-	0.08629***	3.22509
Ln X <sub>4</sub> x Ln X <sub>4</sub>	$\beta_{10}$	-	-	-0.00548	-0.15746
Ln X <sub>5</sub> x Ln X <sub>5</sub>	$\beta_{11}$	-	-	-0.17555**	-1.97206
Ln X <sub>6</sub> x Ln X <sub>6</sub>	$\beta_{12}$	-	-	-0.47077**	-2.30417
Ln X <sub>1</sub> x Ln X <sub>2</sub>	$\beta_{13}$	-	-	0.02238***	0.08841
Ln X <sub>1</sub> x Ln X <sub>3</sub>	$\beta_{14}$	-	-	-0.21902**	-2.08172
Ln X <sub>1</sub> x Ln X <sub>4</sub>	$\beta_{15}$	-	-	-0.34772***	-2.98692
Ln X <sub>1</sub> x Ln X <sub>5</sub>	$\beta_{16}$	-	-	-0.01519	-0.07083
Ln X <sub>1</sub> x Ln X <sub>6</sub>	$\beta_{17}$	-	-	0.92179***	2.71673
Ln X <sub>2</sub> x Ln X <sub>3</sub>	$\beta_{18}$	-	-	-0.04185	-0.68130
Ln X <sub>2</sub> x Ln X <sub>4</sub>	$\beta_{19}$	-	-	-0.18338*	-1.73789
Ln X <sub>2</sub> x Ln X <sub>5</sub>	$\beta_{20}$	-	-	0.46272***	3.03556
Ln X <sub>2</sub> x Ln X <sub>6</sub>	$\beta_{21}$	-	-	-0.30251	-1.27172
Ln X <sub>3</sub> x Ln X <sub>4</sub>	$\beta_{22}$	-	-	-0.07313**	-2.15759
Ln X <sub>3</sub> x Ln X <sub>5</sub>	$\beta_{23}$	-	-	0.07281	0.94844
Ln X <sub>3</sub> x Ln X <sub>6</sub>	$\beta_{24}$	-	-	0.13279	0.99296
Ln X <sub>4</sub> x Ln X <sub>5</sub>	$\beta_{25}$	-	-	0.02049	0.22763
Ln X <sub>4</sub> x Ln X <sub>6</sub>	$\beta_{26}$	-	-	0.56468***	3.37801
Ln X <sub>5</sub> x Ln X <sub>6</sub>	$\beta_{27}$	-	-	-0.20888	-0.85362
<b>Inefficiency Model</b>					
Intercept	$\delta_0$	-2.71358	-1.60431	-3.19604**	-2.37611
EXPERIENCE	$\delta_1$	0.02652*	1.70008	0.03161**	2.49135
EDUCATION	$\delta_2$	0.59905*	1.81157	0.86594**	2.37613
HSIZE	$\delta_3$	-0.03301	-1.58264	-0.09435*	-1.99631
OFF-FARM	$\delta_4$	-0.36591	-1.41754	-0.44124**	-2.12623
FMLYLBOR	$\delta_5$	0.92596	1.64717	0.21261	0.89593
LSEGMENT	$\delta_6$	0.17590**	2.22275	0.08836***	2.16400
LNDOWNR	$\delta_7$	-1.31317**	-2.42846	-0.29433	-1.54436
LOCNHRN	$\delta_8$	1.64662*	1.93193	1.18174***	2.68159
LOCNACKL	$\delta_9$	1.61760**	1.96370	1.12603***	2.70968
IRRGFREQ	$\delta_{10}$	0.06700	1.14677	0.14315**	2.34143
<b>Diagnostics</b>					
Sigma-squared	$\sigma^2$	0.25618**	2.41275	0.17952***	3.16563
Gamma	$\gamma = \sigma_u^2 / (\sigma_v^2 + \sigma_u^2)$	0.91644***	29.04133	0.91630***	23.72817
Sigma V-squared	$\sigma_v^2$	0.02141	---	0.01502	---
Sigma U-squared	$\sigma_u^2$	0.23477	---	0.16449	---
Log Likelihood	$\ln L(y \beta, \sigma, \gamma)$	23.11763	---	42.08589	---

Source: Authors, (2023).

Table 6: Output elasticities of inputs used in cotton production.

Inputs	Cobb-Douglas	Translog Frontier	Inputs	Cobb-Douglas	Translog Frontier
SEED	0.00684	0.07933	PESTICIDE	0.09822	0.05897
FERTILIZER	0.02476	0.09948	CAPITAL	0.14152	0.01843
LABOR	0.00158	0.02593	LAND	0.69347	0.66910
<b>Return to Scale</b>	<b>0.96639</b>	<b>0.95124</b>			

Source: Authors, (2023).

Table 7: Hypothesis tests for the stochastic frontier and inefficiency effects models.

Null Hypotheses	Log Likelihood	$\chi^2$ Statistic	$\chi^2_{0.95}$ Critical	Decision
<b>Cobb-Douglas</b>				
Unrestricted Model	23.11763			
1. $H_0: \gamma = \delta_0 = \delta_1 = \delta_2 = \dots = \delta_{10} = 0$	-1.89620	50.02766	22.40	Reject $H_0$
2. $H_0: \gamma = \delta_0 = 0$	13.44472	19.34582	5.99	Reject $H_0$
3. $H_0: \delta_1 = \delta_2 = \dots = \delta_{10} = 0$	11.98264	22.26998	18.30	Reject $H_0$
4. $H_0: \delta_0 = 0$	20.97651	4.28224	3.84	Reject $H_0$
<b>Translog</b>				
Unrestricted Model	42.08589			
1. $H_0: \gamma = \delta_0 = \delta_1 = \delta_2 = \dots = \delta_{10} = 0$	17.20815	49.75548	22.40	Reject $H_0$
2. $H_0: \gamma = \delta_0 = 0$	35.37227	13.42724	5.99	Reject $H_0$
3. $H_0: \delta_1 = \delta_2 = \dots = \delta_{10} = 0$	30.52162	23.12854	18.30	Reject $H_0$
4. $H_0: \delta_0 = 0$	38.51215	7.14748	3.84	Reject $H_0$
<b>Testing Cobb-Douglas</b>				
Unrestricted Model = Translog	42.08589			
5. $H_0: \beta_7 = \beta_8 = \beta_9 = \beta_{10} = \dots = \beta_{27} = 0$	<b>23.11763</b>	<b>37.93652</b>	<b>32.7</b>	<b>Reject <math>H_0</math></b>

Source: Authors, (2023).

The coefficients of the variables designated HSIZE and OFF-FARM are estimated to be negative, implying that household size and off-farm employment availability have a beneficial influence on efficiency, albeit these coefficients are only significant in the translog frontier model. This is not consistent with the findings by Sesabo and Tol (2007) [25]. The estimates for the coefficients of the share of the family labor force in total labor input and the number of irrigation applied to turn out to be positive showing evidence of lowered efficiency levels as they tend to increase. However, the coefficients of the share of family labor input are not significant in both models while the coefficient of irrigation frequency is only significant at the 5% level in the translog stochastic frontier model. Although these findings about family labor input and irrigation frequency satisfy our initial expectations there are no similar results in the literature to which we can compare our findings.

The signs of the estimates for the coefficients of land disintegration as measured by the number of parcels under ownership or tenancy are estimated to be positive which translates into a negative impact on efficiency, i.e., the greater the plot size the lower the efficiency. This finding runs along similar lines to the results obtained by Coelli and Battese (1996) and Wadud (2003) [30], [35]. The estimates for the coefficients of the dummy variable capturing the land ownership status have negative signs indicating that land owners are associated with higher efficiency levels than

tenants (only significant in the Cobb-Douglas stochastic frontier model). This is perhaps because landowners would feel more responsible for tracts they operate on resulting in greater engagement of infrastructural investments and that would in turn result in greater efficiency levels. Last but not least, the outcomes of the two models show that the efficiency is negatively impacted by the location dummies for the districts of Harran and Akcakale. This indicates that farmers in the province of Sanliurfa's core area are associated with higher efficiency levels. This conclusion may be explained by the fact that farmers in the central district have easier access to financial instruments such as credits, derivative products, etc.

Results indicate that farm households have technical efficiency scores which substantially differ across the sample. Technical efficiency scores for the Cobb-Douglas frontier model range from 0.30 to 0.98, with a mean of 0.87 and a standard deviation of 0.12, while technical efficiency scores for the translog stochastic frontier model are predicted to range from 0.28 to 0.97, with a mean of 0.88 and a standard deviation of 0.11. The technical efficiency scores' frequency distributions are shown in Table 8 along with their summary statistics. The table shows that it is possible to enhance farm income and thereby welfare by improving efficiency. Production costs could be reduced by 12 percent if full technical efficiency levels were attained by farmer operations.

Table 8: Frequency distribution of farm-specific technical efficiency.

Efficiency Distribution (%)	Cobb-Douglas Stochastic Frontier		Translog Stochastic Frontier	
	Number of Farms	% of Farms	Number of Farms	% of Farms
0-60	3	2.38	5	3.97
60-65	5	3.97	2	1.59
65-70	4	3.17	2	1.59
70-75	3	2.38	1	0.79
75-80	3	2.38	5	3.97
80-85	17	13.49	16	12.70
85-90	26	20.63	17	13.49
90-95	54	42.86	54	42.86
95-100	11	8.73	24	19.05
Mean	86.5		87.9	
Minimum	30.4		28.2	
Maximum	97.5		97.4	
<b>Standard Deviation</b>	<b>11.5</b>		<b>11.2</b>	

Source: Authors, (2023).



#### IV. CONCLUSIONS

The Cobb-Douglas and translog stochastic frontier models are used in this study to examine the potential for finding technical inefficiency in terms of its patterns and sources for the case of local cotton growers working on Türkiye's Harran Plain. A specialized maximum likelihood estimation model is applied to estimate these efficiency scores along with their determinants simultaneously with the incorporation of stochastic frontiers and inefficiency effects into a single equation system. The inefficiency effects include such factors, namely education, farm experience, household size, off-farm job availability, the share of the family labor force, land fragmentation, land ownership status, irrigation frequency, and location of the farm relative to the central district of Sanliurfa. The system generates parameters of output elasticities calculated from both the stochastic frontier models, with their signs pointing in the desired directions. The study's findings demonstrate that the sampled local farm households exhibit slightly declining returns to scale in cotton production. The two well-known stochastic models, namely the Cobb-Douglas and the translog frontiers, generate wide ranges of technical efficiency scores that vary from 30% to 98% with a mean of 87% and 28% to 97% with a mean of 88%, respectively. It was detected that full technical efficiency levels attained by farmers ensure a reduction in production cost by 12%.

The findings of the study show that technical efficiency is significantly impacted by farm-specific explanatory factors included in the technical inefficiency effects model. Ironically the older, experienced farm Households with greater education tend to operate farming activities inefficiently. Technically speaking, the farm households operating in Sanliurfa's central region are more productive than those in Akcakale and Harran districts. Moreover, farm households that operate on larger, more fragmented land holdings are inherently less efficient. The well-being of farm households should be improved by robust agricultural policies targeting to reduce land fragmentation and increase technical efficiency and thereby improving farm income.

#### V. AUTHOR'S CONTRIBUTION

**Conceptualization:** Tamer Işgın, Remziye Özel, Abdulkaki Bilgiç and Mehmet Reşit Sevinç.

**Methodology:** Tamer Işgın, Remziye Özel and Abdulkaki Bilgiç.

**Investigation:** Tamer Işgın, Remziye Özel, Abdulkaki Bilgiç and Mehmet Reşit Sevinç.

**Discussion of results:** Tamer Işgın, Remziye Özel and Abdulkaki Bilgiç.

**Writing – Original Draft:** Tamer Işgın, Abdulkaki Bilgiç and Mehmet Reşit Sevinç.

**Writing – Review and Editing:** Tamer Işgın, Abdulkaki Bilgiç and Mehmet Reşit Sevinç.

**Resources:** Tamer Işgın, Abdulkaki Bilgiç and Mehmet Reşit Sevinç.

**Supervision:** Tamer Işgın and Abdulkaki Bilgiç

**Approval of the final text:** Tamer Işgın, Remziye Özel, Abdulkaki Bilgiç and Mehmet Reşit Sevinç.

#### VI. ACKNOWLEDGMENTS

The Scientific and Technological Research Council of Türkiye (TUBITAK), which supported our study with reference number 110K374, has our sincere gratitude. Without their significant contributions, this study would not have been possible.

The writers' results, interpretations, and conclusions are their own, and they do not necessarily reflect the opinions of TUBITAK.

#### VII. REFERENCES

- [1] TSI (Turkish Statistical Institute), "Crop production statistics," 2020. <https://biruni.tuik.gov.tr/medas/?kn=92&locale=tr> (accessed Sep. 22, 2023).
- [2] T. Binici, C. R. Zulauf, O. O. Kacira, and B. Karlı, "Assessing the efficiency of cotton production on the Harran Plain, Turkey," *Outlook on Agriculture*, vol. 35, no. 3, pp. 227–232, 2006.
- [3] M. A. Çullu et al., "Implication of groundwater fluctuation on the seasonal salt dynamic in the Harran Plain, Southeastern Turkey," *Irrigation and Drainage*, vol. 59, no. 4, pp. 465–476, 2010.
- [4] H. Basal and V. Sezener, "Turkey cotton report," 2012. [https://www.icac.org/Content/SEEPDocuments/PdfFiles04ba2d90\\_eede\\_4e5a\\_8c3f\\_f14c7f6871a6/Turkey%20Cotton%20Report.pdf](https://www.icac.org/Content/SEEPDocuments/PdfFiles04ba2d90_eede_4e5a_8c3f_f14c7f6871a6/Turkey%20Cotton%20Report.pdf) (accessed May 13, 2022).
- [5] N. P. Russell and T. Young, "Frontier Production functions and the measurement of technical efficiency," *Journal of Agricultural Economics*, vol. 34, no. 2, pp. 139–150, 1983.
- [6] G. E. Battese and G. S. Corra, "Estimation of a production frontier model: With application to the pastoral zone of Eastern Australia," *Australian Journal of Agricultural Economics*, vol. 21, no. 3, pp. 169–179, 1977.
- [7] K. P. Kalirajan and R. T. Shand, "Estimating location-specific and firm-specific technical efficiency: an analysis of Malaysian agriculture," *Journal of Economic Development*, vol. 11, pp. 147–160, 1986.
- [8] T. G. Taylor and J. S. Shonkwiler, "Alternative stochastic specifications of the frontier production function in the analysis of agricultural credit programs and technical efficiency," *Journal of Development Economics*, vol. 21, no. 1, pp. 149–160, 1986.
- [9] G. E. Battese and T. J. Coelli, "A model for technical inefficiency effects in a stochastic frontier production function for panel data," *Empirical Economics*, vol. 20, no. 325–332, 1995.
- [10] P. J. Dawson and J. Lingard, "Measuring farm efficiency over time on Philippine rice farms," *Journal of Agricultural Economics*, vol. 40, no. 2, pp. 168–177, 1989.
- [11] B. E. Bravo-Ureta and L. Rieger, "Alternative production frontier methodologies and dairy farm efficiency," *Journal of Agricultural Economics*, vol. 41, no. 2, pp. 215–226, 1990.
- [12] G. E. Battese and T. J. Coelli, "Frontier production functions, technical efficiency and panel data: With application to paddy farmers in India," *Journal of Productivity Analysis*, vol. 3, pp. 153–169, 1992.
- [13] T. Coelli, S. Rahman, and C. Thirtle, "A stochastic frontier approach to total factor productivity measurement in Bangladesh crop agriculture, 1961-92," *Journal of International Development*, vol. 15, no. 3, pp. 321–333, 2003.
- [14] T. Binici, V. Demircan, and C. R. Zulauf, "Assessing production efficiency of dairy farms in Burdur province, Turkey," *Journal of Agriculture and Rural Development in the Tropics and Subtropics*, vol. 107, no. 1, pp. 1–10, 2006.
- [15] F. Lambarra, J. M. Gil, and T. Serra, "Technical efficiency and productivity analysis of Spanish citrus farms," *New Medit*, vol. 10, no. 4, pp. 35–39, 2011.
- [16] A. Musliu, B. Frangu, J. S. Popp, M. Thomsen, and Kemper, "Technical efficiency estimation of dairy farming in Kosovo," *New Medit*, vol. 18, no. 3, pp. 77–84, 2019.
- [17] M. Osmani and A. Kambo, "Efficiency of apple small-scale farming in Albania—a stochastic frontier approach," *New Medit*, vol. 18, no. 2, pp. 71–88, 1999.
- [18] L. M. Seiford and R. M. Thrall, "Recent developments in DEA: the mathematical programming approach to frontier analysis," *Journal of Econometrics*, vol. 46, no. 1–2, pp. 7–38, 1990.
- [19] M. Shafiq and T. Rehman, "The extent of resource use inefficiencies in cotton production in Pakistan's Punjab: an application of data envelopment analysis," *Agricultural Economics*, vol. 22, no. 3, pp. 321–330, 2000.

- [20] K. P. Kalirajan and J. C. Flinn, "The measurement of farm-specific technical efficiency," *Pakistan Journal of Applied Economics*, vol. II, no. 2, pp. 167–180, 1983.
- [21] K. P. Kalirajan, "On measuring the contribution of human capital to agricultural production," *Indian Economic Review*, vol. 24, no. 2, pp. 247–261, 1989.
- [22] K. P. Kalirajan and R. T. Shand, "A generalized measure of technical efficiency," *Applied Economics*, vol. 21, no. 1, pp. 25–34, 1989.
- [23] J. Wang, G. L. Cramer, and E. J. Wailes, "Production efficiency of Chinese agriculture: evidence from rural household survey data," *Agricultural Economics*, vol. 15, no. 1, pp. 17–28, 1996.
- [24] K. R. Sharma, P. S. Leung, and H. M. Zaleski, "Technical, allocative and economic efficiencies in swine production in Hawaii: a comparison of parametric and nonparametric approaches," *Agricultural Economics*, vol. 20, no. 1, pp. 23–35, 1999.
- [25] J. K. Sesabo and R. S. J. Tol, "Technical efficiency and small-scale fishing households in Tanzanian coastal villages: an empirical analysis," *African Journal of Aquatic Science*, vol. 32, no. 1, pp. 51–61, 2007.
- [26] M. Bozoğlu and V. Ceyhan, "Measuring the technical efficiency and exploring the inefficiency determinants of vegetable farms in Samsun province, Turkey," *Agricultural Systems*, vol. 94, no. 3, pp. 649–656, 2007.
- [27] G. E. Battese, S. J. Malik, and M. A. Gill, "An investigation of technical inefficiencies of production of wheat farmers in four districts of Pakistan," *Journal of Agricultural Economics*, vol. 47, pp. 37–49, 1996.
- [28] M. J. Farrell, "The measurement of productive efficiency," *Journal of the Royal Statistical Society*, vol. 120, no. 3, pp. 253–290, 1957.
- [29] W. Meeusen and J. Van Den Broeck, "Efficiency estimation from cobb-douglas production functions with composed error," *International Economic Review*, vol. 18, no. 2, pp. 435–444, 1977.
- [30] M. A. Wadud, "Technical, allocative, and economic efficiency of farms in Bangladesh: a stochastic frontier and DEA approach," *The Journal of Developing Areas*, vol. 37, no. 1, pp. 109–126, 2003.
- [31] T. J. Coelli, D. S. Prasada-Rao, C. J. O'donnell, and G. E. Battese, *An introduction to efficiency and productivity analysis*. New York, USA: Springer, 2005.
- [32] T. Coelli, "Guide to FRONTIER Version 4.1: A Computer Program for Stochastic Frontier Production and Cost Function Estimation." 1996. <https://iranarze.ir/wp-content/uploads/2017/07/7209-English-IranArze.pdf> (accessed Mar. 09, 2023).
- [33] Š. Bojnec and L. Latruffe, "Determinants of technical efficiency of Slovenian farms," *Post-Communist Economies*, no. 21, pp. 117–124, 2009.
- [34] K. Larsén, "Effects of machinery-sharing arrangements on farm efficiency: evidence from Sweden," *Agricultural Economics*, vol. 41, no. 5, pp. 497–506, 2010.
- [35] T. J. Coelli and G. E. Battese, "Identification of factors which Influence the Technical Inefficiency of Indian Farmers," *Australian Journal of Agricultural Economics*, vol. 40, no. 2, pp. 103–128, 1996.
- [36] Seyoum, E. T., G. E. Battese, and Fleming, E. M., "Technical efficiency and productivity of maize producers in Eastern Ethiopia: a study of farmers within and outside the Sasakawa-Global 2000 Project," *Agricultural Economics*, vol. 19, no. 3, pp. 341–348, 1998.



## RESEARCH ARTICLE

## OPEN ACCESS

## NEPHROPROTECTIVE EFFECTS OF *ELEUTHERINE AMERICANA MERR* AGAINST LEAD ACETATE-INDUCED CYTOTOXICITY IN MICE BALB/C

Neti Eka Jayanti<sup>\*1,2</sup>, Rozzana Mohd Said<sup>1</sup>, Choo Chee Yan<sup>3</sup>, Suhaidah Mohd Jofrry<sup>4</sup> and Sa'adah Siregar<sup>5</sup>




<sup>1</sup> Institute of Health Technology and Science Wiyata Husada Samarinda, East Kalimantan Indonesia.

<sup>1,2</sup> Department of Basic Sciences in Physiology, Universiti Teknologi MARA, Faculty of Health Sciences, Selangor Malaysia.

<sup>3</sup> MedChem Herbal Research Group, Faculty of Pharmacy, Universitas Teknologi MARA, Selangor Branch, Puncak Alam Campus, 42300, Selangor, Malaysia.

<sup>4</sup> Faculty of Pharmacy, Universitas Teknologi MARA, 42300, Bandar Puncak Alam, Selangor, Malaysia.

<sup>5</sup> Department of medical laboratory technology, Universiti Teknologi MARA, Faculty of Health Sciences, Selangor Malaysia.

<sup>1</sup> <http://orcid.org/0009-0008-9585-7440> , <sup>2</sup> <http://orcid.org/0000-0003-0071-8090> , <sup>3</sup> <http://orcid.org/0000-0002-9084-4818> ,

<sup>4</sup> <http://orcid.org/0000-0001-5132-5751> , <sup>5</sup> <http://orcid.org/0000-0002-0664-4873> 

Email: [\\*neti@itkeswhs.ac.id](mailto:*neti@itkeswhs.ac.id), [rozan480@uitm.edu.my](mailto:rozan480@uitm.edu.my), [choo715@uitm.edu.my](mailto:choo715@uitm.edu.my), [sue82@uitm.edu.my](mailto:sue82@uitm.edu.my), [ghozalirusman@gmail.com](mailto:ghozalirusman@gmail.com)

## ARTICLE INFO

**Article History**

Received: March 29<sup>th</sup>, 2023

Accepted: April 26<sup>th</sup>, 2023

Published: April 29<sup>th</sup>, 2023

**Keywords:**

*E. Americana merr*,  
*Lead Asetat*,  
*Nephroprotective*.

## ABSTRACT

Lead is a poisonous metal, hurtful to most human body organs if exposure surpasses a permissible level of 50 µg/m<sup>3</sup> and an action level of 30 µg/m<sup>3</sup>. This occurs through the initiation of reactive oxygen species (ROS). Studies have indicated that *Eleutherine americana Merr* contains profound biological properties which protects against cancer cells, decreased in prothrombin level, and vessel vasoconstriction. It will be interesting to study the effect of the plant extract on kidneys exposed to lead acetate. This study aimed to evaluate the nephroprotective effects of *Eleutherine americana Merr* extract on lead acetate cytotoxicity in mice BALB/c. A total of 25 BALB/c mice were randomly divided into five groups. Group 1 was given 0.5% Na-CMC orally while Group 2 was treated orally with 0.075 g/kg body weight lead acetate (Pb(CH<sub>3</sub>COO)<sub>2</sub>). Group 3 to 5 was given different dosages of *Eleutherine americana Merr* of 30, 60 and 120 mg/kg body weight accordingly and simultaneously with Pb(CH<sub>3</sub>COO)<sub>2</sub>. All treatment were for 35 days. Mice were sacrificed after 35 days, blood samples were collected for analysis of creatinine and urea while the kidneys were for histological studies. The levels of creatinine and urea was significantly higher in Pb(CH<sub>3</sub>COO)<sub>2</sub> treated mice (p<0.05). Treatment with the plant extract significantly reduced the level of blood creatinine and blood urea at extract concentration of 30mg/kg body weight (p<0.05). Histology studies of the kidneys showed that Pb(CH<sub>3</sub>COO)<sub>2</sub> caused glomeruli atrophy and tubular destructions. Treatment with the plant extract at dosages of 30 and 60 mg/kg body weight seemed to ameliorate the effect Pb(CH<sub>3</sub>COO)<sub>2</sub> on the structure of the nephrons. Extract of *Eleutherine americana Merr* was shown to have nephroprotective effect against the assault of Pb(CH<sub>3</sub>COO)<sub>2</sub> in mice.



Copyright ©2023 by authors and Galileo Institute of Technology and Education of the Amazon (ITEGAM). This work is licensed under the Creative Commons Attribution International License (CC BY 4.0).

## I. INTRODUCTION

Lead (Pb) is a conceivably poisonous component that, when consumed by the body, amasses in blood and bones, just as in organs like the liver, kidneys, cerebrum and skin. Its negative wellbeing impacts can be both intense and constant, on the

grounds that the human body inadequately discharges Pb. Exposure to high levels of lead can result in adverse health outcomes in people, lead has been displayed to influence the capacity of reproductive, hepatic, endocrine, immune and gastrointestinal systems frameworks, some even leading to death [1-3] Exposure happens through ingestion of debased food,

drinking water, and residue, just as smoking and inward breath of dirtied air in regions with hefty traffic or industrial emissions [4, 5].

The kidney is one of the objective organs for lead harmfulness [5, 6] for being a significant course of discharge from the body and works with kidney harm by means of oxidative pressure and lipid peroxidation (LP). Intense lead harming (blood lead levels > 80–100 µg/dL) upsets both capacity both proximal tubular structure and function [6].

Lead might assume a significant part in producing oxidative stress [7] lead been known to be nephrotoxic at related at high-level [8] The mechanism of lead nephrotoxicity is oxidative stress and the imbalance between antioxidant capacity in the body and the formation of reactive oxygen species (ROS) in the kidney [9, 10].

A few investigations have detailed that lead has prompted oxidative pressure [7] Recent studies investigations show ROS or free extremists like superoxide particle (O<sub>2</sub><sup>-</sup>), hydroxyl radical (OH<sup>-</sup>), and nitrogen oxide (NO) have a vital job in lead-actuated nephrotoxicity [11, 12].

Natural plants have consistently been utilized as the significant constituent of medication in the traditional system [13]. Natural products or medicinal plants having cancer prevention agent antioxidant properties for lessening free radical free revolutionary prompted tissue harm has been accounted for. Restorative plants have upper hands over the ordinarily utilized medications, which has a high price are pricey and known to have hurtful incidental effects for the treatment of different sicknesses [14].

The agent action antioxidant or hindrance of free radicals assumes an urgent part in against protection weighty metal incited nephrotoxicity. In this way, it has been guaranteed that defensive specialists against free radicals, like cancer prevention agents, may be useful therapeutics for weighty metal harmfulness in the kidneys [12]. In the current investigation, we zeroed in on the concentrate of plant *Eleutherine Americana* Merr pods as a natural antioxidant [15].

Indications of the content of *Eleutherine Americana* Merr extricates from phytochemical screening results containing: flavonoids, saponins, tannins, triterpenoids, alkaloids, anthraquinones, naphthoquinones, and steroids [16, 17]. Dayak onions have been displayed to have antioxidant [18, 19], antifungal [20] antimutagenic [21] and antiacne [22].

## II. METHODS

### II.1 EXPERIMENTAL ANIMALS

This study was a true experimental study using randomization with a post-test-only control group design. The experiment was conducted at the Biomedical Laboratory of the Institute of Technology Health and Science, Wiyata Husada Samarinda. The experimental animals used were 25 male mice *mus musculus* BALB/C. The maintenance room was illuminated for 12 h (06.00–18.00). The experimental mice given food and ad libitum drinking water. The rats used were aged 3 months old, with an average initial body weight of 25–30 g. The experimental animals were divided into five groups, each group consisting of five mice.

### II.2 RESEARCH DESIGN

The research was conducted in March 2021 at the Biomedical Laboratory, Fof the Institute of Technology Health and Science, Wiyata Husada Samarinda. The research design used a laboratory experiment with a completely randomized design, five treatments.

The treatment groups were detailed as follows:

Group 1 = Standard control, given 0.5% Na-CMC

Group 2 = Negative control, Exposed Pb Acetate 0.075 g/kg body weight

Group 3 = Exposed by Pb Acetate and had extract at a dose of 30 mg/kg body weight

Group 4 = Exposed by Pb Acetate and had extract at a dose of 60 mg/kg body weight

Group 5 = Exposed by Pb Acetate and had extract at a dose of 120 mg/kg body weight

### II.3 RESEARCH PROCEDURE

#### II.3.1 Extract Preparation of *Eleutherine Americana* Merr (Dayak onion)

Dayak onion bulbs are peeled first, dried and then mashed. Dayak onion bulbs that have been dried are then ground and made into simplicia. Simplicia 500 grams was macerated with 96% ethanol for 48-72 hours and filtered using a Buechner funnel and concentrated using a rotary evaporator.

#### II.3.2 Exposure to Lead Asetat and Intervention of *Eleutherine Americana* Merr Extract

Before interventions, the mice were put in adaptation in a standard cage for 7 days in a room with a temperature of 23 ± 2°C. The mice were individually caged. The lighting was set to 12 h of daylight-dark cycles. During the adaptation period, ad libitum (AL) food and drink were administered daily at 7 am and 5 p.m. After the adaptation, the mice were divided randomly into five groups, each consisting of 5 mice.

The normal control Group 1 was a standard control group with 0.5% Na-CMC administration. Days 1-3 Group 2 was given 0.5% Na-CMC, Group 3 - Group 5 was given Dayak onion extract at a dose of Group 3 (30mg/kgBW) Group 4 (60 mg/kgBW) Group 5 (120 mg/kgBW). Days 4-38 Group 2 was given 0.1 ml of lead acetate, Group 3 - Group 5 was given 0.1 ml of lead acetate + extract Group 3 (30mg/kgBW) Group 4 (60 mg/kgBW) Group 5 (120 mg/kgBW). Then on day 39 all mice were sacrificed for data examination.

#### II.3.3 Sampling

The collection of mouse blood serum begins with taking a certain volume of blood through the heart and then put it into a microtube. Then the blood was centrifuged at 4000 rpm for 20 minutes and the supernatant was taken at the top in the form of a slightly yellowish clear liquid. Blood serum was taken and stored at -20°C until used for creatinine and blood urea analysis. In addition, after the abdomen was opened, the kidney was taken for Histological examination of tissue.

#### II.3.4 Ethical clearance

This research has been approved by the Veterinary Research Ethics Committee of the Faculty of Veterinary Medicine, Universitas Airlangga through approval letter No. 658/EC/KEPK/FKUA/2017.

### III. RESULTS AND DISCUSSIONS

#### III.1 RESULTS

Before the interventions, the randomly grouped mice were first measured for the weights to ensure that they were in the same condition at the beginning of the study. The results of one-way ANOVA test showed no difference in the mean body weight among the groups before the treatment ( $p > 0.05$ ).

#### III.1.1 Creatinine Levels

The result of experimental data on biochemical parameters in this study was the measurement of creatinine levels. Analysis of mice's creatinine levels showed that the highest was found in group G2 (2,41) followed by group G3 and group G5 (Figure 1). The one-way ANOVA test yielded  $p < 0.05$  ( $p = 0.024$ ), indicating a significant difference in the mean creatinine level between the five groups. The LSD (Least Significance Different) test also found a significant difference between the groups.

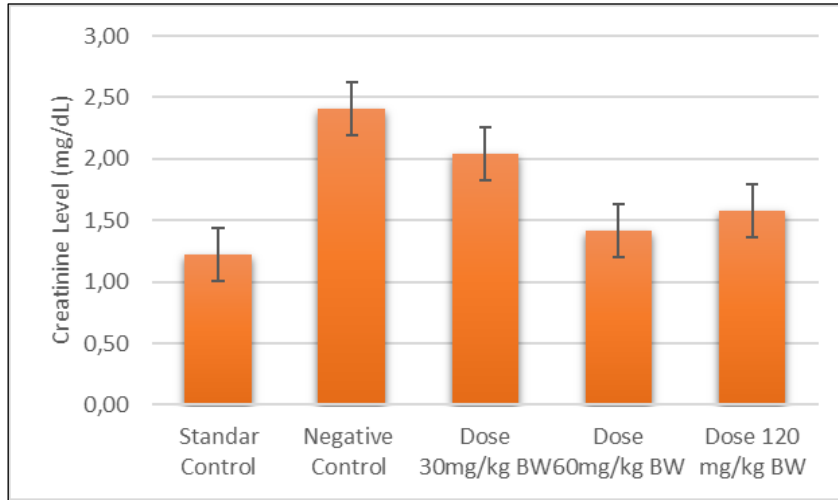


Figure 1: The Creatinine Levels.

Source: Authors, (2022).

Creatinine levels showed the results that a dose of 60 mg/kg showed lowest creatinine level. Average result of each level group is shown in Figure 1.

Normality test was performed by Kolmogorov-Smirnov test, Sig.  $> 0.05$ , creatinine data were normally distributed. Levene Sig test results. 0.91 ( $p > 0.05$ ), it means that the creatinine data is homogeneous. One Way Anova statistical analysis test shows the value of sig. 0.024 ( $p < 0.05$ ). There was a significant difference between the treatment groups for creatinine. LSD Post Hoc Test. The results showed that all doses had nephroprotective activity as seen from the significant difference with the negative control. The dose of 60 mg/kg did not show a significant difference with the dose of 120 mg/kg, meaning that the nephroprotective ability was the same as the treatment at the

highest dose, but this dose showed a significant difference with the negative control. Meanwhile, the dose of 30 mg/kg showed a significant difference with the doses of 60 and 120 mg/kg, and also showed a significant difference with the negative control.

#### III.1.2 Blood Urea Levels

The result of experimental data on biochemical parameters in this study was the measurement of blood urea levels. Analysis of mice's blood urea levels showed that the highest was found in group G2 (73) followed by group G3 and group G5 (Figure 1). The one-way ANOVA test yielded  $p < 0.05$  ( $p = 0.000$ ), indicating a significant difference in the mean creatinine level between the five groups. The LSD (Least Significance Different) test also found a significant difference between the groups.

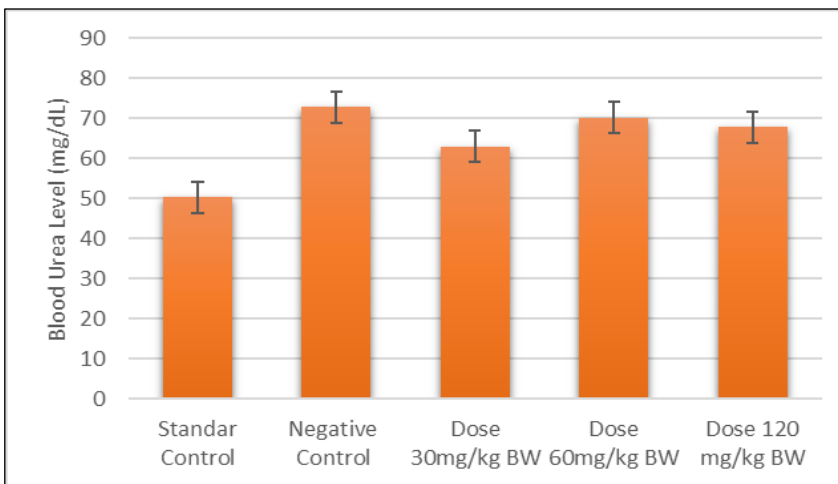


Figure 2: Blood Urea levels.

Source: Authors, (2022).

Blood Urea levels showed that the dose of 30 mg/kg had the lowest levels. The results of the average level of each group are shown in Figure 2.

Normality test was carried out by Kolmogorov-Smirnov and Sig. > 0.05. Urea levels were normally distributed. Levene, significant 0.058 ( $p > 0.05$ ), homogeneously distributed data. One way ANOVA statistical analysis test showed that there was a significant difference between the treatment groups in urea. Post hoc using LSD analysis.

The results showed that the dose of 30mg/kg had nephroprotective activity as seen from the significant difference with the negative control. Doses of 60 and 120 mg/kg did not show a significant difference with negative control, which means that there is a decrease in nephroprotective activity.

### III.1.3 Kidney Histopathology

Histopathological examination was carried out using a light microscope. Microscopic examination of normal kidneys showed intact tubules and glomeruli. In the lead acetate treatment group, kidney tissue showed the most severe glomerular atrophy and tubular destruction of all groups. Administration of Eleutherine Americana Merr extract at doses of 30 and 60 mg/kg BW but not at a dose of 120 mg/kg BW significantly changed histopathology to normal (Figure 3).

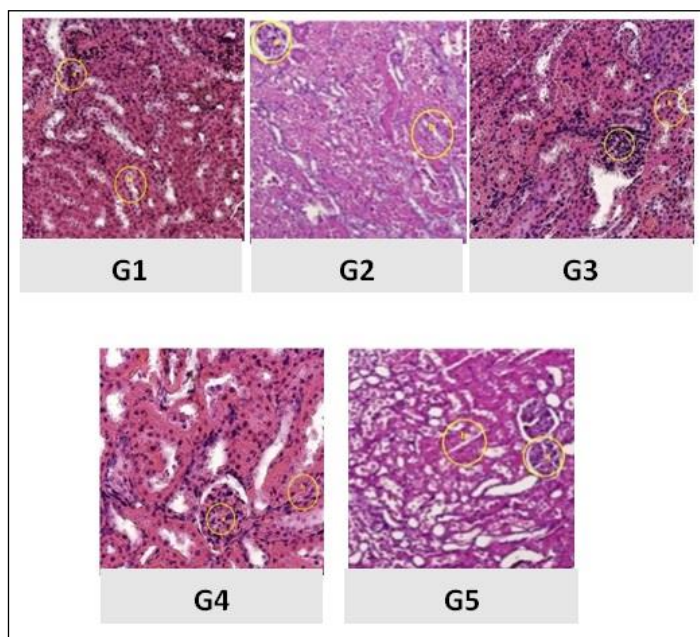


Figure 3: Histology of the kidney (40× objectives, scale bar 50 μm). G1: normal control, G2: negative control. G3, G4 and G5 were treated with 30, 60, and 120 mg/kg BW ethanolic extract of eleutherine americana merr, respectively. A: glomerular, B: tubules. Source: Authors, (2022).

Nephrotoxicity occurs as a result of lead exposure because the kidneys are the main route of lead disposal. Lead is absorbed by the proximal renal tubular cells, where it binds to specific lead-binding proteins. Acute lead poisoning (blood lead levels > 80–100 g/dL) disrupts the structure and function of the proximal tubules, where protein pools that result in obstruction of delivery through the renal tubules also stimulate tubular necrosis.

The result shown in figure 5, the cast is in the negative control. In the treatment except normal controls, changes in the shape of the proximal tubule were found.

In the Pb Acetate negative control group, glomerular atrophy and tubular destruction were the most severe of all groups, and the administration of Eleutherine Americana Merr could reduce the damage caused by Pb Acetate administration of 0.75 mg/kg bw. At the extract dose of 120 mg/kg bw there was still glomerular atrophy and tubular destruction, while at doses of 30 and 60 mg/kg bw the glomerulus and tubules were normal.

Glomerular damage (glomerular atrophy) causes disruption of the filtration process, thus causing kidney problems, namely reduced ability to filter blood. If the ability to filter blood is reduced, then blood cells and proteins can come out with the urine or even accumulate urea in the tubules because they can pass through the filtration process [23].

## III.2 DISCUSSION

Elevated blood urea and creatinine levels were evident in group G2 which provided evidence that administration of 0.075g/kg BW of lead acetate could induce kidney injury. Administration of eleutherine americana merr extract at doses of 30 mg/kg and 60 mg/kg BW together with lead acetate significantly inhibited the increase in markers of kidney injury, namely blood urea and creatinine.

Creatinine is produced by the digestion of protein in the muscles, with most of the creatinine filtered through the blood by the kidneys and excreted in the urine. The glomerular filtration rate (GFR) is an important tool for measuring the renal excretion limit. In clinical practice, GFR is obtained from creatinine freedom in urine tests collected over 24 hours [23]. The level of creatinine clearance was significantly higher in the extract group with a dose of 60 (medium dose) this indicates the ability of eleutherine americana merr extract to remove creatinine from the blood into the urine, which in turn normalizes the creatinine content in the blood and extract at a dose of 120 (high dose) there was an increase in creatinine again this could be due to the active compound content in the eleutherine americana merr extract which had reached the highest level which in turn caused the active content in the extract to become toxic again.

In renal infection, serum urea accumulates and causes uremia because the rate of serum urea production exceeds the clearance rate [24, 25]. Significantly high blood urea in the G2 negative group indicates kidney injury. Administration of eleutherine americana merr extract prevented lead acetate-induced nephrotoxicity, significantly reduced urea accumulation in the 60 mg/kg bw extract group (medium dose) and the extract at 120 doses (high dose) increased blood urea return.

Lead acetate-induced nephrotoxicity is due to the formation of reactive oxygen species (ROS), especially the superoxide anion. Nephrotoxicity induced by ROS and NAPQI is largely offset by glutathione in the early stages of toxicity [26]

The content of creatinine and urea in the blood at a dose of 30 and a dose of 60 mg/kg bw decreased significantly compared to the control group, this provides evidence that eleutherine americana merr extract is able to minimize the toxic effects of lead acetate. The biochemical results were also confirmed by histologic findings, which showed preservation of the glomeruli and tubules.

Most lead acetate induces renal injury affecting the proximal tube, glomerulus, or more distal part of the nephron [27]. Gavage administration of lead acetate into the G2 negative group caused severe kidney damage, with tubular degeneration, wide lumina, damaged glomeruli, whereas pretreatment of eleutherine americana merr extract resulted in significant dose-

dependent nephroprotection against lead acetate-induced nephrotoxicity. Taken together, these results suggest that *eleutherine americana* merr extract may protect the kidneys from lead acetate-induced damage and may be a potential therapeutic candidate for lead acetate-induced nephrotoxicity.

Administration of lead acetate can cause substantial peroxidation of membrane lipids and depletion of antioxidants in renal tissue leading to severe kidney damage through the production of highly reactive free radicals [28, 29]. Decreased antioxidant status in renal tissue has been shown to partially explain the mechanism of lead acetate-induced nephrotoxicity as a result of free radical production [30]. In addition, previous studies have shown that *eleutherine americana* merr extract has antioxidant and anti-inflammatory effects and a protective effect against lead acetate-induced toxicity [31].

#### IV. CONCLUSIONS

The present study demonstrated the dose-dependent nephroprotective activity of the extract *eleutherine americana* merr in a mice strain BALB/C model of lead acetate-induced nephrotoxicity. Pretreatment with extract *eleutherine americana* merr dose-dependently prevented kidney injury as evidenced by serum and urine biochemical analysis and kidney histopathology. In conclusion, *eleutherine americana* merr is a potential nephroprotective agent against lead acetate-induced nephrotoxicity.

#### V. AUTHOR'S CONTRIBUTION

**Conceptualization:** Neti Eka Jayanti, Rozzana Mohd Said and Choo Chee Yan.

**Methodology:** Neti Eka Jayanti and Rozzana Mohd Said.

**Investigation:** Choo Chee Yan and Suhaidah Mohd Joffry.

**Discussion of results:** Neti Eka Jayanti and Sa'adah Siregar.

**Writing – Original Draft:** Neti Eka Jayanti and Sa'adah Siregar.

**Writing – Review and Editing:** Neti Eka Jayanti and Sa'adah Siregar.

**Resources:** Rozzana Mohd Said and Choo Chee Yan.

**Supervision:** Neti Eka Jayanti and Suhaidah Mohd Joffry.

**Approval of the final text:** Neti Eka Jayanti and Suhaidah Mohd Joffry.

#### VI. REFERENCES

- [1] Krzywy, I., et al., [Lead--is there something to be afraid of?]. *Annales Academiae Medicae Stetinensis*, 2010. 56(2): p. 118-128.
- [2] Debnath, B., W. Singh, and K. Manna, Sources and toxicological effects of lead on human health. *Indian Journal of Medical Specialities*, 2019. 10: p. 66.
- [3] Nigra, A.E., et al., Environmental Metals and Cardiovascular Disease in Adults: A Systematic Review Beyond Lead and Cadmium. *Curr Environ Health Rep*, 2016. 3(4): p. 416-433.
- [4] Chain, E.P.o.C.i.t.F., Scientific Opinion on lead in food. *EFSA Journal*, 2010. 8(4): p. 1570.
- [5] Skerfving, S. and I.A. Bergdahl, Chapter 43 - Lead, in *Handbook on the Toxicology of Metals (Fourth Edition)*, G.F. Nordberg, B.A. Fowler, and M. Nordberg, Editors. 2015, Academic Press: San Diego. p. 911-967.
- [6] Rana, M.N., J. Tangpong, and M.M. Rahman, Toxicodynamics of lead, cadmium, mercury and arsenic-induced kidney toxicity and treatment strategy: a mini review. *Toxicology reports*, 2018. 5: p. 704-713.
- [7] Flora, G., D. Gupta, and A. Tiwari, Toxicity of lead: a review with recent updates. *Interdisciplinary toxicology*, 2012. 5(2): p. 47.
- [8] Ekong, E., B. Jaar, and V. Weaver, Lead-related nephrotoxicity: a review of the epidemiologic evidence. *Kidney international*, 2006. 70(12): p. 2074-2084.
- [9] Patrick, L., Lead toxicity part II: the role of free radical damage and the use of antioxidants in the pathology and treatment of lead toxicity. *Altern Med Rev*, 2006. 11(2): p. 114-27.
- [10] Hussein, S.A., R. Mohammed, and A.H. Ali, Protective effects of alpha-lipoic acid against lead-induced oxidative stress in erythrocytes of rats. *Benha Vet Med J*, 2014. 27(2): p. 382-395.
- [11] Xu, J., et al., Lead induces oxidative stress, DNA damage and alteration of p53, Bax and Bcl-2 expressions in mice. *Food and chemical toxicology*, 2008. 46(5): p. 1488-1494.
- [12] Ghoniem, M.H., et al., Efficacy of curcumin on lead induced nephrotoxicity in female albino rats. *Journal of American Science*, 2012. 8(6): p. 502-510.
- [13] Negi K, Mirza A. Nephroprotective and Therapeutic Potential of Traditional Medicinal Plants in RenalDiseases. *J Drug Res AyurvedicSci* 2020;5(3):177–185.
- [14] Aziz, F., I. Maulood, and M. Chawsheen, Effects of melatonin, vitamin C and E alone or in combination on lead-induced injury in liver and kidney organs of rats. *IOSR J Pharm*, 2012. 2(5): p. 13-18.
- [15] Couto, C.L., et al., *Eleutherine bulbous* (Mill.) Urb.: A review study. *Journal of Medicinal Plants Research*, 2016. 10(21): p. 286-297.
- [16] Kuntorini, E.M. and L.H. Nugroho, Structural development and bioactive content of red bulb plant (*Eleutherine americana*); a traditional medicines for local Kalimantan people. *Biodiversitas Journal of Biological Diversity*, 2010. 11(2).
- [17] Mierza, V., D. Suryanto, and M. Nasution. Screening test phytochemicals and antibacterial effects of ethanol extracts of onion bulbs sabrang (*Eleutherine palmifolia* Merr.). in *Proceedings of the National Biology Seminar: Enhancing the Role of Biology in Creating National Achievement with Global Reach*. North Sumatra, Indonesia. 2011.
- [18] Mahmudah, S., A. Muntaha, and A. Muhlisin, Effectiveness of Dayak (*Eleutherine palmifolia* (L.) Merr) Extracts Against *Escherichia coli* In Vitro. *Tropical Health and Medical Research*, 2019. 1(2): p. 44-48.
- [19] Harlita, T.D. and A.A. Oedjijono, The antibacterial activity of dayak onion (*Eleutherine palmifolia* (L.) merr) towards pathogenic bacteria. *Tropical life sciences research*, 2018. 29(2): p. 39.
- [20] Diana, N. and M. Siti Khotimah, Penghambatan Pertumbuhan Jamur Fusarium oxysporum Schlecht Pada Batang Padi (*Oryza sativa* L.) Menggunakan Ekstrak Metanol Umbi Bawang Mekah (*Eleutherine palmifolia* Merr.). *Protobiont*, 2014. 3(2).
- [21] Efendi, A., I. Ahmad, and A. Ibrahim, Efek Antimitosis Ekstrak Bawang Dayak (*Eleutherina americana* L. Merr) Terhadap Sel Telur Bulu Babi (*Tripneustes gratilla* Linn.). *Jurnal Sains dan Kesehatan*, 2015. 1(3): p. 99-104.
- [22] Syamsul, E.S., et al., Ethanolic extract formulation of bawang tiwai (*Eleutherine americana*) in antiacne cream. *Majalah Obat Tradisional*, 2015. 20(3): p. 149-157.
- [23] Hirsova, P., et al., Lipotoxic lethal and sublethal stress signaling in hepatocytes: relevance to NASH pathogenesis[S]. *Journal of Lipid Research*, 2016. 57(10): p. 1758-1770.
- [24] Adeneye, A., et al., Nephroprotective effects of the aqueous root extract of *Harungana madagascariensis* (L.) in acute and repeated dose acetaminophen renal injured rats. *Int J Appl Res Nat Prod*, 2008. 1(1): p. 6-14.
- [25] Mayne, P., *The kidneys and renal calculi. Clinical chemistry in diagnosis and treatment*. 6th ed. London: Edward Arnold Publications, 1994: p. 2-24.
- [26] Miettinen, T.P. and M. Björklund, NQO2 is a reactive oxygen species generating off-target for acetaminophen. *Molecular pharmaceutics*, 2014. 11(12): p. 4395-4404.
- [27] Nashar, K. and B.M. Egan, Relationship between chronic kidney disease and metabolic syndrome: current perspectives. *Diabetes, Metabolic Syndrome and Obesity: Targets and Therapy*, 2014. 7: p. 421.

- [28] Hamid, Z.A., et al., Nephroprotective effects of Zingiber zerumbet Smith ethyl acetate extract against paracetamol-induced nephrotoxicity and oxidative stress in rats. *Journal of Zhejiang University Science B*, 2012. 13(3): p. 176-185.
- [29] Adelman, R., et al., Frusemide enhancement of netilmicin nephrotoxicity in dogs. *Journal of antimicrobial chemotherapy*, 1981. 7(4): p. 431-440.
- [30] Ahmad, S.T., et al., Hesperidin alleviates acetaminophen induced toxicity in Wistar rats by abrogation of oxidative stress, apoptosis and inflammation. *Toxicology letters*, 2012. 208(2): p. 149-161.
- [31] Varghese, C.P., et al., Antioxidant and anti-inflammatory activity of *Eurycoma longifolia* Jack, a traditional medicinal plant in Malaysia. *Int. J. Pharm. Sci. Nanotechnol.*, 2013. 5(4): p. 1875-1878.





ISSN ONLINE: 2447-0228



### RESEARCH ARTICLE

### OPEN ACCESS

## INFLUENCE OF GRADATION ON THE PERFORMANCE OF ASPHALTIC MIXES

Akintunde Akinola Oyedele\*<sup>1</sup>

<sup>1</sup> Department of Physics, Ekiti State University, Ado – Ekiti, Nigeria.

<sup>1</sup> <http://orcid.org/0000-0003-0428-7566> 

Email: [\\*akintunde.oyedele@eksu.edu.ng](mailto:*akintunde.oyedele@eksu.edu.ng)

### ARTICLE INFO

#### Article History

Received: April 01<sup>th</sup>, 2023

Accepted: April 26<sup>th</sup>, 2023

Published: April 29<sup>th</sup>, 2023

#### Keywords:

Aggregates,  
Asphaltic mixes,  
Marshall mix design,  
Pavement failure,  
Specifications.

### ABSTRACT

An assessment of asphaltic mixes on failed sections along Ado – Ikere road, Southwest Nigeria has been carried out. The study has been designed to fully understand and account for the incessant pavement failures aside soil characterization. Samples of asphalt concrete were collected from failed sections along the road. The samples were subjected to density measurements, bitumen extraction, sieve analysis, hot mix Marshall Stability and flow tests. Values ranging between 6.01 – 6.45 %, 320 – 365 kg, 3.6 – 5.9 mm, 4.2 – 6.0 % were obtained for bitumen content, stability, flow, voids in total mix, respectively. The results revealed influence of gradation on the performance of asphaltic mixes. Poor gradation of aggregates resulting in low stability and flow as well as excess voids in the concrete was apparent and capable of inducing pavement failure. The asphaltic mixes significantly fell out of the limits in the criteria of the 2007 Federal Ministry of Works and Housing Standard Specifications for Roads and Bridges (FMW). Strict adherence to standards regarding asphalt concrete mix used for pavement construction is imperative to rule out the nature of asphaltic mixes as a possible cause of premature failure of road pavements.



Copyright ©2023 by authors and Galileo Institute of Technology and Education of the Amazon (ITEGAM). This work is licensed under the Creative Commons Attribution International License (CC BY 4.0).

### I. INTRODUCTION

Hot mix asphalt (HMA) is the most common material used for surface course of asphalt pavements in different countries. There are several methods for designing asphalt mixtures, such as the Marshall, Hveem and Superpave methods. The Marshall mix design has been the most widely used method in many countries including Nigeria and the tropical countries [1 - 3]. The method is based on empirical experiments. It is a process to manipulate three variables of aggregate, asphalt binder content and the ratio of aggregate to asphalt binder with the objective of obtaining an HMA that is deformation resistant, fatigue resistant, moisture damage resistant, skid resistant, durable and workable [2, 4, 5]. It is noted that the optimum asphalt content of a mix is highly dependent on aggregate characteristics such as gradation and absorptiveness. Aggregate gradation is directly related to optimum asphalt content [6, 7].

A minimum amount of air void should be maintained to avoid instability during compaction process and to provide space

for bitumen flow in long-term consolidation under traffic loads. A sufficient amount of air voids should be designed to make room for expansion of binder in hot weather conditions and compaction by road traffic to avoid bleeding and loss of stability which may occur and the pavement will deform readily under severe loads. However, an air void content on the very high side allows for intrusion of air and water. It also increases the rate of hardening of binders which promotes premature embrittlement of pavements and differential compaction subject to traffic loads with the resultant formation of ruts and grooves along the wheel track [8, 9].

Beside the physical properties of aggregate, gradation plays a vital role in durability of asphalt pavement. It is one of the crucially important features of aggregate blend. The gradation of the aggregate should be so adjusted that voids in mineral aggregate (VMA), voids in total mix (VTM) and asphalt film thickness criteria are also met. The gradation within the specified grading envelope is most desirable [7, 9, 10].

## II. THEORETICAL REFERENCE

An asphalt concrete mixture must be designed, produced and placed in order to obtain the desirable mix properties including stability, durability, flexibility, fatigue resistance, skid resistance, impermeability and workability. It must resist water damage, deformation and cracking, provide a good tractive surface, and be obtained at economic rate. The asphalt content is expected to ensure that the resulting air-void content and percent voids filled with asphalt fall within prescribed limits, that the Marshall stability exceeds a specified minimum level, and that the flow value does not exceed a prescribed maximum value [2, 5, 11].

The percentage of air voids in asphalt directly relates to the longevity of the pavement. The level of compaction any asphalt mix receives directly impacts the quality and lifetime of that

pavement. Understandably, the more air voids a pavement has, the more that pavement is compromised in terms of pavement strength, fatigue life, durability, raveling, rutting and susceptibility to moisture damage.

In order to meet these demands, the mindful and effective manipulation of the three variables; the aggregate, asphalt binder and the ratio of asphalt binder to aggregate is mandatory. Aggregates constitute approximately 95% of asphalt mix by weight [7, 8]. The durable asphalt mix is attributed to the properties of aggregates (physical and chemical), properties of binder, percentage of binder used and arrangement of aggregate particles (or gradation).

This research work seeks to assess the Influence of Gradation on the performance of asphaltic mixes with regards to road failure along Ado-Ikere Road, southwest, Nigeria (Figure 1).

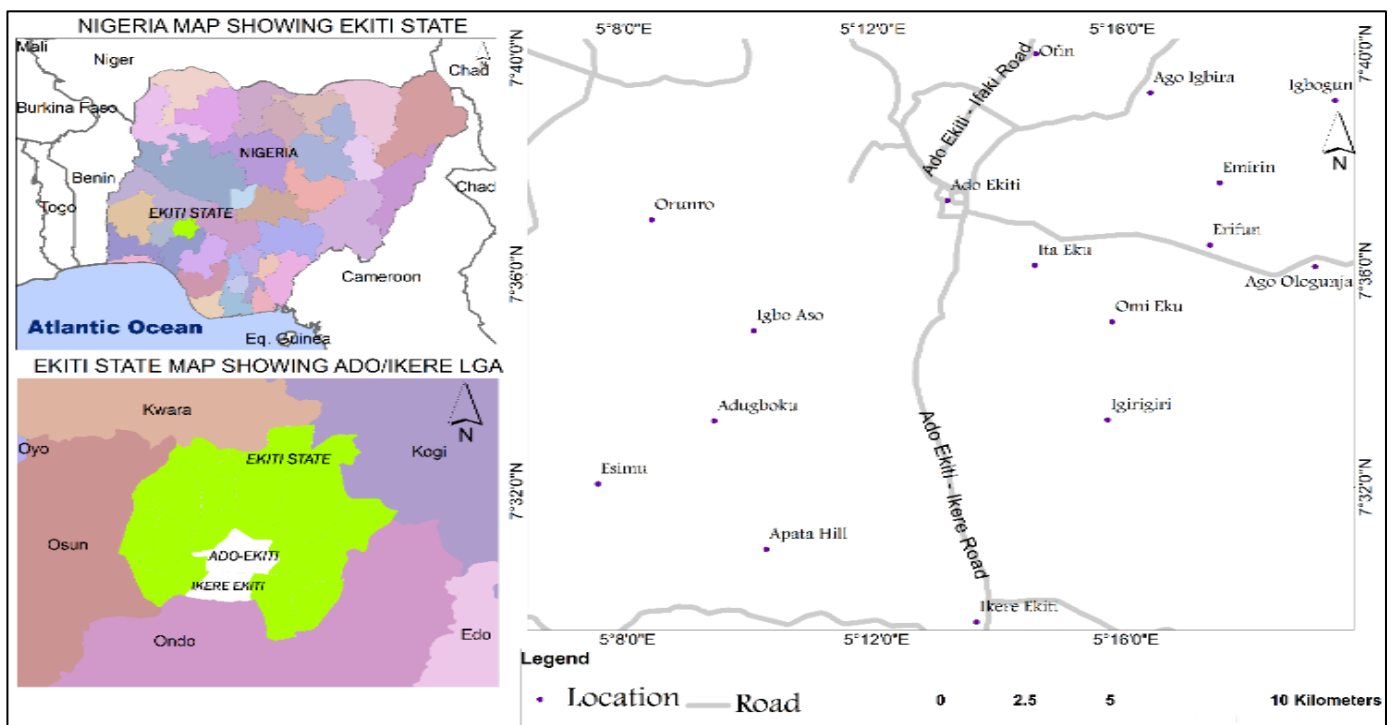


Figure 1: Location map showing Ado – Ikere Road.  
Source: Author, (2023).

## III. MATERIALS AND METHODS

Samples of asphalt concrete were collected from three failed sections along Ado-Ikere road, Ekiti State, Nigeria (Figure 1). The laboratory work utilized integrated investigations involving determination of the asphalt density, binder contents, Marshall stability, Marshall flow, void in mix, void filled with bitumen and grading envelope.

Bitumen Extraction and Grain-size Analysis experiments for gradation of aggregates were carried out on the samples. The bitumen extraction test enabled the separation of the binder from the mineral aggregates in the asphaltic paving mixture. The Centrifuge method for Bitumen Extraction Test as per standard by American Society for Testing Materials ASTM 2172 [12] was adopted.

The procedure in AASHTO T 27 / ASTM C 136 [16] was adopted for the gradation and sieve analysis test [13 - 15]. In the void and density analysis, the bulk density, voids in total mix (VTM), voids in mineral aggregate (VMA), and voids filled with asphalt (VFA) were determined. The Marshall stability test was performed as per Standard ASTM D 1559 / AASHTO T-245 [11].

The Marshall stability and flow test provides the performance prediction measure for the Marshall mix design method. The stability portion of the test measures the maximum load supported by the test specimen at a loading rate of 50.8 mm/minute. Selecting the required proportions of aggregates (fine and coarse), fillers, and bitumen for the design of pavement is critical to achieving the expected properties of the asphaltic concrete [4, 13].

The results obtained were examined in the context of the provisions of the 2007 Federal Ministry of Works and Housing Standard Specifications for Roads and Bridges to determine the compliance [2, 10].

## IV. RESULTS AND DISCUSSIONS

### IV.1 PROPERTIES OF ASPHALT CONCRETE

Values ranging from 6.01 – 6.45 %, 320 – 365 kg, 3.6 – 5.9 mm, and 4.2 – 6.0 % were obtained for bitumen content, stability, flow, voids in total mix, respectively (Table 1). The results revealed varying levels of compliance with the criteria of the FMW Standard Specifications (Figures 2 – 6) [10].

Table 1: Properties of asphalt concrete along Ado-Ikere Road.

Location	Properties	Test Results	FMW Limits
POINT A	BC	6.45	5.0 – 8.0 %
	Stability	365	≥ 350 kg
	Flow	3.6	2 mm – 4 mm
	Voids in mix	4.5	3 % - 5 %
POINT B	BC	6.19	5.0 – 8.0 %
	Stability	355	≥ 350 kg
	Flow	4.0	2 mm – 4 mm
	Voids in mix	4.2	3 % - 5 %
POINT C	BC	6.01	5.0 – 8.0 %
	Stability	320	≥ 350 kg
	Flow	5.9	2 mm – 4 mm
	Voids in mix	6.0	3 % - 5 %

BC = Bitumen Content.  
Source: Authors, (2023).

**IV.1.1 Bitumen Content**

With regards to bitumen content, Figure 2, all samples met the standard [10]. HMA that has too little asphalt binder can have lowered fatigue resistance and problems with raveling and

stripping. Bitumen should satisfy all the specifications laid down relating to penetration, softening point, ductility, flash point, wax content, loss on heating and retained penetration, solubility, viscosity at 60 °C and 135 °C [7, 8].

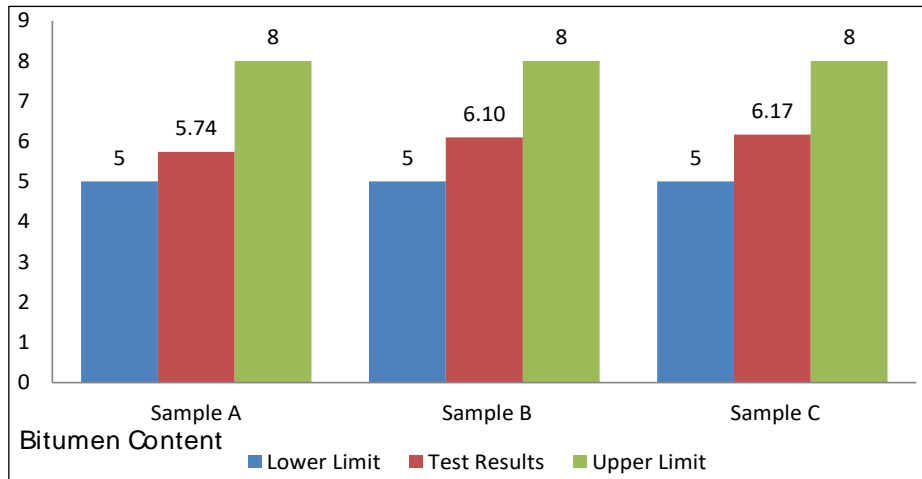


Figure 2: Bitumen content test results for bitumen samples.  
Source: Author, (2023).

**IV.1.2 Marshall Stability and Flow**

The standard of excess of 350 kg (≥ 350 kg) is prescribed for Marshall stability with a flow limit of 2 mm – 4 mm [10]. As low as 320 kg obtained, Figure 3, is a pointer to pavement failure.

A mix with a very high value of stability but a low flow value is not desirable (Figure 4). Requisite examination of the aggregates for their compliance with the standard specifications and the proportions selected are essential for optimum results.

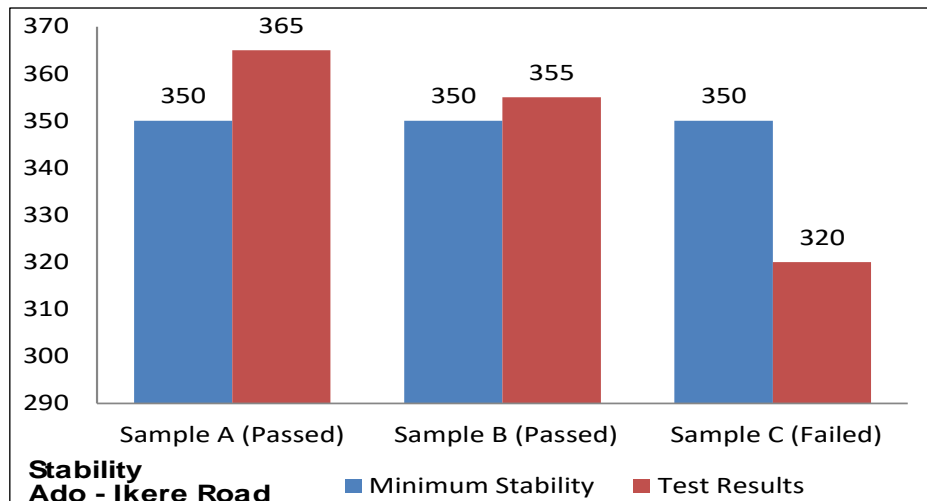


Figure 3: Stability test results for bitumen samples.  
Source: Author, (2023).

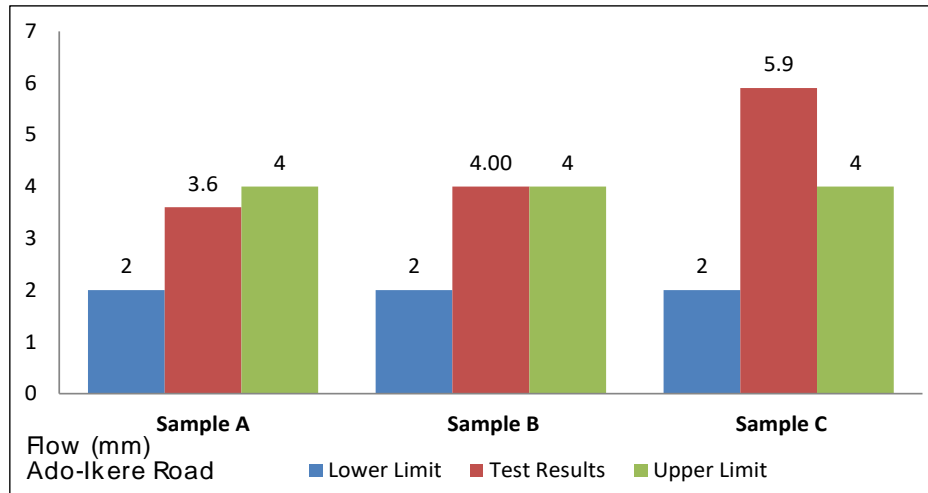


Figure 4: Flow test results for bitumen samples.  
Source: Author, (2023).

#### IV.1.3 Voids in Mix

A range of 3 % - 5 % void in mix is prescribed according to the provisions of FMW [10]. The air void content of bituminous materials is an important control parameter for the quality of

bitumen being laid and compacted. Asphalt without sufficient air entrapped in the layer will deform under traffic and result in a rutted and rough surface. Almost all samples fulfilled the standard criterion except at a point with value of 6% void in mix (Figure 5).

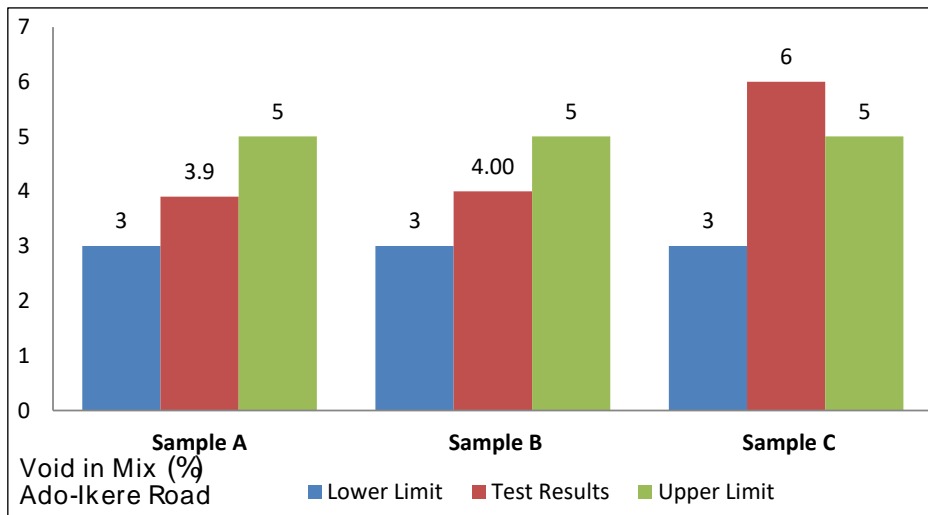


Figure 5: Void in mix test results for bitumen samples.  
Source: Author, (2023).

#### IV.1.4 Sieve Analysis

The sieve analysis of aggregates at the three points along the road (Tables 2 - 4) yielded the grading envelope for the segments as presented in Figure 6.

Table 2: Sieve analysis of aggregates extracted from sample A (ADO-IKERE PT A).

Sieve No	Weight retain (g)	% ret	% pass	SPECIFICATION	
25	0	0.00	100.00	100	100
19	55.6	5.56	94.44	100	100
12.5	132.5	13.25	81.19	85	100
9.5	39.7	3.97	77.22	75	92
4.75	183.9	18.39	58.83	65	82
2.36	172.9	17.29	41.54	50	65
1.18	83.4	8.34	33.20	36	51
0.6	79.4	7.94	25.26	26	40
0.3	61.6	6.16	19.10	18	30
0.15	63.6	6.36	12.74	13	24
0.075	28	2.80	9.94	7	14

Source: Author, (2023).

Table 3: Sieve analysis of aggregates extracted from sample B (ADO-IKERE PT B).

Sieve No	Weight retain (g)	% ret	% pass	SPECIFICATION	
25	0	0.00	100.00	100	100
19	53.3	5.33	94.67	100	100
12.5	130.4	13.04	81.63	85	100
9.5	37.5	3.75	77.88	75	92
4.75	185.4	18.54	59.34	65	82
2.36	170.6	17.06	42.28	50	65
1.18	86.7	8.67	33.61	36	51
0.6	80.4	8.04	25.57	26	40
0.3	63.4	6.34	19.23	18	30
0.15	60.2	6.02	13.21	13	24
0.075	30.1	3.01	10.20	7	14

Source: Author, (2023).

Table 4: Sieve analysis of aggregates extracted from sample C (ADO-IKERE PT C).

Sieve No	Weight retain (g)	% ret	% pass	SPECIFICATION	
25	31.8	3.18	96.82	100	100
19	62	6.20	93.80	100	100
12.5	195	19.50	74.30	85	100
9.5	53.5	5.35	68.95	75	92
4.75	171	17.10	51.85	65	82
2.36	158.6	15.86	35.99	50	65
1.18	63.2	6.32	29.67	36	51
0.6	58.7	5.87	23.80	26	40
0.3	49.2	4.92	18.88	18	30
0.15	51.8	5.18	13.70	13	24
0.075	17.3	1.73	11.97	7	14

Source: Author, (2023).

#### IV.2 INFLUENCE OF GRADATION

The grading curves and grading envelope obtained (Figure 6) showed that none of the samples fell completely within the lower and upper limits specified by FMW standard specifications. The

non-compliance of the extracted aggregates with the specification could hinder some other properties of asphalt concrete [2, 10].

The particle size distribution of the constituent aggregates is one of the most influential characteristics in determining how an HMA mixture will perform as a pavement material. Aggregate gradation influences almost every important.

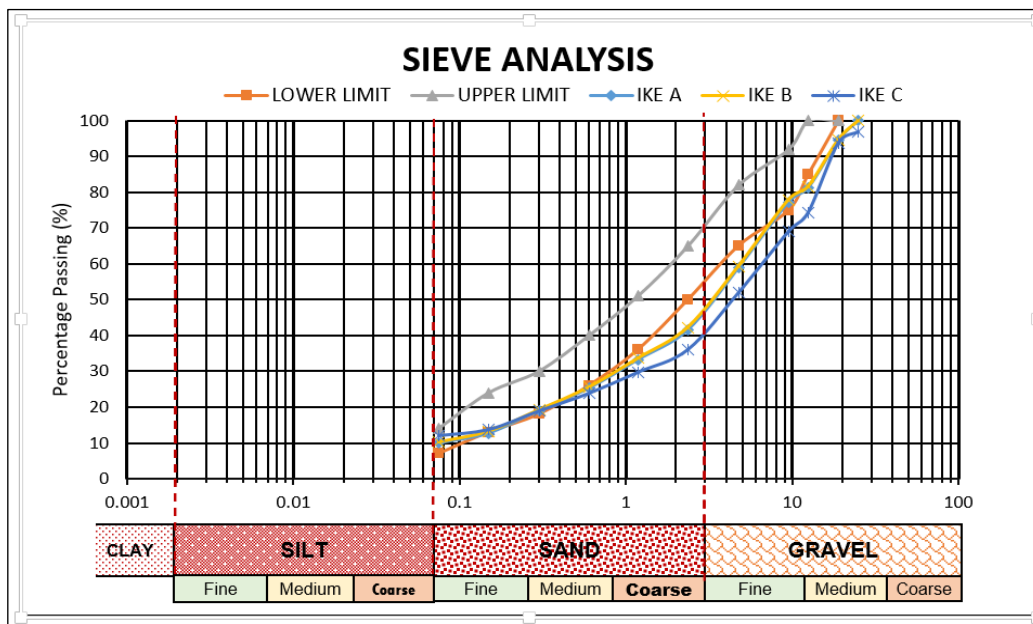


Figure 6: Grading curves and grading envelope.

Source: Author, (2023).

HMA property including stiffness, stability, durability, permeability, workability, fatigue resistance, skid resistance and resistance to moisture damage [2, 6, 9].

Poor gradation of aggregates resulting in low stability and flow as well as excess voids in the concrete was apparent and capable of inducing pavement failure. This results agreed with the

works of similar authors including [3], [6] and [16]. Voids of the order of 6.0 % and flow of 6.3 mm observed along Ado – Ikere road with associated poor stability as low as 320 kg could compromise the integrity of the asphaltic concrete for road construction within the given geological environment. The road is characterized by a grading envelope indicating poor gradation with all curves completely falling out of the envelope and attendant poor stability, excess flow and voids (Figure 6). These would readily precipitate pavement failure along the road.

The main purpose of highway pavement traditionally has been to provide smooth surface over which vehicles can move safely from one place to another. However, the flexible pavements under investigation readily show defects like rutting, fatigue failure, low skid resistance and so on, causing the pavement to fail before design life [2, 12, 16]. The poor gradation of aggregates has led to unsatisfactory results which significantly impact on the performance of asphalt concrete leading to premature failure of the pavement. It is essential to put in place an effective procedure for quality assurance quality control (QA/QC) and subsequent characterization.

## V. CONCLUSIONS

An assessment of the asphaltic mix on failed sections of Ikere-Ado Ekiti road has been carried out. The results revealed varying levels of compliance with the criteria of Federal Ministry of Works and Housing Standard Specifications for Roads and Bridges. Well graded aggregates and mineral filler resulting in maximum density when mixed with optimum quantity of bitumen readily yields a mix with very high stability.

The use of poorly graded mineral aggregates resulted in the mix having poor stability, inadequate flow and excess voids. These unsatisfactory results significantly impact the performance of asphalt concrete leading to premature failure of the pavement.

In order to ensure satisfactory behaviour and performance of the mixture under traffic, a mix design must be performed under strict compliance with the standard specifications. Quality assurance test must be ensured before the commencement of work and during project execution. This should take cognizance of soil characterization results in line with the anticipated axle load and capacity. Asphaltic mixes used as wearing course of the pavements should receive considerable attention.

## VI. AUTHOR'S CONTRIBUTION

**Conceptualization:** Akintunde Akinola Oyedele.

**Methodology:** Akintunde Akinola Oyedele.

**Discussion of results:** Akintunde Akinola Oyedele.

**Writing – Original Draft:** Akintunde Akinola Oyedele.

**Writing – Review and Editing:** Akintunde Akinola Oyedele.

**Resources:** Akintunde Akinola Oyedele.

**Supervision:** Akintunde Akinola Oyedele.

**Approval of the final text:** Akintunde Akinola Oyedele.

## VII. ACKNOWLEDGMENTS

The useful suggestions of the Editor-in-Chief and the anonymous reviewers are appreciated.

## VIII. REFERENCES

[1] Almeida, J.R., Boeira, F.D., Specht, L.P., Cervo, T.C., Pereira, D.S., Centofante R., Barbosa JR., Silva, C.C. "Avaliação laboratorial do tipo e teor de ligante e da granulométrica deformação permanente de misturas asfálticas." *Transportes*, vol. 26, no. 2, pp. 1-15. DOI:10.14295/transportes.v26i2.1407, 2018.

[2] Akinleye, M.T., Tijani, M.A. "Assessment of Quality of Asphalt Concrete used in Road Construction in South West Nigeria." *Nig J. Technol Dev*, vol. 14, no. 2, pp. 52-55, 2017.

[3] Carmo, C.A.T., Pereira, G.S., Marques, G.L.O., Borges, P.R. "Structural sensitivity of an asphalt pavement to asphalt binder content and mix design method." *TRANSPORTES*, vol. 28, no. 4, ISSN: 2237-1346, 2021.

[4] Al-Humeidawi, B.H. "Experimental characterization of rutting performance of HMA designed with aggregate gradations according to Superpave and Marshall methods." *World J. Eng & Technol*, vol. 4, pp. 477-487. DOI: 10.4236/wjet.2016.43048, 2016.

[5] Hemida, A., Abdelrahman, M., Deef-Allah, E. "Quantitative evaluation of asphalt binder extraction from hot mix asphalt pavement using ashing and centrifuge methods." *Transportation Eng.*, vol. 3, 100046, <https://doi.org/10.1016/j.treng.2021.100046>, 2021.

[6] Akijie, I., Oyekan, G.L. "Stabilization assessment of aggregates in asphalt concrete mixtures." *Int J. Scient & Eng Researc.*, vol. 3, no. 4. pp. 695-699, 2012.

[7] Eberhardsteiner, L., Blab, R. "Design of bituminous pavements – a performance-related approach". *Road Mat & Pavement Design*, vol. 20, no. 2, pp. 244-258, DOI: 10.1080/14680629.2017.1380689, 2019.

[8] Mohammed, A., Aliyu, I., Sulaiman, T.A., Umar, H.A., Jubril, Y. "Appraisal of Asphalt Concrete with Coal Bottom Ash as Mineral Filler." *FUOYE J. Eng & Technol.*, vol. 6, no. 2, pp. 105-110, 2021.

[9] Roberts, F.L., Kandhal, P.S., Brown, E.R., Lee, D-Y., Kennedy, T.W. "Hot Mix Asphalt Materials, Mixture Design, and Construction." Vol. 8, National Asphalt Pavement Association, Research and Education Foundation, Lanham. 603 p. 1996.

[10] Federal Ministry of Works and Housing - FMW. "Pavement and materials design in highway manual part 1: Design." 3. Federal Ministry of Works, Abuja, Nigeria. 2007.

[11] Fang, M., Park, D., Singuranayo, J.L., Chen, H., Li, Y. "Aggregate gradation theory, design and its impact on asphalt pavement performance: a review." *Int J. Pavement Eng.*, vol. 20, no. 12, pp.1408-1424, DOI: 10.1080/10298436.2018.1430365, 2019.

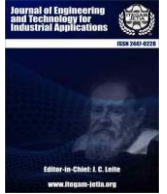
[12] ASTM D2172-05. "Standard test methods for quantitative extraction of asphalt binder from asphalt mixtures." ASTM International. West Conshohocken, PA. 2005.

[13] ASTM (American Society for Testing and Materials). "Standard test method for sieve analysis of fine and coarse aggregates. C136." West Conshohocken, PA, USA. 2001.

[14] American Association of State Highway and Transportation Officials (AASHTO). "Standard Specifications for Transportation Materials and Methods of Sampling and Testing, Twentieth Edition." American Association of State Highway and Transportation Officials, Washington, D.C. 2000.

[15] ASTM (American Society for Testing and Materials). "Standard test method for Marshall stability and flow of asphalt mixtures. D6927". West Conshohocken, PA, USA. 2005.

[16] Ogundipe, O.M. "Marshall stability and flow of lime-modified asphalt concrete." *Transportation Researc Procedia*, vol. 14, pp. 685 – 693, 2016.









### RESEARCH ARTICLE

### OPEN ACCESS

## DESIGN AND CONSTRUCTION OF A FUZZY LOGIC SOLAR TRACKER PROTOTYPE FOR THE OPTIMIZATION OF A PHOTOVOLTAIC SYSTEM

Omar Beltrán González<sup>1</sup>, Jesús Hernández Aguilar<sup>2</sup>, Francisco Eneldo López Monteagudo<sup>\*3</sup>, Rafael Villela Varela<sup>4</sup>, Aurelio Beltrán Telles<sup>5</sup> and Claudia Reyes Rivas<sup>6</sup>

<sup>1, 2, 3, 4, 5, 6</sup> Autonomous University of Zacatecas, Av. López Velarde No. 801 CP 98060 Zacatecas, México.

<sup>1</sup> <http://orcid.org/0009-0006-6647-7014> , <sup>2</sup> <http://orcid.org/0009-0000-6461-0762> , <sup>3</sup> <http://orcid.org/0000-0001-6082-1546> ,  
<sup>4</sup> <http://orcid.org/0000-0003-0088-4718> , <sup>5</sup> <http://orcid.org/0000-0001-8757-2041> , <sup>6</sup> <http://orcid.org/0000-0001-9028-2096> 

Email: [omar@uaz.edu.mx](mailto:omar@uaz.edu.mx), [jesush@uaz.edu.mx](mailto:jesush@uaz.edu.mx), [\\*eneldolm@yahoo.com](mailto:*eneldolm@yahoo.com), [wrwrmx@yahoo.com.mx](mailto:wrwrmx@yahoo.com.mx), [abeltral@uaz.edu.mx](mailto:abeltral@uaz.edu.mx), [clausy\\_17@yahoo.com](mailto:clausy_17@yahoo.com)

### ARTICLE INFO

#### Article History

Received: March 29<sup>th</sup>, 2023

Accepted: April 26<sup>th</sup>, 2023

Published: April 29<sup>th</sup>, 2023

#### Keywords:

Photovoltaic panels,  
Solar energy,  
Solar tracker.

### ABSTRACT

In this article, a fuzzy logic solar tracker was designed and implemented to increase the efficiency of a photovoltaic system by updating the position of the panel throughout the day for optimal use of solar radiation. In the design and implementation of the solar tracker, different control strategies were analyzed, concluding that the fuzzy control satisfies all the requirements of the photovoltaic system with a solar tracker, the developed prototype underwent different tests in a determined period of time to validate the performance of the solar tracker. system compared to one with a fixed position, achieving an increase of 40% compared to fixed solar systems.



Copyright ©2023 by authors and Galileo Institute of Technology and Education of the Amazon (ITEGAM). This work is licensed under the Creative Commons Attribution International License (CC BY 4.0).

## I. INTRODUCTION

At present, the predominant energy medium is from fossil fuels, which is being diminished due to industrial growth, means of transportation and population, increasing demand for it, to meet this increase in demand. demand the most viable alternative is renewable energy. Within these renewable energies, solar energy is the most viable because it is a resource that occurs anywhere, it does not depend on its geographical location, unlike other alternative energies [1].

Photovoltaic solar energy is that which is obtained through the direct transformation of the sun's energy into electrical energy through solar cells [2].

Solar energy is one of the most viable alternative sources since it is present throughout the planet, the energy from the sun is inexhaustible and contributes to reducing current environmental problems that have been a consequence of the irrational use of fuels. fossils [3].

The energy produced by solar panels depends directly on the position of the sun with respect to said panel. The constant change of position of the sun considerably limits the efficiency of a panel in a fixed state, therefore, through the use of solar trackers,

it is sought to make the most of the irradiation of the sun's rays, increasing the power level. electricity generated in the photovoltaic system compared to fixed systems [4].

The photoelectric cells transform solar energy into electricity in the form of direct current and this is transformed into alternating current by means of an inverter to guarantee the parameters of the electrical network in interconnected systems, so that the converter works in the zone of maximum efficiency solar trackers are used [5].

In photovoltaic systems connected to the electrical grid, the inverter is the central core and must have certain protections in situations that may occur in the electrical grid, such as voltage out of range, grid outage, grid phase shift. [6].

Solar trackers, depending on the type of movement, can be one-axis or two-axis [7].

In single-axis solar trackers, the solar panels remain approximately perpendicular to the sun's rays, following the sun from east to west, with a minimum degree of complexity and lower cost compared to other types of trackers. The limitation of this type of tracker is that it cannot fully track the sun, since it can only track the azimuth or the solar inclination, but not both [8].

Two axis solar trackers have two degrees of freedom and are capable of fully tracking the sun, both in inclination and azimuth, although the performance of the installation may be superior compared to single-axis ones, their cost is much higher [9].

The tracker described in this article belongs to the classification of trackers of an azimuthal axis whereby the panels remain approximately perpendicular to the sun's rays, following the sun from sunrise to sunset.

## II. METHODOLOGY

The objective of this article was to design and implement a control system that allows the photovoltaic system to follow the path of the sun to improve the efficiency in the generation of electrical energy compared to fixed systems.

Fuzzy logic has played a vital role in advancing practical solutions for a wide variety of applications in automatic control engineering, digital signal processing, communications, expert systems, medicine, etc. However, the most significant applications of fuzzy systems have been concentrated specifically in the area of automatic control.

Different studies applied to fuzzy control theory have shown that fuzzy learning and/or fuzzy control algorithms are one of the most active and fruitful areas of research in recent years within the field of fuzzy logic [10].

### II.1 ESTRUCTURA DE LOS SISTEMAS DIFUSOS

The Different studies applied to fuzzy control theory have shown that fuzzy learning and/or fuzzy control algorithms are one of the most active and fruitful areas of research in recent years within the field of fuzzy logic.

From the conceptual point of view, the design of fuzzy systems from input-output pairs have been classified into two types. The first type of classification suggests that the rules are generated through the input-output pairs and the structure of the fuzzy system is built from these rules, from the fuzzy inference mechanism of the fuzzifier and the defuzzifier. In the second classification, the structure of the fuzzy system is specified first so that some parameters in the fuzzy structure are free to change and these are determined according to the input-output pairs. Although regularly some applications of fuzzy control to industrial processes have produced results superior to their equivalents obtained by classical control, the domain of these applications has experienced a serious limitation when expanding it to more complex systems, due to the fact that There is not yet a complete theory to determine the performance of the systems from the change in its parameters or variables.

Fuzzy inference systems have currently found several successful applications within a wide variety of areas such as automatic control, data classification, decision analysis, expert systems, time series prediction, etc. robotics and pattern recognition. Because of their multidisciplinary nature, fuzzy inference systems are known as expert systems, fuzzy models, fuzzy logic controllers, or just fuzzy systems.

Essentially a fuzzy system, it is a structure based on knowledge defined through a set of fuzzy rules, which contain a fuzzy logical quantification of the expert's linguistic description of how to perform adequate control. Figure 1 illustrates the block diagram and the basic components of a fuzzy system where the classical sets  $U_i$  and  $Y_i$  are called the universe of discourse for  $u_i$  and  $y_i$  respectively. In particular,  $u_i \in U_i$  with  $i = 1, 2, 3, \dots, n$  and

$y_i \in Y_i$  with  $i = 1, 2, \dots, m$ , where  $u_i$  and  $y_i$  correspond to the inputs and outputs of the fuzzy system.

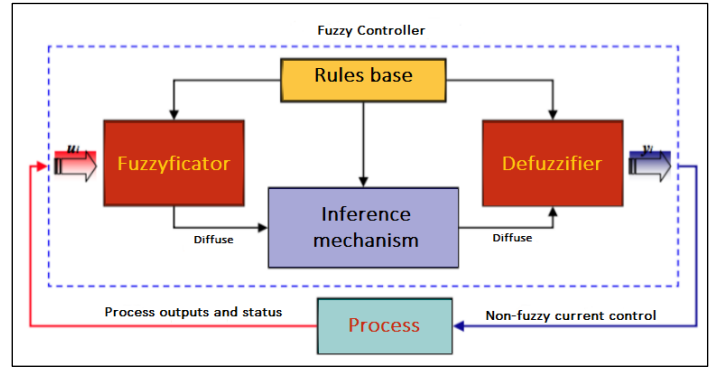


Figure 1: General scheme of fuzzy control.

Source: [12].

In figure 1, it can be seen that the fuzzy system uses fuzzy sets, defined by the fuzzy rule base, to quantify the information in the rule base and that the inference mechanism operates on these fuzzy sets to produce new sets. Therefore, it is necessary to specify how the system will convert the numerical inputs  $u_i \in U_i$  into fuzzy sets, a process called "fuzzification", such that they can be used by the fuzzy system. Similarly, the process called defuzzification describes the mapping of a space of fuzzy control actions into non-fuzzy control actions. Defuzzification therefore generates a non-fuzzy control action which we generally denote by  $y_{qcrips}$  and is the best representation of an inferred fuzzy output.

The fuzzification process consists of a transformation of a datum from a classical set to its corresponding fuzzy set, therefore, we denote by  $U_i^*$ , the set of all possible fuzzy sets that can be defined by  $U_i$  and given  $u_i \in U_i$ , let us denote the fuzzy transformation of  $u_i$  to a fuzzy set by  $A_{ifuz}$ , which is defined in the universe of discourse  $U_i$ . The transformation from a classical set to a fuzzy set is produced by using the fuzzification operator  $F$ , [11], defined by  $F: U_i \rightarrow U_i^*$ , where  $F(u_i) = A_{ifuz}$ . Regularly the use of the singleton type fuzzifier is the most widely used for applications in the area of automatic control and this is defined as a fuzzy set  $A_{ifuz} \in U^* \cdot i$  with membership function.

$$\mu_{A_i}^{fuz}(x) = \begin{cases} 1 & \text{si } x = u_i \\ 0 & \text{en otro caso} \end{cases} \quad (1)$$

Any fuzzy set with the form 1 in its membership function is called "singleton", figure 2.

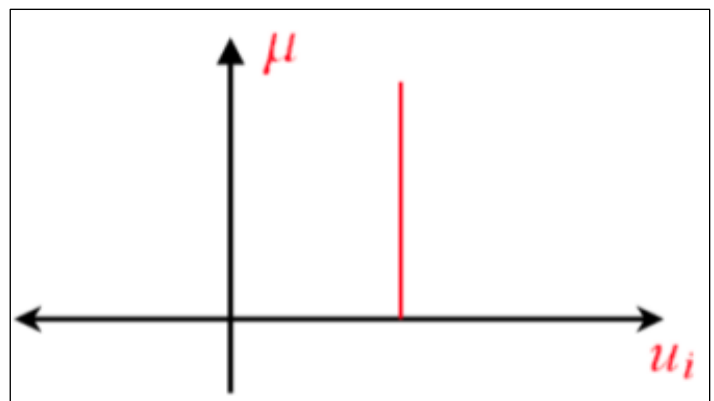


Figure 2: Singleton membership function.

Source: [12].



The first step for the control design is the transformation of the domain so that the values delivered by the sensors are transformed to fuzzy inputs. For each input and output it is required to have an adequate number of labels that adequately describe their behavior. A universe of discourse with more labels is more accurate than one with few labels, however, it will also require more processing time. Also, an excessive number of labels can lead to an unstable fuzzy system.

### II.2 FUZZY INFERENCE MECHANISM

The fuzzy inference mechanism is the core of any fuzzy controller. Its behavior is generally characterized by a set of fuzzy rules of the form:

$$\text{If } x \text{ is } A \text{ then } y \text{ is } B \quad (2)$$

Where A and B are linguistic values defined by a fuzzy set in a universe X and Y respectively. The If clause, an antecedent, is a control action given to the process under control. With a set of fuzzy rules, the fuzzy inference mechanism is capable of deriving a control action for a set of input values, determining a control action for the observed inputs, which represent the state of the process to be controlled. -side by using control rules. The expression "If x is A then y is B," which is regularly abbreviated  $A \rightarrow B$ , is essentially a binary relation R of the variables x and y on the product space  $X \times Y$ . There are several fuzzy inference methods that can be formulated through the t-norm and s-norm operators to calculate the fuzzy relation  $R = A \rightarrow B$ .

### II.3 FUZZY INFERENCE MECHANISM

Defuzzification is defined as a mapping from a fuzzy set B' in  $V \subset R$  (which is the output of fuzzy inference) to an element of a classical set  $yq^{crisp} = y * \in V$ .

Conceptually, the task of defuzzifying is to specify a point, an element of V, that reflects the best representation of the fuzzy set B'. To date there is no optimal algorithm for defuzzification, however, there are different defuzzification techniques that are easy to implement.

There are different fuzzy controllers, the most widely used are Mamdani and Sugeno, which have been used successfully in a wide variety of applications in the fuzzy control community. Although, the objective of the Mamdani fuzzy controller is to represent a successful human operator, the Sugeno-type fuzzy controller is suggested to be more efficient in computational and learning methods.

## III. SOLAR TRACKER CONTROL PLATFORM DESIGN

For the design of the control platform, two degrees of freedom were used, considering an azimuthal axis and a polar axis, allowing the photovoltaic cell system to position itself parallel to the sun's rays, achieving its highest efficiency. regardless of your geographical position or time of day. For the implementation of the controller, an Arduino card was used through which the movement of the two motors is controlled, positioning the platform in its different axes.

The support structure was designed considering the type of movement desired for the solar tracker, the size of the solar panels and the available space.

The control system uses optical sensors, which monitor the variations in light levels emitted by the sun in order to know the position in which it is located. In this way, analog signals are

obtained that will later be converted to digital signals and implemented as variables in a program in charge of feeding the motors to move the structure and position it parallel to the incidence of the sun's rays.

The built mechanical structure is made up of various parts:

1. Structure support
2. Rectangular panel support
3. Concrete base
4. Counterweight
5. DC motors
6. Toothed disk azimuthal movement
7. Worm azimuthal movement
8. Polar movement worm
9. Toothed disc polar movement

In the figure 3 shows the parts of the mechanical structure.



Figure 3: Parts of the structure.  
Source: Authors, (2022).

In the figure 4 shows the parts of the azimuthal axis.

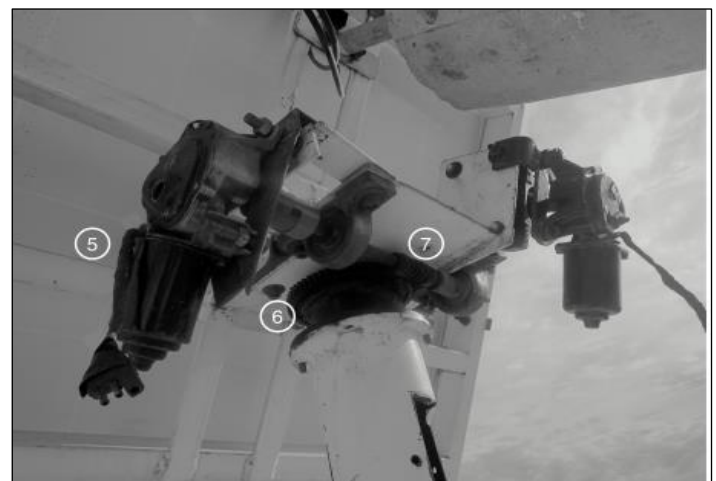


Figure 4: Parts of the azimuthal axis structure.  
Source: Authors, (2022).

In the figure 5 shows the parts of the polar axis.

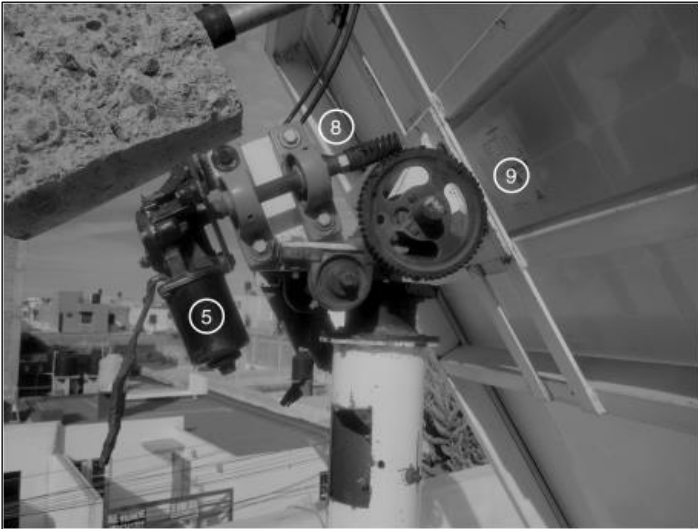


Figure 5: Shows the parts of the azimuthal axis.  
Source: Authors, (2022).

In the figure 6 shows the solar panel used.

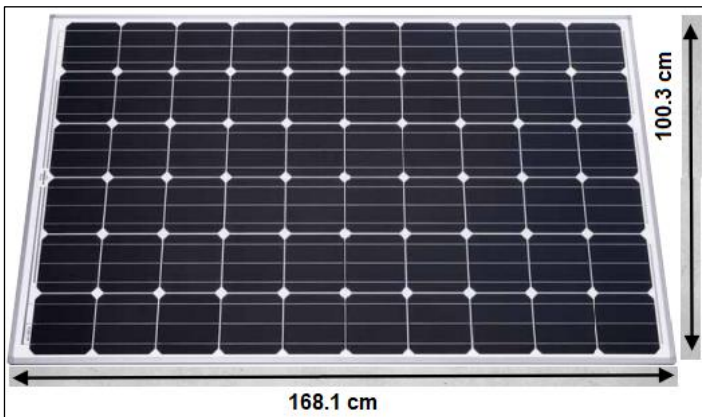


Figure 6: Used solar panel (Produced in Germany).  
Source: Authors, (2022).

In order to monitor the solar movement throughout the day and during the seasons of the year, a circuit was implemented to compare the reading of a pair of photoresistive components (LDR), located parallel to each other on the surface and separated by a perpendicular plate that provides a shadow that makes the readings of said devices vary, generating an inequality unless they are located parallel to the sun, this inequality in the readings of said elements is used to locate the panel in the optimal position. The circuit was located in a translucent container conditioned to avoid the interference of solar rays with incidents not necessary for its application. The circuit shown in figure 5 has an arrangement of L298N, which can handle a voltage of up to 46 Volts, through the two output terminals the direction of rotation of the motor is controlled, the supply voltage for this motor is 17 volts which are obtained from an external source, the control system has three terminals for the direction and speed control signals of the motor to be controlled. If both inputs are low, the motor will be off and there is no power consumption, the speed being controlled by PWM (Pulse Width Modulation). Applying the PWM signal to one of the control inputs of the bridge.

To control the system, an Arduino card supported on a free Hardware platform was used, based on a board with a

microcontroller, which is programmed using its own language and a free integrated development environment (IDE). As it is a free Hardware development platform, both its design and its implementation are free without the need to previously acquire a license.

The developed platform used an Arduino UNO with an ATmega328 microcontroller (data-sheet). It has 14 digital input/output pins (of which 6 of them were used as PWM outputs), 6 analog inputs, a 16MHz crystal oscillator, a USB connection, a power jack, an ICSP header, and a reset button. The microcontroller connects to a computer via USB, is powered by an AC/DC adapter, or a battery. The Arduino Uno Board differs from its predecessor in that it does not require the use of the FTDI USB-to-serial driver chip. Instead, it has the Atmega8U2 programmed as a USB-to-serial converter. ONE.

Atmega328 has 32 KB of flash memory for code storage (of which 0.5 KB is used for the bootloader); it also has 2 KB of SRAM and 1 KB of EEPROM (which can be read and written with the EEPROM library).

Each of the 14 digital pins on the Arduino UNO board can be used as input or output, using the pinMode (), digitalWrite (), and digitalRead () functions. They all operate at 5 volts, each pin can supply or receive a maximum of 40 mA and have an internal pull-up resistor (disconnected by default) of 20-50 KΩ. In addition, some pins have specialized functions. The configuration of the Arduino UNO used is shown in figure 7.

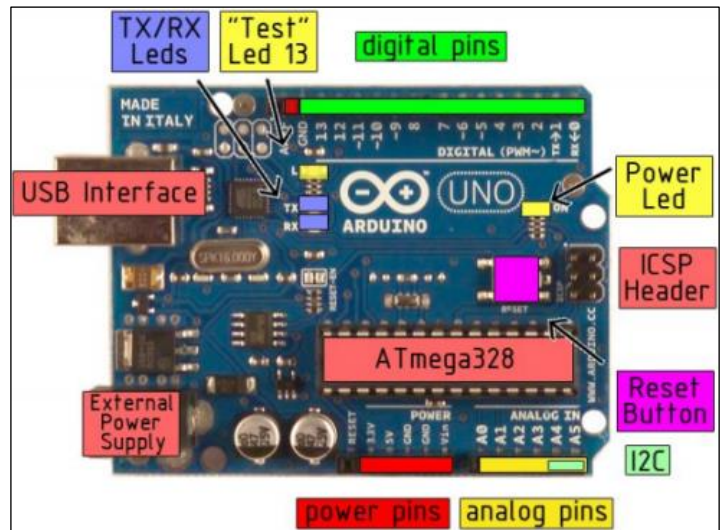


Figure 7: Arduino UNO Configuration.  
Source: [10].

The Hardware of the card used consists of a board with an Atmel AVR microcontroller and input/output ports.

#### IV. PROGRAMMING OF THE MEMBER UNIONS OF THE SOLAR TRACKER

For the elaboration of the control program of the solar tracker, knowing the behavior of the different devices that will make possible the control of the system, the member functions that are used in the programming will be elaborated, to corroborate the correct operation, the Fuzzy Logic Controller Design package from the LabView program, this was only used for the simulation of the control algorithms since Arduino does not have a simulation environment. For each of the input and output variables, the universe of discourse is defined in which the member functions of each of the variables will be contained.

For the fuzzy control, a natural language was used through which the functions of each variable are expressed with a name to distinguish them and use them later.

Table 1: Input variables.

Name	Range	Number of member functions
Photo_l $0 \geq 600$ 4	Photo_l $0 \geq 600$ 4	Photo_l $0 \geq 600$ 4
Photo_r $0 \geq 600$ 4	Photo_r $0 \geq 600$ 4	Photo_r $0 \geq 600$ 4
Pot_A 660 $\geq 880$ 3	Pot_A 660 $\geq 880$ 3	Pot_A 660 $\geq 880$ 3
Pot_G Trapezoide 3	Pot_G Trapezoide 3	Pot_G Trapezoide 3

Source: Authors, (2022).

In the table 2 shows the output variables.

Table 2: Output variables.

Name	Range	Number of member functions
ACCW	$0 \geq 255$	3
ACW	$0 \geq 255$	3
GCW	$0 \geq 255$	3
Pot_G	$0 \geq 255$	3

Source: Authors, (2022).

In the table 3 shows the member functions of Photo l.

Table 3: Photo member functions l.

Membership Function	Shape	Points
DL	Trapezoide	500 ; 525 ; 600 ; 600
DML	Trapezoide	300 ; 400 ; 400 ; 500
ML	Trapezoide	100 ; 200 ; 200 ; 300
BL	Trapezoide	0 ; 0 ; 75 ; 100

Source: Authors, (2022).

Obtaining the graph shown in figure 8 for the member functions of Photo l.

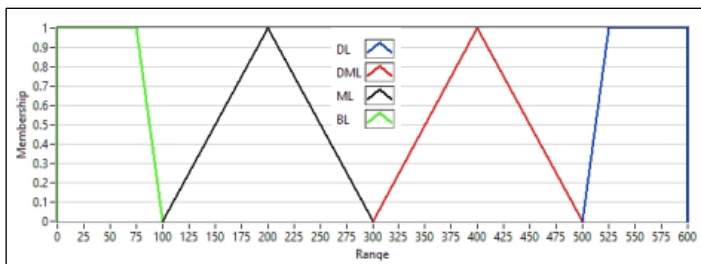


Figure 8: Graph of member functions of Photo l.

Source: Authors, (2022).

In the table 4 shows the member functions of Photo r.

Table 4: Photo member functions r.

Membership Function	Shape	Points
DR	Trapezoide	500 ; 525 ; 600 ; 600
DMR	Trapezoide	300 ; 400 ; 400 ; 500
MR	Trapezoide	100 ; 200 ; 200 ; 300
BR	Trapezoide	0 ; 0 ; 75 ; 100

Source: Authors, (2022).

Obtaining the graph shown in figure 9 for the member functions of Photo r.

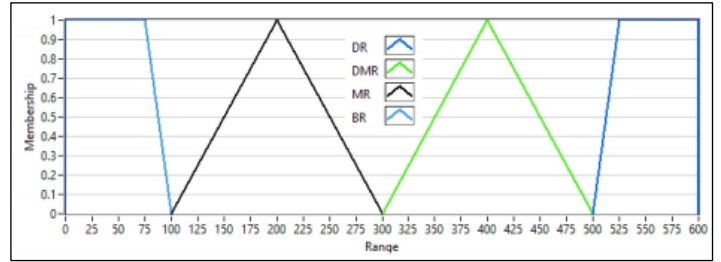


Figure 9: Graph of member functions of Photo r.

Source: Authors, (2022).

In the table 5 shows the member functions of potentiometer A.

Table 5: Member functions of potentiometer A.

Membership Function	Shape	Points
Amin	Trapezoide	660 ; 660 ; 660 ; 700
Asafe	Trapezoide	700 ; 700 ; 840 ; 840
Amax	Trapezoide	840 ; 880 ; 880 ; 880

Source: Authors, (2022).

Obtaining the graph shown in figure 10 for the member functions of potentiometer A.

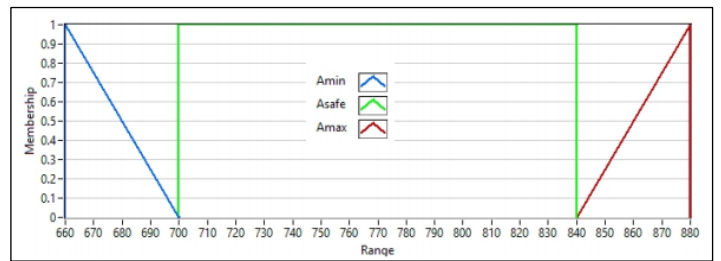


Figure 10: Graph of member functions of Potentiometer A.

Source: Authors, (2022).

In the table 6 shows the member functions of potentiometer G.

Table 6: Member functions of potentiometer G.

Membership Function	Shape	Points
Gmin	Trapezoide	450 ; 450 ; 450 ; 500
Gsafe	Trapezoide	500 ; 500 ; 900 ; 900
Gmax	Trapezoide	900 ; 950 ; 950 ; 950

Source: Authors, (2022).

Obtaining the graph shown in figure 11 for the member functions of potentiometer G.

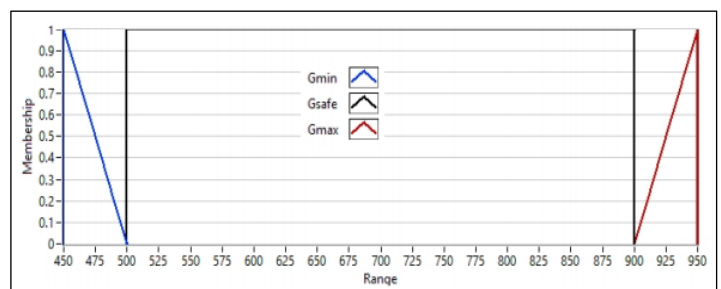


Figure 11: Graph of member functions of Potentiometer G.

Source: Authors, (2022).

In the table 7 shows the member functions of the Polar motion motor.

Table 7: Functions member of the Polar motion motor.

Membership Function	Shape	Points
OFF_ACCW	Trapezoide	0
M_ACCW	Trapezoide	100 ; 140 ; 140 ; 180
ON_ACCW	Trapezoide	180 ; 200 ; 240 ; 255

Source: Authors, (2022).

Obtaining the graph shown in figure 12 for the member functions of the Polar movement motor.

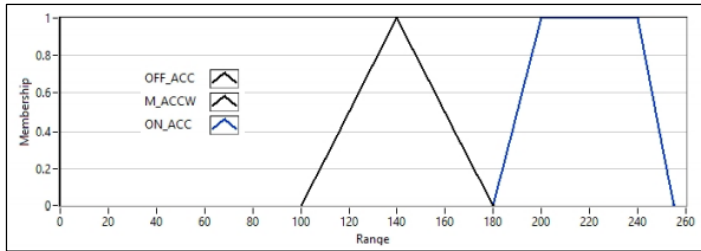


Figure 12: Graph of member functions of the Polar motion motor. Source: Authors, (2022).

In the table 8 shows the member functions of the Polar motion engine.

Table 8: Functions member of the Polar motion engine.

Membership Function	Shape	Points
OFF_ACW	Singleton	0
M_ACW	Trapezoide	100 ; 140 ; 140 ; 180
ON_ACW	Trapezoide	180 ; 200 ; 240 ; 255

Source: Authors, (2022).

Obtaining the graph shown in figure 13 for the member functions of the Polar movement motor.

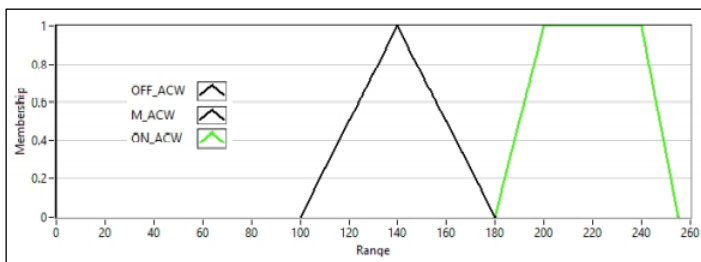


Figure 13: Graph of member functions of the Polar motion motor. Source: Authors, (2022).

In the table 9 shows the member functions of the Azimuthal movement motor.

Table 9: Functions member of the Polar motion motor.

Membership Function	Shape	Points
OFF_GCCW	Singleton	0
M_GCCW	Trapezoide	120 ; 130 ; 170 ; 180
ON_GCCW	Trapezoide	180 ; 200 ; 240 ; 255

Source: Authors, (2022).

Obtaining the graph shown in figure 14 for the member functions of the Azimuthal movement motor.

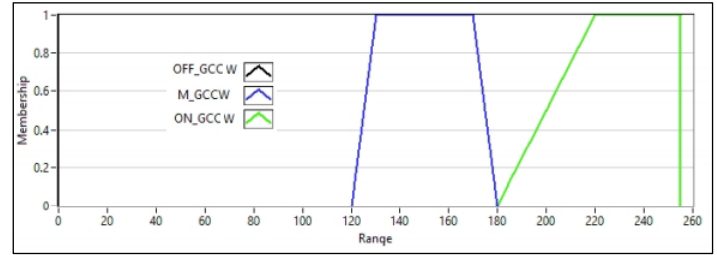


Figure 14: Graph of member functions of the Azimuthal movement motor. Source: Authors, (2022).

In the table 10 shows the member functions of the Azimuthal movement motor.

Table 10: Azimuthal moving engine member functions.

Membership Function	Shape	Points
OFF_GCW	Singleton	0
M_GCW	Trapezoide	120 ; 130 ; 170 ; 180
ON_GCW	Trapezoide	180 ; 220 ; 255 ; 255

Source: Authors, (2022).

Obtaining the graph shown in figure 15 for the member functions of the Azimuthal movement motor.

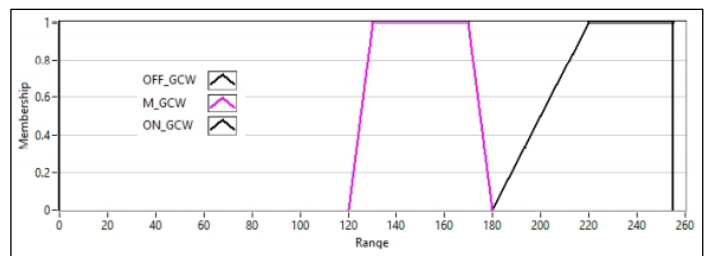


Figure 15: Graph of member functions of the Azimuthal motion motor. Source: Authors, (2022).

## V. RESULTS AND DISCUSSIONS

From the analysis of the data, the hypothesis on the increase in the level of electrical power generated in the photovoltaic system using solar trackers, unlike fixed systems, is corroborated.

In the present research work, a functional fuzzy control system was designed and implemented in a mechanical structure; to which different tests were carried out with satisfactory results. The results were obtained by means of the Arduino card, sensing the photoresistive elements between the values of 0 to 1023, varying the readings in a range of 0 to 600 depending on the incidence of solar rays.

In order to verify the correct operation of the control system of the solar tracker, calibration tests were carried out making a greater amount of light fall on one of the photosensitive elements and checking that the motor rotates in that direction.

To corroborate the objective set out in the investigation "A control system was designed to improve the efficiency for the generation of electrical energy with a solar tracker". Measurements were made to compare the energy generated by a fixed panel and the automated system with the implemented fuzzy control, for which I connect a load made up of five 60-watt spotlights placed in series.

Data acquisition was carried out over three days during the month of November 2020, obtaining a total of 113 samples for each

day; using for this purpose four multimeters connected to the load: two of them used for voltage readings and the other two for current readings in both cases, both in the fixed state and in the mobile state.

A test was carried out with a moving solar panel taking into account only the polar movement of the structure from an initial position of 15o inclination on said axis and facing east for sunrise. The control system designed maintained the orthogonality between the panel and the incidence of the sun's rays in order to obtain the

greatest possible efficiency throughout the course of the day, controlling the position through the use of a card. Arduino through the values delivered by the photoresistors moving it as appropriate.

Voltage and current measurements were carried out between 8:40 a.m. and 5:00 p.m. and 6:00 p.m. and with these readings the power and energy generated by the solar panel were determined.

In the table 11 shows the measurements of the first day between 8:40 a.m. and 5:00 p.m. and 6:00 p.m.

Table 11: Comparative measurements of the first day.

Hour	fixed panel			mobile panel		
	Voltage	Current	Power	Voltage	Current	Power
8:40	29.86	1.065	31.8009	33.1	1.1	36.41
8:45	30.25	1.075	32.5187	33.4	1.11	37.07
8:50	30.69	1.084	33.2679	33.3	1.11	36.96
8:55	30.89	1.067	32.9596	33.2	1.11	36.85
9:00	31.14	1.093	34.0360	33.1	1.11	36.74
9:05	31.44	1.098	34.5211	33.1	1.11	36.74
9:10	31.47	1.098	34.5540	33.2	1.11	36.84
9:15	31.66	1.102	34.8893	33.2	1.11	36.85
9:20	31.9	1.105	35.2495	33.3	1.11	36.95
9:25	32.02	1.108	35.4781	33.3	1.11	36.96
9:30	32.09	1.11	35.6199	33.1	1.11	36.74
9:35	32.09	1.11	35.6199	33	1.11	36.63
9:40	32.19	1.12	36.0528	33	1.11	36.63
9:45	32.27	1.114	35.9487	32.8	1.1	36.08
9:50	32.22	1.113	35.8608	32.8	1.1	36.08
9:55	32.37	1.115	36.0925	32.9	1.1	36.19
10:00	32.19	1.112	35.7952	32.8	1.1	36.08
10:05	32.19	1.113	35.8274	32.8	1.1	36.08
10:10	32.2	1.113	35.8386	32.8	1.1	36.08
10:15	32.13	1.112	35.7285	32.6	1.1	35.86
10:20	32.19	1.113	35.8274	32.7	1.1	35.97
10:25	32.22	1.114	35.8930	32.5	1.1	35.75
10:30	32.21	1.114	35.8819	32.6	1.1	35.86
10:35	32.22	1.113	35.8608	32.5	1.1	35.75
10:40	32.27	1.115	35.9810	32.8	1.1	36.08
10:45	32.29	1.115	36.0033	32.9	1.1	36.19
10:50	32.28	1.114	35.9599	32.8	1.11	36.40
10:55	32.18	1.112	35.7841	32.6	1.1	35.86
11:00	32.1	1.11	35.631	32.4	1.1	35.64
11:05	32.1	1.112	35.6952	32.4	1.1	35.64
11:10	32.13	1.112	35.7285	32.6	1.1	35.86
11:15	32.14	1.112	35.7396	32.7	1.1	35.97
11:20	32.01	1.111	35.5631	32	1.1	35.2
11:25	31.39	1.1	34.529	32.2	1.1	35.42
11:30	31.74	1.105	35.0727	32	1.1	35.2
11:35	31.73	1.106	35.0933	32.1	1.1	35.31
11:40	31.77	1.107	35.1693	32.2	1.1	35.42
11:45	31.72	1.105	35.0506	32.1	1.1	35.31
11:50	31.84	1.108	35.2787	32.5	1.1	35.75
11:55	31.89	1.108	35.3341	32.6	1.1	35.86
12:00	31.8	1.105	35.139	32.8	1.1	36.08
12:05	31.72	1.103	34.9871	32.5	1.1	35.75
12:10	31.68	1.102	34.9113	32.5	1.1	35.75
12:15	31.66	1.102	34.8893	32.5	1.1	35.75
12:20	31.74	1.104	35.0409	32.4	1.1	35.64

Hour	fixed panel			mobile panel		
	Voltage	Current	Power	Voltage	Current	Power
12:25	31.66	1.103	34.9209	32.2	1.1	35.42
12:30	31.68	1.103	34.9430	32.4	1.1	35.64
12:35	32.15	1.112	35.7508	33.2	1.11	36.85
12:40	31.96	1.109	35.4436	33	1.1	36.3
12:45	31.74	1.106	35.1044	32.6	1.1	35.86
12:50	31.78	1.107	35.1804	32.8	1.1	36.08
12:55	31.7	1.106	35.0602	32.8	1.1	36.08
13:00	31.51	1.096	34.5349	32.3	1.1	35.53
13:05	30.1	1.084	32.6284	32	1.09	34.88
13:10	31.1	1.083	33.6813	31.09	1.09	33.88
13:15	30.85	1.084	33.4414	32.2	1.09	35.09
13:20	30.86	1.087	33.5448	32.2	1.1	35.42
13:25	29.72	1.084	32.2164	31.08	1.09	33.88
13:30	30.51	1.081	32.9813	31.8	1.09	34.66
13:35	30.69	1.083	33.2372	31.8	1.09	34.66
13:40	30.56	1.085	33.1576	32	1.09	34.88
13:45	30.95	1.087	33.6426	32.6	1.1	35.86
13:50	30.18	1.088	32.8358	32.2	1.1	35.42
13:55	29.68	1.085	32.2028	31.9	1.09	34.77
14:00	30.59	1.082	33.0983	31.9	1.09	34.77
14:05	30.75	1.083	33.3022	31.09	1.09	33.89
14:10	30.68	1.083	33.2264	32.5	1.1	35.75
14:15	30.76	1.086	33.4053	32.4	1.1	35.64
14:20	30.75	1.084	33.333	32.2	1.1	35.42
14:25	30.74	1.085	33.3529	32.6	1.1	35.86
14:30	30.73	1.084	33.3113	32.4	1.1	35.64
14:35	30.7	1.07	32.849	32.5	1.1	35.75
14:40	30.69	1.064	32.6541	32.5	1.1	35.75
14:45	30.7	1.063	32.6341	32.4	1.1	35.64
14:50	30.5	1.061	32.3605	32.3	1.09	35.20
14:55	30.7	1.063	32.6341	32.3	1.09	35.21
15:00	30.58	1.061	32.4453	32.4	1.1	35.64
15:05	30.66	1.061	32.5302	32.4	1.1	35.64
15:10	30.45	1.077	32.7946	32.3	1.1	35.53
15:15	30.53	1.063	32.4533	32.5	1.1	35.75
15:20	12.77	0.726	9.27102	10.5	0.66	6.93
15:25	31.09	1.069	33.2352	33.2	1.11	36.85
15:30	30.95	1.065	32.9617	33.1	1.11	36.74
15:35	6.59	0.588	3.87492	6.7	0.56	3.752
15:40	6.6	0.587	3.8742	7.9	0.6	4.74
15:45	31	1.091	33.821	34.6	1.13	39.09
15:50	6.6	0.547	3.6102	8.7	0.64	5.568
15:55	24.5	0.854	20.923	27.5	0.95	26.13
16:00	30.56	1.081	33.0353	34.9	1.14	39.78
16:05	29.56	1.062	31.3927	33.7	1.12	37.74
16:10	28.45	1.043	29.6733	33.1	1.11	36.74
16:15	27.62	1.029	28.4209	32.7	1.1	35.97
16:20	27.11	1.02	27.6522	32.7	1.1	35.97
16:25	26.11	1.002	26.1622	32.7	1.1	35.97
16:30	25.17	0.985	24.7924	32.7	1.1	35.97
16:35	24.01	0.963	23.1216	32.6	1.1	35.86
16:40	22.48	0.935	21.0188	32.6	1.1	35.86
16:45	19.91	0.887	17.6601	32.7	1.1	35.97
16:50	16.91	0.826	13.9676	32.3	1.09	35.20

Hour	fixed panel			mobile panel		
	Voltage	Current	Power	Voltage	Current	Power
16:55	16.69	0.822	3.71918	32.4	1.09	35.31
17:00	14.26	0.773	11.0229	32.2	1.09	35.09
17:05	12.11	0.727	8.80397	32.2	1.09	35.10
17:10	8.28	0.637	5.27436	32.1	1.09	34.98
17:15	1.1	0.233	0.2563	1.9	0.32	0.608
17:20	0.958	0.211	0.20213	1.6	0.29	0.464
17:25	0.869	0.195	0.16945	1.6	0.29	0.464
17:30	1.033	0.221	0.22829	1.28	0.69	0.883
17:35	0.684	0.16	0.10944	1.3	0.25	0.325
17:40	0.719	0.167	0.12007	26.1	0.91	23.75
17:45	0.551	0.131	0.07218	15.1	0.74	11.17
17:50	0.419	0.102	0.04273	0.6	0.13	0.078
17:55	0.333	0.08	0.02664	0.4	0.09	0.036
18:00	0.264	0.065	0.01716	0.3	0.07	0.021

Source: Authors, (2022).

Obtaining the graph of power generated for the first day with a fixed panel shown in figure 16.

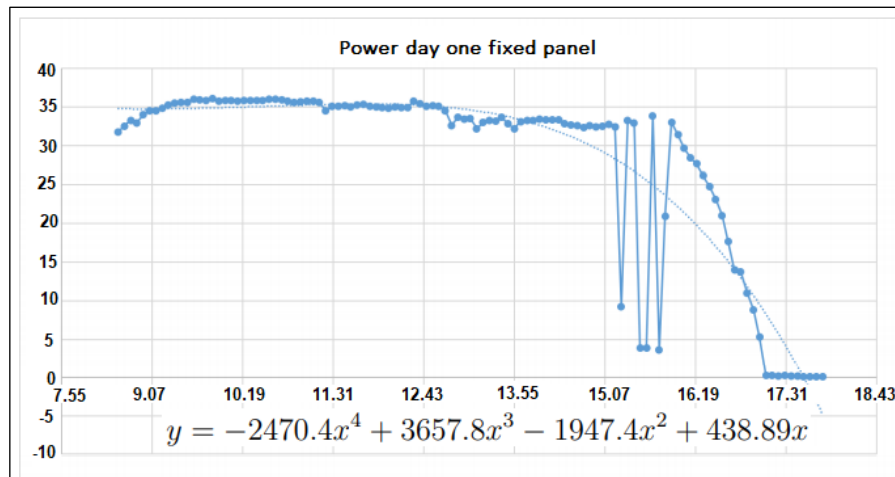


Figure 16: Graph of power generated first day with fixed panel.  
Source: Authors, (2022).

Obtaining the graph of power generated for the first day with a mobile panel shown in figure 17.

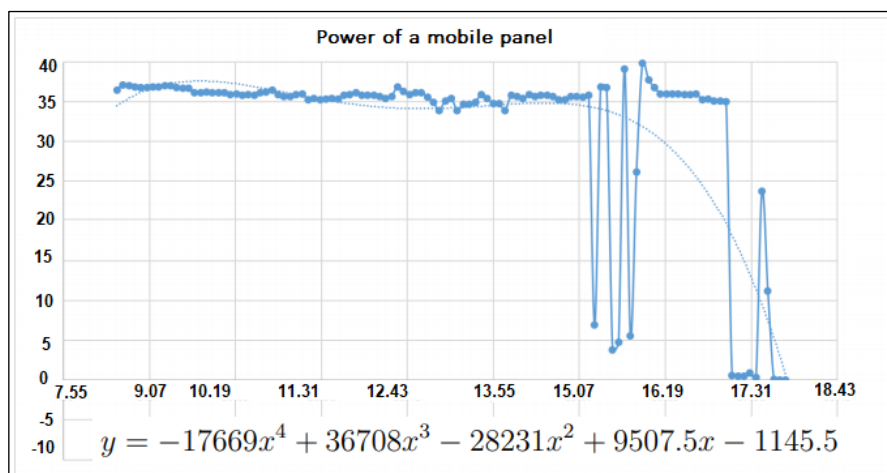


Figure 17: Graph of generated power, day one mobile panel  
Source: Authors, (2022).

With the measurements of the second day, the graph of power generated with a fixed panel is obtained, shown in figure 18.

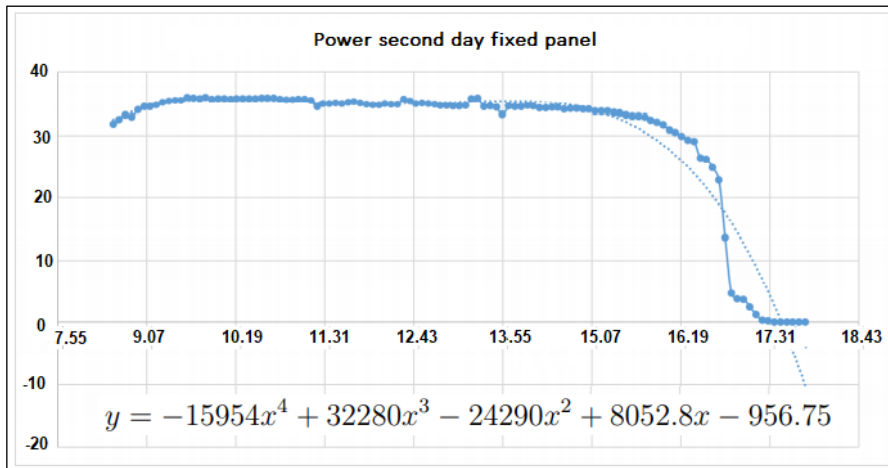


Figure 18: Graph of power generated second with fixed panel.  
Source: Authors, (2022).

With the measurements of the second day, the graph of power generated with the mobile panel is obtained, which is shown in figure 19.

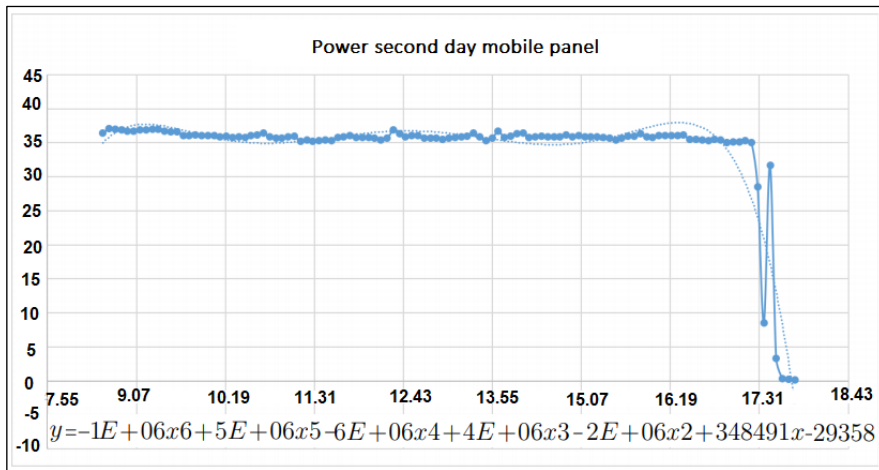


Figure 19: Graph of power generated second day with mobile panel.  
Source: Authors, (2022).

With the measurements of the third day, the graph of power generated with a fixed panel is obtained, which is shown in figure 20.

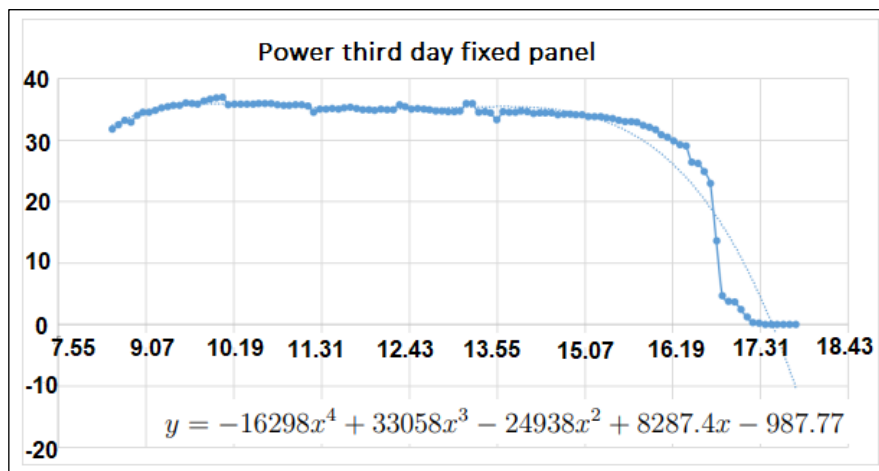


Figure 20: Graph of power generated third with fixed panel.  
Source: Authors, (2022).



With the measurements of the third day, the graph of power generated with the mobile panel is obtained, which is shown in figure 21.

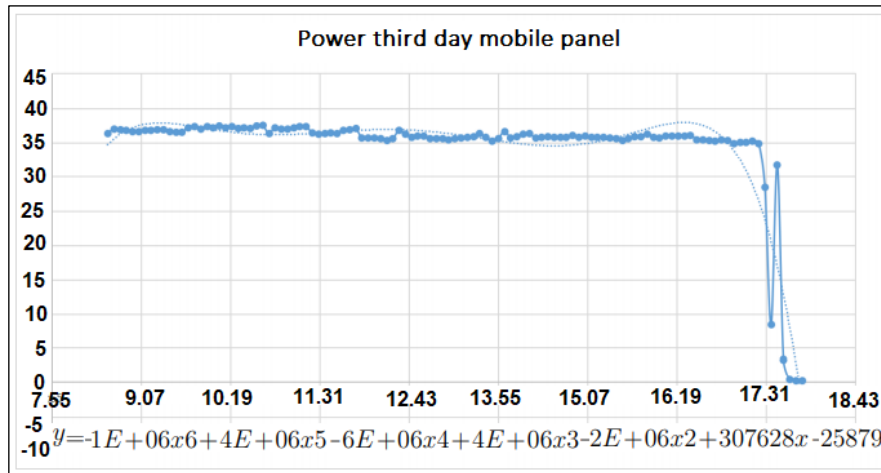


Figure 21: Graph of power generated third day with mobile panel.  
Source: Authors, (2022).

## VI. CONCLUSIONS

The built prototype complies with the required characteristics of tracking the sun on the polar axis from an initial position of the structure of 15o inclination on said axis and facing east for sunrise, by means of a fuzzy control system. which with respect to the classic controls is easier to understand the algorithm since it handles a linguistic programming method. To control the position of the panel with respect to the incidence of light, photoresistive elements were used, achieving a 40% increase in efficiency in solar panels with a mobile system with respect to fixed solar systems. The developed software allows maintaining the perpendicularity of the solar panel with respect to the incidence of solar rays, which is demonstrated with the data collected during the testing stage. The tests of the fixed system and the mobile system controlled by fuzzy control were carried out simultaneously, so the comparison made in the data collected has a higher degree of sustainability, since they were carried out under the same climatic conditions. It was not possible to carry out an implementation of a two-axis solar tracker system due to certain movement limitations in the structure and the short time in which the tests were carried out for the design used. The program used is designed to function exclusively for the structure used, however it is easily adjustable to a different structure that has a similar system.

## VII. AUTHOR'S CONTRIBUTION

**Conceptualization:** Omar Beltrán González, Jesús Hernández Aguilar, Francisco Eneldo López Monteagudo and Rafael Villela Varela.

**Methodology:** Omar Beltrán González, Jesús Hernández Aguilar, Francisco Eneldo López Monteagudo and Rafael Villela Varela

**Investigation:** Omar Beltrán González, Jesús Hernández Aguilar, Francisco Eneldo López Monteagudo, Rafael Villela Varela, Aurelio Beltrán Telles and Claudia Reyes Rivas.

**Discussion of results:** Omar Beltrán González, Jesús Hernández Aguilar, Francisco Eneldo López Monteagudo, Rafael Villela Varela, Aurelio Beltrán Telles and Claudia Reyes Rivas.

**Writing – Original Draft:** Omar Beltrán González and Jesús Hernández Aguilar

**Writing – Review and Editing:** Omar Beltrán González, Jesús Hernández Aguilar, Francisco Eneldo López Monteagudo and Rafael Villela Varela.

**Resources:** Omar Beltrán González and Jesús Hernández Aguilar, Francisco Eneldo López Monteagudo and Rafael Villela Varela.

**Supervision:** Francisco Eneldo López Monteagudo and Rafael Villela Varela.

**Approval of the final text:** Omar Beltrán González, Jesús Hernández Aguilar, Francisco Eneldo López Monteagudo and Rafael Villela Varela.

## VIII. ACKNOWLEDGMENTS

We thank the Autonomous University of Zacatecas and the Zacatecano council of science and technology for the support for the realization of this article.

## IX. REFERENCES

- [1] H. M. F. da Silva e F. J. C. Araújo, "Energia solar fotovoltaica no brasil: uma revisão bibliográfica", rease, vol. 8, n° 3, p. 859–869, mar. 2022.
- [2] M. Quijano and G. González, "Study of the Penetration of Photovoltaic Energy at the Self-consumption Customer Level using the IEEE 13-Node Test Feeder adapted to Panama," 2022 IEEE 40th Central America and Panama Convention (CONCAPAN), Panama, Panama, 2022, pp. 1-5, doi: 10.1109/CONCAPAN48024.2022.9997607.
- [3] J. N. Maciel, J. Javier Giménez Ledesma and O. Hideo Ando Junior, "Forecasting Solar Power Output Generation: A Systematic Review with the Proknow-C," in IEEE Latin America Transactions, vol. 19, no. 4, pp. 612-624, April 2021, doi: 10.1109/TLA.2021.9448544.
- [4] L. H. Vera, M. Cáceres, A. Firman, R. Gonzales Mayans and A. Busso, "Diseño y simulación de microrred híbrida aislada," 2022 IEEE Biennial Congress of Argentina (ARGENCON), San Juan, Argentina, 2022, pp. 1-7, doi: 10.1109/ARGENCON55245.2022.9939734.
- [5] F. R. Riccio Anastacio, Seguidor solar a dos ejes cuya posición se calcula utilizando los ángulos de elevación y Azimut del sol en Guayaquil, RECIMUNDO, vol. 6, n.º 1, pp. 225-231, feb. 2022.
- [6] E. Chacón-Pinzón, D. Arenas, y B. J. Parra, «Revisión del estado actual de los Sistemas de Energía Fotovoltaica», rinte, vol. 11, jul. 2021.
- [7] J. M. Rey et al., "A Review of Microgrids in Latin America: Laboratories and Test Systems," in IEEE Latin America Transactions, vol. 20, no. 6, pp. 1000-1011, June 2022, doi: 10.1109/TLA.2022.9757743.

- [8] A. -H. I. Mourad, H. Shareef, N. Ameen, A. H. Alhammadi, M. Iratni and A. S. Alkaabi, "A state-of-the-art review: Solar trackers," 2022 Advances in Science and Engineering Technology International Conferences (ASET), Dubai, United Arab Emirates, 2022, pp. 1-5, doi: 10.1109/ASET53988.2022.9735074.
- [9] A.Z. Hafez, A.M. Yousef, N.M. Harag, "Solar tracking systems: Technologies and trackers drive types – A review, Renewable and Sustainable Energy Reviews", Volume 91, 2018, Pages 754-782, ISSN 1364-0321, <https://doi.org/10.1016/j.rser.2018.03.094>.
- [10] A. Bahrami, C. Onyeka Okoye, "The performance and ranking pattern of PV systems incorporated with solar trackers in the northern hemisphere, Renewable and Sustainable Energy Reviews", Volume 97, 2018, Pages 138-151, ISSN 1364-0321, <https://doi.org/10.1016/j.rser.2018.08.035>.
- [11] A. -T. Nguyen, T. Taniguchi, L. Eciolaza, V. Campos, R. Palhares and M. Sugeno, "Fuzzy Control Systems: Past, Present and Future," in IEEE Computational Intelligence Magazine, vol. 14, no. 1, pp. 56-68, Feb. 2019, doi: 10.1109/MCI.2018.2881644.
- [12] Y. Hong, Hans J. Pasma, N. Quddus, M. Sam Mannan, "Supporting risk management decision making by converting linguistic graded qualitative risk matrices through interval type-2 fuzzy sets, Process Safety and Environmental Protection", Volume 134, 2020, Pages 308-322, ISSN 0957-5820, <https://doi.org/10.1016/j.psep.2019.12.001>.
- [13] O. Beltrán González, and J. Hernández Aguilar, "Design of a control system for a solar tracker implementing fuzzy logic in arduino", Bachelor's thesis, Electrical Engineering Academic Unit Autonomous University of Zacatecas, Mexico 2015.